

DESIGN AND DEVELOPEMENT OF ENERGY EFFICIENT MINIATURE DEVICES  
FOR ENERGY HARVESTING, THERMAL MANAGEMENT AND BIOMEDICAL  
APPLICATIONS

by  
A. TAHA ÇIKIM

Submitted to the Graduate School of Engineering and Natural Sciences  
In partial fulfilment of  
the requirements for the degree of  
Master of Science

SABANCI UNIVERSITY

January 2014

DESIGN AND DEVELOPEMENT OF ENERGY EFFICIENT MINIATURE DEVICES  
FOR ENERGY HARVESTING, THERMAL MANAGEMENT AND BIOMEDICAL  
APPLICATIONS

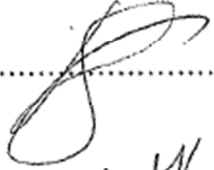
APPROVED BY:

Assoc. Prof. Dr. Ali Koşar

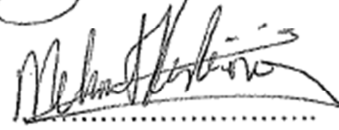


(Thesis Supervisor)


Assoc. Prof. Dr. Devrim Gözüaçık



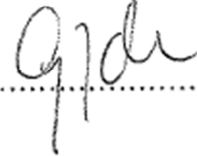
Assoc. Prof. Dr. Mehmet Keskinöz



Asst. Prof. Dr. Burç Mısırlıoğlu



Asst. Prof. Dr. Gözde Özaydın İnce



DATE OF APPROVAL: 13/ 01/ 2014

© A. Taha ıkım 2013

All Rights Reserved

DESIGN AND DEVELOPEMENT OF ENERGY EFFICIENT MINIATURE DEVICES  
FOR ENERGY HARVESTING, THERMAL MANAGEMENT AND BIOMEDICAL  
APPLICATIONS

A. Taha ÇIKIM

Mechatronics Engineering, M.Sc Thesis, 2013

Thesis Supervisor: Assoc. Prof. Dr. Ali KOŞAR

Keywords: Energy harvesting, Ferrofluid, PEI, SPION, Transfection, Magnetic Actuation, MCF-7, Crosslinked pHEMA Coating, Heat Transfer Enhancement, Flow Boiling, Micro Scale Boiling, Black ghost knife fish; external fluid flow; miniature power generators; power reclamation

**ABSTRACT**

This thesis aims to make contributions to the literature in the field of energy efficient miniature devices for energy harvesting, thermal management and biomedical applications.

In the first part, experimental results related to energy harvesting capability of a miniature power reclamation device based on external liquid flows are represented. The device's reclamation principle depends on the conversion of mechanical energy into electrical energy. The mechanical energy in the device was generated by capturing vibrations caused by external liquid flows via the device's tails, which were designed by taking inspiration from the body shape of the black ghost knife fish, apteronotus albifrons. The reclaimed power was obtained through magnetic polarization, which was generated by rotating circular waterproof magnet structures as a result of rotating movements of the mentioned tails and is transferred to 3.76 V (Ni-Mg) batteries. Power reclamation was also simulated using COMSOL 4.2 software in order to compare the maximum reclaimable theoretical energy harvesting capacity to the experimental results. Experimental tests were performed within a range of flow velocities (1.0 m/s ~ 5.0 m/s) for various fluid densities (plain water, low-salt and high-salt water) in order to obtain extensive experimental data related to the device in response to



external fluid flows. According to experimental results, the device could generate powers up to 17.2W. On the other hand, the maximum reclaimable power was obtained as 25.7W from COMSOL Multiphysics 4.2 simulations. Promising energy harvesting results imply that the output from this device could be used as a power source in many applications such as in lighting and GPS (Global positioning system) devices.

In the second part of the thesis, a miniature system was used for flow boiling in mini/microtubes. Flow boiling was investigated with surface enhancements provided by crosslinked polyhydroxyethylmethacrylate (pHEMA) coatings, which were used as a crosslinker coating type with different thicknesses (~50 nm, 100 nm and 150 nm) on inner microtube walls. Flow boiling heat transfer experiments were conducted on microtubes (with inner diameters of 249  $\mu\text{m}$ , 507  $\mu\text{m}$  and 908  $\mu\text{m}$ ) coated with crosslinked pHEMA coatings. pHEMA nanofilms were deposited with the initiated chemical vapor deposition (iCVD) technique. De-ionized water was utilized as the working fluid. Experimental results obtained from coated microtubes were compared to their plain surface counterparts at two different mass fluxes (5,000  $\text{kg/m}^2\text{s}$  and 20,000  $\text{kg/m}^2\text{s}$ ), and significant enhancements in Critical Heat Flux (up to 29.7 %) and boiling heat transfer (up to 126.2 %) were attained. The enhancement of boiling heat transfer was attributed to the increase in nucleation site density and incidence of bubbles departing from surface due to porous structure of crosslinked pHEMA coatings. The underlying mechanism was explained with suction-evaporation mode. Moreover, thicker pHEMA coatings resulted in larger enhancements in both CHF and boiling heat transfer.

In the third part, a platform for gene delivery via magnetic actuation of nanoparticles was developed. The importance of high transfection efficiency has been emphasized in many studies investigating methods to improve gene delivery. Accordingly, non-viral transfection agents are widely used as transfection vectors to condense oligonucleotides, DNA, RNA, siRNA, deliver into the cell, and release the cargo. Polyethyleneimine (PEI) is one of the most popular non-viral transfection agents. However, the challenge between high transfection efficiency and toxicity of the polymers is not totally resolved. The delivery of necessary drugs and genes for patients and their transport under safe conditions require carefully designed and controlled delivery systems and constitute a critical stage of patients' treatment. Compact systems are considered as the strongest candidate for the preparation and delivery of drugs and genes under leak free and safe conditions because of their low energy consumption, low waste disposal, parallel and fast processing capabilities, removal of human

factor, high mixing capabilities, enhanced safety, and low amount of reagents. Motivated by this need in the literature, The use of PEI-SPION (Super paramagnetic iron oxide nanoparticles) as transfection agents in in-vitro studies was investigated with the effect of varying magnetic fields provided by a special magnetic system design, which was used as a miniature magnetic actuator device offering different magnet's turn speeds in the system. Experimental results obtained from experimental magnetic actuator systems were compared to the experiments without magnetic actuation, and it was observed that significant enhancements in transfection efficiency (up to 25-30 %) in MCF-7 and PC-3 cells were attained.

ENERJİ ÜRETİMİ, TERMAL YÖNETİM VE BİOMEDİKAL UYGULAMALARI İÇİN  
ENERJİ VERİMLİLİĞİ YÜKSEK MİNYATÜR CİHAZLARIN TASARIM VE  
GELİŞTİRİLMESİ

A. Taha ÇIKIM

Mekatronik Mühendisliği, Yüksek Lisans Tezi, 2012

Tez Danışmanı: Doç. Dr. Ali KOŞAR

Anahtar Kelimeler: Enerji üretimi, Ferrofluid, PEI, SPION, Transfeksiyon, Manyetik Aktivasyon, MCF-7, PC-3, Çaprazbağlı pHEMA Kaplama, Isı Transfer Geliştirme, Akış Kaynamaları, Mikro Ölçekli Kaynama, Siyah Hayalet Kılıç Balığı, Harici Sıvı Akışı, Minyatür Güç Jeneratörleri, Güç Üretimi

**ÖZET**

İşbu çalışma, enerji üretimi, termal yönetim ve biomedikal uygulamaları için enerji verimliliği yüksek minyatür cihazların tasarım ve geliştirilmesi ile ilgili literatürdeki bilgi boşluğuna katkı sağlamak amacı taşımaktadır.

Birinci kısımda, harici sıvı akışına dayanarak güç üretebilen bir minyatür cihazın enerji üretim kapasitesi incelenmiştir. Cihazın enerji üretimi, mekanik enerjinin elektrik enerjisine dönüşmesiyle gerçekleşir. Mekanik enerji, latince apteronotus albifrons olarak adlandırılan siyah hayalet bıçak balığının vücut şeklinden ve iskelet yapısından esinlenerek tasarlanmış kuyrukların, harici sıvı akışlarını yakalayıp titremesiyle oluşur. Elde edilen güç, su geçirmez manyetik yapıların hareket etmesiyle, manyetik kutuplaşmadan dolayı oluşan enerjinin 3.76 V (Ni-Mg) pile aktarmasıyla oluşur. Cihazın teorik olarak üretebileceği maksimum gücü ölçmek için, COMSOL 4.2 yazılımı ile simülasyon yapılmış ve bulunan sonuçlar deneysel sonuçlar ile karşılaştırılmıştır. Deneysel 1 m/s ile 5 m/s arasında değişen akış hızları ve değişik sıvı yoğunlukları (saf su, az tuzlu su, çok tuzlu su) altında, farklı harici sıvı akışlarına göre geniş çaplı deney sonuçları elde etmek için yapılmıştır. Deneysel sonuçlar cihazın 17.2

Watt'a kadar enerji üretebildiğini gösterirken, COMSOL 4.2 yazılımı kullanılarak yapılan simülasyon sonuçları cihazın 25.7 Watt enerji üretebileceğini göstermiştir. Gelecek vaat eden enerji üretimi sonuçları göstermiştir ki cihaz GPS ve ışıklandırma gibi birçok amaç için güç kaynağı olarak kullanılabilir.

İkinci kısımda, mini ve mikro kanal kaynama akışlarında, çapraz bağlayıcı olarak kullanılan polyhydroxyethylmethacrylate (pHEMA) mikro kanal iç duvar yüzeyi kaplaması, farklı kalınlıklarda (~50 nm, 100 nm ve 150 nm) incelenmiştir. Kaynama akışı deneyleri, çapraz bağlayıcı pHEMA kaplı farklı mikro kanal yarıçaplarında (~249 µm, 507 µm ve 998 µm) gerçekleştirilmiştir. pHEMA nanofilm kaplaması, (iCVD) başlatılmış kimyasal buhar çöküntü yöntemiyle kaplanmıştır. Çalışma sıvısı olarak iyonsuzlaştırılmış su kullanılmıştır. Kaplanmış mikro kanallardan elde edilmiş sonuçlar, farklı kütle akıları (~5,000 kg/m<sup>2</sup>s ve ~20,000 kg/m<sup>2</sup>s) altında kaplanmamış mikro kanallardan elde edilmiş sonuçlar ile karşılaştırılmış, kritik ısı akısında (CHF) % 29.7, kaynayan ısı transfer oranında ise % 126.2'ye varan artış gözlemlenmiştir. Kaynama ısı transferindeki artış, çekirdeklenme yoğunluğuna ve çapraz bağlı pHEMA kaplamanın porlu yapısından dolayı yüzeyden ayrılan baloncuk sıklığının artmasına atfedilmiştir. Buradaki mekanizma emme-buharlaşma mekanizması ile açıklanmıştır. Ayrıca kaplama kalınlığı ince mikro kanallarda hem kritik ısı akısı hem de kaynama ısı transferinde daha çok artış görüldüğü gözlemlenmiştir.

Üçüncü kısımda ise nanoparçacıkların manyetik aktivasyon ile taşınmasını sağlayan bir platform geliştirilmiştir. Yüksek transfeksiyon verimliliğinin önemi, gen taşımayı geliştiren bir method üzerinde vurgulanmıştır. Benzer şekilde, oligo nükleotidleri, DNA, RNA ve siRNA moleküllerini yoğunlaştırmak için transfeksiyon vektörü olarak bilinen viral olmayan transfeksiyon araçlarının hücre içine taşıma ve yük atma işlemleri için kullanıldıkları bilinmektedir. Polyethyleneimine (PEI), bilinen en popüler viral olmayan transfeksiyon araçlarından biridir. Ancak, yüksek transfeksiyon verimliliği ve polimerin toksitliği arasındaki zorluklar tamamen çözülmüş değildir. Gerekli ilaçların ve genelerin hastalara güvenli koşullar altında ulaştırılması gelişmiş dizayn ve kontrol gerektirmekle birlikte, hastalığın kritik seviyelerinden önce yapılmasını gerektirmektedir. Bu nedenle ilaç ve genlerin hazırlanması ve taşınmasında kompakt sistemler, düşük enerji tüketimi, düşük atık oranı, paralel ve hızlı işlem kapasitesi, insan faktörünü yok etmesi, yüksek karıştırma kapasitesi, gelişmiş güvenlik seviyesi ve düşük malzeme kullanımı yönünden güçlü

adaylardır. Bu kısımda, in vitro çalışmalarında PEI-SPION (Süper paramaynetik demir oksit) nanoparçacıklarının transfeksiyon aracı olarak kullanılması, farklı yönlere dönebilme özelliklerinden ötürü deęişken manyetik alan gücüne sahip özel olarak dizayn edilmiş bir manyetik aktivator minyatür cihazı ile incelenmiştir. Minyatür manyetik aktivator cihazı ile elde edilmiş sonuçlar, manyetik aktivator kullanılmadan yapılan transfeksiyon sonuçları ile karşılaştırılmış, MCF-7 ve PC-3 hücrelerinde gerçekleşen transfeksiyon verimliliğinde % 25-30 arası deęişen artış elde edilmiştir.

## *ACKNOWLEDGEMENTS*

I feel a dept of gratitude for my thesis supervisor Assc. Prof. Ali KOŞAR because of his self-sacrifice, sympathy and helpfulness during my whole undergraduate and graduate period (from sophomore to M.S) for any kind of issue in terms of both academic and personal aspects, which constitute milestones of my life. I am grateful and proud for being one of his students and having millions of academic opportunities, which he proposed me even after graduation. I will be always proud of working with him and, continuously needing his endless support and guidance. I hope our collaboration would last forever.

I also would like to thank to Dr. Devrim Gözüaık, his research team and Dr. Özlem Oral for their enthusiastic support and help for my research.

I would like to thank Dr. Gözde Özaydın-İnce, her research team and Dr. Meltem Sezen for their contributions to this thesis.

I am very grateful to my thesis committee members Dr. Devrim Gözüaık, Dr. Gözde Özaydın-İnce, Dr. Burç Mısırlıođlu and Dr. Mehmet Keskinöz for giving their valuable time for evaluating my M.Sc thesis.

I would like to thank to Eren Yalçın for his friendliness and all moral and academic support especially when I had troubles.

I would like to thank to my tablemate Mostafa Shojaeian for sharing not only table, but also for having several adventures and supporting my work.

I would like to thank my best friends Mehmet Emre Kara and Erdem Görgün for having unforgettable adventures and coming to help wherever I call them.

I would like to thank the Sabancı University Nanotechnology Research and Application Center (SUNUM) for the continued equipment and characterization support.

This work was supported by Turkish Scientific Council, grant number: 112M940 and TUBA (Turkish Academy of Science) Outstanding Young Investigator Support Program (GEBIP).

# TABLE OF CONTENTS

|   |             |
|---|-------------|
| <b>ABSTRACT .....</b>   | <b>II</b>   |
| <b>ÖZET.....</b>  | <b>V</b>    |
| <b>ACKNOWLEDGEMENT .....</b>  | <b>VIII</b> |
| <b>TABLE OF CONTENTS.....</b>   | <b>IX</b>   |
| <b>LIST OF FIGURES .....</b>  | <b>XI</b>   |
| <b>LIST OF TABLES .....</b>   | <b>XIV</b>  |
| <b>NOMENCLATURE.....</b>  | <b>XV</b>   |
| <br>  |             |
| 1. INTRODUCTION.....  | 1           |
| 1.1 Objectives and Major Challenges of This Work.....   | 2           |
| 1.2 Literature Survey of Miniature Energy Harvesting Device Using External Fluid<br>Flows (First Part) .....                                  | 2           |
| 1.3 Literature Survey of Miniature System for Flow Boiling Enhancement in<br>Microtubes with Crosslinked pHEMA Coatings (Second Part) .....   | 6           |
| 1.4 Literature Survey of Miniature Magnetic Actuator for Targeted Gene Delivery of<br>Nucleic Acid Based Molecules (Third Part) .....         | 9           |
| <br>  |             |
| 2. EXPERIMENTAL SETUP AND PROCEDURE .....   | 16          |
| 2.1 Experimental Test Setup of Miniature Energy Harvesting Device Using External<br>Fluid Flows using external fluid flows (First Part) ..... | 16          |
| 2.1.1 Device Overview .....   | 16          |
| 2.1.2 Tail Design .....   | 18          |

|       |  |    |
|-------|--|----|
| 2.2   | Experimental Test Setup of Miniature System for Flow Boiling Enhancement in Microtubes with Crosslinked pHEMA Coatings (Second Part) | 21 |
| 2.3   | Experimental Test Setup of Miniature Magnetic Actuator for Targeted Gene Delivery of Nucleic Acid Based Molecules (Third Part)       | 22 |
| 2.4   | Experimental Procedure of Miniature Energy Harvesting Device Using External Fluid Flows using external fluid flows (First Part)      | 24 |
| 2.5   | Experimental Procedure of Miniature System for Flow Boiling Enhancement in Microtubes with Crosslinked pHEMA Coatings (Second Part)  | 25 |
| 2.6   | Experimental Procedure of Miniature Magnetic Actuator for Targeted Gene Delivery of Nucleic Acid Based Molecules (Third Part)        | 26 |
| 2.6.1 | Preparation of Polyethyleneimine-Superparamagnetic Nanoparticles   | 27 |
| 2.6.2 | Plasmid DNA isolation and Cell Culture   | 27 |
| 2.6.3 | Cell Transfection  | 28 |
| 2.7   | Model and Simulations  | 28 |
| 2.7.1 | Governing Equations  | 29 |
| 2.7.2 | Mesh and Solver Settings   | 30 |
| 2.7.3 | Post Processing of the Results   | 31 |
| 2.8   | Data Reduction   | 35 |
| 3.    | MOTIVATION   | 38 |
|       | RESULTS AND DISCUSSION   | 40 |
| 3.1   | First Part - Power Reclamation Efficiency of Miniature Energy Harvesting Device Using External Fluid Flows                           | 40 |
| 3.1.1 | Simulation Results   | 40 |
| 3.1.2 | Experimental Results   | 40 |
| 3.2   | Second Part - Flow Boiling Enhancement in Microtubes with Crosslinked pHEMA Coating Having Different Coating Thickness Flows         | 43 |
| 3.2.1 | Boiling Curves   | 44 |
| 3.2.2 | Heat Transfer Results  | 50 |
| 3.2.3 | Raman Spectroscopy Results   | 56 |
| 3.2.4 | Visualization Tests  | 58 |
| 3.3   | Third Part - Varying Magnetic Field on Targeted Gene Delivery of Nucleic Acid-Based Molecules  | 62 |
| 3.3.1 | PEI Transfection Results   | 62 |
| 3.3.2 | PEI-SPION Transfection Results   | 64 |



|   |           |
|---|-----------|
| MAJOR FINDINGS .....                    | 69        |
| 4. CONTRIBUTION TO THE LITERATURE ..... | 71        |
| 5. CONCLUSION .....                     | 73        |
| <b>REFERENCES.....</b>                  | <b>75</b> |

# LIST OF FIGURES

## CHAPTER 2

|   |    |
|---|----|
| Figure 2.1: Isometric view of the power reclamation device .....                                      | 17 |
| Figure 2.2: Schematic of the miniature energy harvesting device including its components .            | 17 |
| Figure 2.3: The design based on skeleton of Black Ghost Night Fish tail .....                         | 19 |
| Figure 2.4: Surface of the Black Ghost Night Fish Tail Design .....                                   | 19 |
| Figure 2.5: Illustration of the tail layers of the miniature energy harvesting device.....            | 20 |
| Figure 2.6: Schematic of the heat transfer experiment setup .....                                     | 21 |
| Figure 2.7: Schematic of the test section.....  | 21 |
| Figure 2.8: Magnetic field direction on magnetic rotors.....  | 23 |
| Figure 2.9: Schematic of the magnetic actuator .....  | 24 |
| Figure 2.10: Experimental Setup of Miniature Energy Harvesting Device .....                           | 25 |
| Figure 2.11: Fixed Mesh for Virtual Environment Cube .....  | 30 |
| Figure 2.12: Moving Mesh for the Tail in the Cube .....   | 31 |
| Figure 2.13: Zoom in View of Moving Mesh for the tail*.....   | 32 |
| Figure 2.14: Initial Position of the Tail.....  | 33 |
| Figure 2.15: Tail at a Displacement Value of 2 cm due to Vibrations Caused by Flow Oscillations ..... | 34 |
| Figure 2.16: Flow Streamlines for the Initial Position of the Tail.....                               | 34 |

## CHAPTER 3

|  |    |
|--|----|
| Figure 3.1: Outlet Power Result of COMSOL Simulation (Plain Water) and Experimental Results under Different Working Fluids .....   | 42 |
| Figure 3.2: Friction factor – Reynolds number profiles.....  | 43 |
| Figure 3.3: Boiling Curves for Plain Surface Microtubes and pHEMA Coated Microtubes (50 nm, 100 nm and 150 nm thick coatings) with an Inner Diameter of 249 $\mu\text{m}$ at the Mass Flux of 5,000 $\text{kg}/\text{m}^2\text{s}$ ..... | 44 |
| Figure 3.4: Boiling Curves for Plain Surface Microtubes and pHEMA Coated Microtubes (50 nm, 100 nm and 150 nm thick coatings) with an Inner Diameter of 507 $\mu\text{m}$ at the Mass Flux of 5,000 $\text{kg}/\text{m}^2\text{s}$ ..... | 45 |

|   |    |
|---|----|
| Figure 3.5: Boiling Curves for Plain Surface Microtubes and pHEMA Coated Microtubes (50 nm, 100 nm and 150 nm thick coatings) with an Inner Diameter of 998 $\mu\text{m}$ at the Mass Flux of 5,000 $\text{kg}/\text{m}^2\text{s}$ .....                        | 46 |
| Figure 3.6: Boiling Curves for Plain Surface Microtubes and pHEMA Coated Microtubes (50 nm, 100 nm and 150 nm thick coatings) with an Inner Diameter of 249 $\mu\text{m}$ at the Mass Flux of 20,000 $\text{kg}/\text{m}^2\text{s}$ .....                       | 47 |
| Figure 3.7: Boiling Curves for Plain Surface Microtubes and pHEMA Coated Microtubes (50 nm, 100 nm and 150 nm thick coatings) with an Inner Diameter of 507 $\mu\text{m}$ at the Mass Flux of 20,000 $\text{kg}/\text{m}^2\text{s}$ .....                       | 48 |
| Figure 3.8: Boiling Curves for Plain Surface Microtubes and pHEMA Coated Microtubes (50 nm, 100 nm and 150 nm thick coatings) with an Inner Diameter of 998 $\mu\text{m}$ at the Mass Flux of 20,000 $\text{kg}/\text{m}^2\text{s}$ .....                       | 49 |
| Figure 3.9: Two Phase Heat Transfer Coefficient for Plain Surface Microtubes and pHEMA Coated Microtubes (50 nm, 100 nm and 150 nm Thick Coatings) with an Inner Diameter of 249 $\mu\text{m}$ at the Mass Flux of 5,000 $\text{kg}/\text{m}^2\text{s}$ .....   | 51 |
| Figure 3.10: Two Phase Heat Transfer Coefficient for Plain Surface Microtubes and pHEMA Coated Microtubes (50 nm, 100 nm and 150 nm Thick Coatings) with an Inner Diameter of 507 $\mu\text{m}$ at the Mass Flux of 5,000 $\text{kg}/\text{m}^2\text{s}$ .....  | 52 |
| Figure 3.11: Two Phase Heat Transfer Coefficient for Plain Surface Microtubes and pHEMA Coated Microtubes (50 nm, 100 nm and 150 nm Thick Coatings) with an Inner Diameter of 998 $\mu\text{m}$ at the Mass Flux of 5,000 $\text{kg}/\text{m}^2\text{s}$ .....  | 53 |
| Figure 3.12: Two Phase Heat Transfer Coefficient for Plain Surface Microtubes and pHEMA Coated Microtubes (50 nm, 100 nm and 150 nm Thick Coatings) with an Inner Diameter of 249 $\mu\text{m}$ at the Mass Flux of 20,000 $\text{kg}/\text{m}^2\text{s}$ ..... | 54 |
| Figure 3.13: Two Phase Heat Transfer Coefficient for Plain Surface Microtubes and pHEMA Coated Microtubes (50 nm, 100 nm and 150 nm Thick Coatings) with an Inner Diameter of 507 $\mu\text{m}$ at the Mass Flux of 20,000 $\text{kg}/\text{m}^2\text{s}$ ..... | 55 |
| Figure 3.14: Two Phase Heat Transfer Coefficient for Plain Surface Microtubes and pHEMA Coated Microtubes (50 nm, 100 nm and 150 nm Thick Coatings) with an Inner Diameter of 998 $\mu\text{m}$ at the Mass Flux of 20,000 $\text{kg}/\text{m}^2\text{s}$ ..... | 56 |
| Figure 3.15: Raman Spectrum Taken from the Inner Surface of the Untreated Sample Microtube Having 249 $\mu\text{m}$ Inner Diameters.....  | 57 |
| Figure 3.16: Raman Spectrum Taken from the Inner Surface of the Treated Sample Microtube Having 249 $\mu\text{m}$ Inner Diameters.....  | 58 |
| Figure 3.17: The Schematic of the Experimental Setup for Visualization.....   | 60 |
| Figure 3.18: Bubbles emerging from the non-coated Plate.....  | 61 |
| Figure 3.19: Bubbles emerging from the Crosslinked pHEMA coated Plate .....   | 61 |

|   |    |
|---|----|
| Figure 3.20: Transfection results of 2.5 g/ml DNA with 25 microgram PEI.....  | 63 |
| Figure 3.21: Transfection results of 0.5 g/ml DNA with 5 microgram PEI.....   | 63 |
| Figure 3.22: Magnetic actuator setup inside incubator at 37 C° .....  | 64 |
| Figure 3.23: Power vs velocity curve for magnetic rotors .....  | 65 |
| Figure 3.24: MCF-7 Breast Cancer Cells.....   | 66 |
| Figure 3.25: Experimental results without device MCF-7 cell under Fluorescent light (a) and light microscopy (b) image..... | 67 |
| Figure 3.26: Experimental results with device MCF-7 cell under Fluorescent light (a) and light microscopy (b) image.....    | 67 |
| Figure 3.27: Experimental results without device PC-3 cell under Fluorescent light (a) and light microscopy (b) image.....  | 68 |
| Figure 3.28: Experimental results without device PC-3 cell under Fluorescent light (a) and light microscopy (b) image.....  | 68 |

# LIST OF TABLES

## CHAPTER 2

Table 2.1: Uncertainties of measured values..... 37

## CHAPTER 3

Table 3.1: Uncertainties Estimated Working Duration of the Energy Harvesting Device to Run Given Daily Used Devices for ~1 Hour..... 40

## NOMENCLATURE

| Symbol           | Description                       | Units   |
|------------------|-----------------------------------|---|
| $A_c$            | cross-sectional area              | $\text{m}^2$                                    |
| $c_p$            | specific heat of water            | $\text{kJ kg}^{-1} \text{ }^\circ\text{C}^{-1}$ |
| $d_i$            | channel inner diameter            | $\text{M}$                                      |
| $G$              | mass flux                         | $\text{kg m}^{-2} \text{s}^{-1}$                |
| $h_{FG}$         | latent heat of vaporization       | $\text{J kg}^{-1} \text{K}^{-1}$                |
| $h_{tp}$         | boiling heat transfer coefficient | $\text{W cm}^{-2} \text{K}^{-1}$                |
| $I$              | electric current                  | <b>Amp</b>                                      |
| $L_h$            | heated length                     | $\text{M}$                                      |
| $\hat{n}$        | unit normal vector                | -   |
| $\dot{m}$        | mass flow rate                    | $\text{kg s}^{-1}$                              |
| $p$              | pressure                          | <b>Pa</b>                                       |
| $P$              | power                             | $\text{W}$                                      |
| $R$              | resistance                        | $\Omega$  |
| $x_e$            | exit mass quality                 | -   |
| $q''$            | heat flux                         | $\text{W cm}^{-2}$                              |
| $\dot{q}$        | volumetric heat generation        | $\text{W m}^{-3}$                               |
| $\dot{Q}_{loss}$ | heat loss                         | $\text{W}$                                      |
| $T_{diss}$       | dissociation temperature          | $^\circ\text{C}$                                |
| $T_h$            | heating temperature of monomer    | $^\circ\text{C}$                                |
| $T_i$            | inlet temperature                 |   |
| $T_{sat}$        | saturation temperature            | $^\circ\text{C}$                                |
| $T_{w,i}$        | inner wall temperature            | $^\circ\text{C}$                                |
| $T_{w,o}$        | outer wall temperature            | $^\circ\text{C}$                                |

| <b>Subscript</b> | <b>Description</b>  | <b>Units</b> |
|------------------|---------------------|--------------|
| <i>atm</i>       | atmospheric         | -            |
| <i>CHF</i>       | critical heat flux  | -            |
| <i>e</i>         | exit                | -            |
| <i>elec</i>      | electric            | -            |
| <i>h</i>         | heated              | -            |
| <i>i</i>         | inlet, inner        | -            |
| <i>m</i>         | mechanical          | -            |
| <i>sat</i>       | value at saturation | -            |
| <i>w</i>         | wall                | -            |

| <b>Greek Symbols</b> | <b>Description</b>  | <b>Units</b>            |
|----------------------|---------------------|-------------------------|
| $\delta$             | stress              | <b>Pa</b>               |
| $\nu$                | kinematic Viscosity | <b>kg/ms</b>            |
| $\mu$                | dynamic Viscosity   | <b>m<sup>2</sup>/s</b>  |
| $\rho$               | density             | <b>kg/m<sup>3</sup></b> |

# CHAPTER 1

## INTRODUCTION

### 1.1 Objectives and Major Challenges of This Work

The proposed thesis aims to make a contribution to the literature in the field of energy efficient miniature devices for energy harvesting, thermal management and biomedical applications.

In the first part, the objective is to design a miniature power reclamation device based on external liquid flows are represented. The device's reclamation principle depends on the conversion of mechanical energy into electrical energy. The mechanical energy in the device will be generated by capturing vibrations caused by external liquid flows via the device's tails, which should be designed by taking inspiration from the body shape of the black ghost knife fish, *apteronotus albifrons*. The reclaimed power will be obtained through magnetic polarization, which will be generated by rotating circular waterproof magnet structures as a result of rotating movements of the mentioned tails and is transferred to 3.76 V (Ni-Mg) batteries. The second objective is to simulate power reclamation using COMSOL 4.2 software in order to compare the maximum reclaimable theoretical energy harvesting capacity to the experimental results. The potential of this device will be revealed for the use in applications such as in lighting and GPS (Global positioning system) devices.

In the second part of the thesis, the main objective is to investigate flow boiling in mini/micro channels with surface enhancements provided by crosslinked polyhydroxyethylmethacrylate (pHEMA) coatings, which will be used as a crosslinker coating type with different thicknesses (~50 nm, 100 nm and 150 nm) on inner microtube walls. Flow boiling heat transfer experiments will be conducted on microtubes (with inner diameters of 249  $\mu\text{m}$ , 507  $\mu\text{m}$  and 908  $\mu\text{m}$ ) coated with crosslinked pHEMA coatings. pHEMA nanofilms will be deposited with initiated chemical vapor deposition (iCVD) technique. De-ionized water will be utilized as the working fluid in this study. Experimental results obtained from coated



microtubes will be compared to their plain surface counterparts at two different mass fluxes (5,000 kg/m<sup>2</sup>s and 20,000 kg/m<sup>2</sup>s), and potential enhancements in Critical Heat Flux and boiling heat transfer will be reported.

In the third part, the objective is to develop an energy efficient platform for gene delivery via magnetic actuation of nanoparticles. The use of PEI-SPION (Super Paramagnetic Iron Oxide Nanoparticles) as transfection agents in in-vitro studies will be investigated with the effect of varying magnetic fields provided by a special magnetic system design, which will be used as miniature magnetic actuator device offering different magnet's turn speeds and directions in the system. Experimental results to be obtained from experimental magnetic actuator systems were compared to the experiments without magnetic actuation, and potential enhancements in transfection efficiency in MCF-7 and PC-3 cells will be reported.

## **1.2 Literature Survey of Miniature Energy Harvesting Device Using External Fluid Flows (First Part)**

Energy harvesting has become an attractive research topic during the last decade. As a natural consequence, the number of studies has been continuously increasing to attain higher power reclamation efficiencies from energy harvesting devices. As indicated in the history of energy harvesting devices, the first experiment was conducted in 1826. In this study, it was found that usage of two dissimilar metals resulted in current flow in a close circuit when they were kept at different temperatures [1]. The principle of generating electric current from magnetism was discovered in 1831. The underlying phenomenon is known as electromagnetic induction [2, 3]. In the same year, direct current generator, which consisted of copper plates rotating between magnetic poles, was discovered by Faraday [4].

The studies about miniature power harvesting devices have a broad range of approaches varying from micro electret power generators to combustion-based thermo electric power generators. Wang et al. [5] developed a piezoelectric energy harvesting device to generate energy from flow-induced vibrations. The device's principle is based on conversion of flow energy into electrical energy via piezoelectric films. The authors obtained an output voltage of 2.2 volts and 0.2 $\mu$ W maximum outlet power for a vibration frequency of 26 Hz. Their results showed that high power outputs could be reached with small vibrations. Matteo et al. [6] studied submerged ionic polymer metal composites (IPMCs). They modelled a framework

to estimate energy harvesting capability of IPMCs as a function of excitation frequency range, electric shunting load and geometrical properties of IPMCs. They treated mechanical vibrations of IPMC strips with Kirchhoff-Love plate theory and claimed that electric shunting impedance should be identical with IPMC impedance in order to obtain the maximum outlet power. According to their experiments for frequency ranges of 2-50 Hz, maximum outlet power was recorded as 1nW. Hobbs and Hu [7] investigated micro energy harvesters inspired by tree trunks swaying in the wind. They used four piezoelectric energy transducers with attached cylinders to study the effects of cylinder space, flow speed and cylinder position. The maximum power outlet was 55 $\mu$ W from four energy transducers, when the flow speed was the maximum, and cylinder spacing was adequately large for Karman vortices. Song et al. [8] conducted an experimental investigation to study conversion of mechanical energy into electrical energy in nanoscale by using a single piezoelectric ZnO wire and belt. They claimed that it was possible to harvest energy without external power via self-powering nanodevices by mechanical movements or vibrational energy sources. They obtained approximately 4mV as the maximum output power from a bent wire. Howells [9] provided proof-of-concept Heel Strike units as a small electric generator, which operated piezoelectric elements to convert oscillatory mechanical energy into electrical energy. According the author, walking motion of a human body could be a source for required mechanical energy to generate electricity. The Heel Strike system had 0.5 W power output with 5A – 50mV shunt resistor and could provide power to a variety communication devices such as cellular phones. Tang et al. [10] studied energy transfer and the concept of flutter mill on cantilevered flexible plates in axial flows. They found that energy could be continuously pumped into the plate from circulating fluid flows if the plate loses its stability at a sufficient flow velocity. Hence, the vibration may be used as an energy source. The dimensions of their flutter mill were 0.58m x 0.2m x 0.58m (length / height / width), and it had a mass ratio of 0.5, while the plate width was 0.2m. According to their analytical results, they expected 10W outlet power. However, only 10 % of wind energy was extracted to electrical energy during their experiments. Akaydin et al. [11] studied piezoelectric generators for energy harvesting capability under unsteady and turbulent fluid flow conditions. The maximum output power of their piezoelectric generator could be obtained, when fluid flow's predominant frequency was identical with natural frequency of piezoelectric generators. The location of the generator directly affected output voltage. In their experimental results, the maximum obtained output power was 4 $\mu$ W, when flow speed was 7.23 m/s, and load resistor was 100k $\Omega$ . Giacomello and Porfiri [12] studied underwater energy harvesting from the instability of a heavy flag via

ionic polymer metal composites (IPMCs). They investigated the relationship between vibration frequency and mean flow speed by attaching IPMCs to the host flag and connecting to an external load varying from 0.1 to 100k $\Omega$ . Their maximum output power was ~10W, when the external load was 10k $\Omega$ . Vanderpool et al. [13] examined the conversation between waste heat and electricity via pyroelectric materials. They simulated a pyroelectric converter using the Finite Elements Method (FEM). They found that energy efficiency could be increased, when the density and specific heat of the working fluid and pyroelectrical material decreased. According to their theoretical investigation, the highest energy efficiency was 40 %. Boland et al. [14] studied the performance of the first micro machined rotational electret power generator. It was suggested that the device could rely on a linearized model of electret power generation. The device consisted of a high-temperature silicon-germanium thermopile and was successfully tested. Muselli et al. [15] investigated the design of a hybrid-photovoltaic power generator, which aimed at the optimization of energy management. With this approach, photovoltaic combined hybrid wave generator could be generated. Taylor et al. [16] introduced a subsurface ocean power generator, which used piezoelectric polymers submerged in oceans to convert flow energy into electrical power. In the work of Kulah and Najafi [17], an electromagnetic micro power generator was introduced, which converted energy of low frequency to higher frequencies so that generators could turn faster with high water speed at a high frequency. Wiegele [18] emphasized on the design and fabrication of a micro-turbo-generator. This study involved one of the pioneering designs of 3D structures. Tsutsumino et al. [19] indicated that the development of a micro electret power generator would be helpful in energy harvesting applications since efficiency could be increased up to 70 % with this approach. Jeon et al. [20] presented an electret-based electrostatic micro-generator, which could resonate at specific frequencies from an external vibration energy source, thereby creating electrical energy via the piezoelectric effect. Soderlund et al. [21] studied a wind power generator for the need of a gearless construction of a wind energy conversion system, which had advantageous features such as less power loss due to fewer used materials. Sarı et al. [22] introduced an electro-magnetic power generator, which generated electrical energy from vibrations. This power generator's working principle was based on the predetermined frequency range (50 to 70 Hz). Yang et al. [23] developed micro thermo photovoltaic power generators, which had the potential of replacing batteries in micromechanical devices. Besides these inventions, Büren and Tröster [24] designed an electromagnetic micro-power generator, which supplied power sensor nodes worn on the body. Williams et al. [25] presented an electromagnetic power generator of 50 mm-scale. The

most important feature of device was the capability of energy harvesting in small scale. The study could be a model for further scale improvements of such miniature devices. White et al. [26] worked on a novel thick-film piezoelectric micro-generator, which was an advanced example of a thick film piezoelectric device able to enhance surface wettability, conductivity, and also scaling effects. Mahmoud et al. [27] focused on low cost and low power losses while introducing a planar electret based micro generator. Beeby et al. [28] introduced a micro machined silicon generator, which used vibrations as the input source. Arakawa and Suzuki [29] presented a solution for increasing power consumption demand of portable electronic devices using a micro seismic power generator based on electret polymer films. Glatz et al. [30] studied the optimization of thick and flexible polymer based thermoelectric micro generator with flat surfaces. Mechanical operations with thick film piezoelectric materials have advantages such as increasing power gain due to lowering power losses. Jacquot et al. [31] designed an in-plane thermoelectric micro generator, which had fine-grained polycrystalline silicon as the active material. Jones et al. [32] used tandem wings and oscillating-wing for micro-hydropower generators. Toriyama et al. [33] investigated a thermoelectric micro power generator in poly silicon-metal. Such thermoelectric materials could be useful for energy harvesting devices, where temperature compatibility is needed. Kwon et al. [34] investigated energy harvesting systems using RED (reverse electro dialysis) with nanoporous polycarbonate track-etch membranes. The authors conducted an experimental study on RED-based energy harvesting system, which converted electrical energy from the concentration gradient between seawater and fresh water. The results indicated that the maximum voltage nonlinearly depended on the concentration difference. Okamoto et al. [35] studied electret-based vibration-driven micro energy harvesters to produce electricity from a vibrating environment via small electronic devices involving electromagnetic methods and piezoelectric materials. The authors indicated that electrostatic methods could be more precise at small scales compared to electro-magnetic methods since the latter could require low resistivity materials at small scale. Danielsson et al. [36] conducted an experimental study on a directly coupled longitudinal flux-type linear permanent magnet generator for wave energy converters. The authors used a combined field and circuit model, which was solved by a time stepping finite element technique for the simulation of armature current level, number of cables per slot and pole width for efficiency, generator size and load angle. The results showed that the generator could provide 10 kW outlet power with a constant piston speed of 0.7 m/s.

In the recent literature, the importance of alternative energy sources is emphasized. One of the most important aims is to design miniature energy harvesting devices, which use natural sources such as water. On the other hand, such devices should be small and have reduced weight. In an attempt to address to the need for these devices, a miniature energy harvesting device was designed in this thesis. Compared to above mentioned devices in the literature, it has an advantage of reduced costs since the materials used in this device are cheap compared to other devices involving piezoelectric materials. Moreover, it does not require any external power in contrast to common energy harvesting devices such the ones involving piezoelectric materials. The current design would be able to run a typical daily device at harsh environmental conditions. After considering many alternatives, we were inspired by the Black Ghost Night Fish and decided on the size and geometry of the device based on this example. The dimensions are chosen in such a way that reasonable output powers could be obtained to operate daily used devices. It was also made sure that the tails have a similar geometry compared to the Black Ghost Night Fish, which enables them to capture vibrations caused by external fluid flows. In this work, experimental results related to energy harvesting capability of a miniature power reclamation device based on external fluid flows are represented. A miniature power harvesting device is designed and analysed in detail its capacity for a range of flow velocities (1.0 m/s ~ 5.0 m/s) at various fluid densities, i.e. in plain water, low-salinity water (with salt concentration of 150 gr per 1000 ml water) and high-salinity water (with salt concentration of 350 gr per 1000 ml water). A series of experimental data related to the power reclamation capability of the device are obtained. The maximum reclaimable power was simulated using COMSOL 4.2 software and compared to the values obtained from the experiments.

### **1.3 Literature Survey of Miniature System for Flow Boiling Enhancement in Microtubes with Crosslinked pHEMA Coatings (Second Part)**

A wide spectrum of micro scale flow boiling applications encourages researchers to study boiling heat transfer mechanisms in micro scale. As a result, many studies related to microscale boiling heat transfer are now available in the literature [37-48]. One of the most significant issues in boiling heat transfer is Critical Heat Flux (CHF) threatening the uniformity of the system. If the CHF condition is reached, unwanted results such as sudden

worsening of heat transfer between heating wall and coolant fluid, sharp decrease in heat transfer coefficient, and physical and chemical damage to the surface (fouling, fracture, etc.) appears, which might be dangerous for the safety of the system [49].

In the literature, extensive research for extending CHF has been conducted by means of micro/nano scale surface enhancements and modification techniques [50-65]. Hwang et al. [50] investigated the effects of uniform porous coatings on CHF enhancement. Copper particles, whose diameters were 40 and 80  $\mu\text{m}$ , were used as coatings with different thicknesses (3 and 5 particle diameters), which significantly increased CHF (about 80 %). Sarwar et al. [51] provided  $\text{Al}_2\text{O}_3$  microporous coatings with particles having sizes smaller than 10  $\mu\text{m}$  and coating thicknesses of 50  $\mu\text{m}$ . A 25 % increase in CHF was obtained. Khanikar et al. [52] utilized carbon nanotubes (CNTs) coatings onto rectangular microtubes to obtain CHF enhancement. The results indicated that CNT coating was a strong alternative for enhancing the boiling curve. Nevertheless, repetitions of tests resulted in damage in CNTs' morphology so that CHF enhancement lost its effect with increasing number of tests. Jeaong et al. [53] used surfactant solutions (tri-sodium phosphate (TSP,  $\text{Na}_3\text{PO}_4 \cdot 12\text{H}_2\text{O}$ )) for surface modification. CHF enhancement was tested at various mass fluxes (100-500  $\text{kg/m}^2\text{s}$ ), and a 48 % increase in CHF was obtained. Kim et al. [54] used different nanoparticles ( $\text{TiO}_2$ ,  $\text{Al}_2\text{O}_3$  and  $\text{SiO}_2$ ) to investigate the flow boiling CHF of aqueous nanofluids. The experiments indicated that CHF was increased when nanoparticles were included in the working fluid. The main reason for CHF enhancement in nanofluids was observed to be nanoparticle deposition after the experiments. In other words, nanoparticles in nanofluids were deposited to the heater surface, and the resulting nanoparticle coating on heater surface altered the surface properties such as surface wettability, surface roughness and maximum capillary wicking height. Şeşen et al. [55] investigated pool boiling on a plate having a planar copper thin film coated on a silicon wafer surface, on which an array of copper nanorods with an average diameter  $\sim 100$  nm and length  $\sim 500$  nm was integrated. They found that using nanostructured surfaces can have the potential to be an effective method of device cooling for small and excessive heat generating microsystem applications due to a significant increase in boiling heat transfer (more than 100 %). For studying the effect of nano-fluids on CHF enhancement, Kim et al. [56] tried to improve CHF by using  $\text{Al}_2\text{O}_3$  nanoparticle based nano-fluids. CHF of  $\text{Al}_2\text{O}_3$  nanoparticle based nano-fluids was greater than CHF of the pure based fluid (up to 70 % increase). To observe the effects of graphene/graphene-oxide nanosheets, Park et al. [57] used graphene/graphene-oxide nanosheets as an additive in nanofluids. The experiments

showed that these nanosheets extended boiling curves. Interestingly, the reason was attributed to neither improved surface wettability nor the capillarity of the nanoparticles deposition layer. This increase was explained by formation of self-porous surface structure of graphene/graphene-oxide nanosheets. Forrest et al. [58] accomplished silica nanoparticle thin film coatings on nickel wire. The experiments showed that coating the nickel wire with silica nanoparticles was a successful method for enhancing CHF (up to 100 %). Surface characterization results indicated that surface wettability was drastically altered with the addition of silica nanoparticles, and CHF was positively affected by this surface modification. Morshed et al. [59] conducted their experiments with copper nanowire (CuNW) coatings on microtubes with a hydraulic diameter of 672  $\mu\text{m}$ . Nanowires on the bottom surface of the microtube were deposited by using the electrochemical deposition technique. Boiling heat transfer experiments at various mass fluxes and subcooling showed that the coating of CuNW in microtubes improved boiling heat transfer coefficient up to ~56 %. For observing the effect of surface wettability on CHF, Phan et al. [60] prepared silicon oxide (SiO), titanium (Ti), diamond-like carbon (DLC), and carbon-doped silicon oxide (SiOC) surfaces, whose static contact angles were 26°, 49°, 63°, and 104° in a single rectangular channel having a height of 0.5 mm, a width of 5 mm and a length of 180 mm, respectively. The experiments conducted at the mass flux of 100  $\text{kg/m}^2\text{s}$  indicated that extended boiling curves could be obtained from surfaces, which had lower static contact angles. Ahn et al. [61] used zircaloy-4 micro/nano structures to enhance CHF under different experimental conditions. Their results indicated that CHF in the annular flow regime might be significantly enhanced by high wettability of zircaloy-4 micro/nanostructures because of the increase in stability of the liquid film and better liquid replenishment as the mass flux increased. Betz et al. [62] investigated pool boiling on surfaces with various wettabilities (from superhydrophobic to superhydrophilic). They found that the highest heat transfer coefficients were reached on uniform surfaces with hydrophilic regions due to high wettability. Saeidi et al. [63] investigated the effect of nanostructured surfaces on pool boiling by utilizing chromic acid and sulphuric acid solutions on aluminium. They found that critical heat flux could be increased by 8 % compared to the untreated aluminium alloy surface. Moreover, boiling heat transfer coefficients were increased by 159 % in weakly etched samples. Tang et al. [64] examined nucleate pool boiling heat transfer performance of a nanoporous copper surface fabricated by the facile hot-dip galvanizing process. They observed that the nanostructured surface reduced wall superheat and increased heat transfer coefficient compared to the unstructured surface at low heat flux conditions. Yongwei et al. [65] investigated pool boiling

on coated surfaces in deionized water and saturated calcium carbonate solution. They found that pool boiling enhancement was observed with thinner nanoscale hydrophobic Titania-Fluoroalkylsilane composite films at higher heat fluxes compared to the thicker coating on stainless steel surfaces.

Encouraged by the abovementioned results with nanostructures and nanofilms deposited on various surfaces in boiling heat transfer, this experimental study examines a new technique for delaying DNB type critical heat flux conditions and increasing subcooled boiling heat transfer in microtubes. In this study, crosslinked pHEMA (polyhydroxyethylmethacrylate) nanofilm coating, which is a type of hydrogels in aqueous medium, was applied to the inner walls of microtubes. pHEMA coating deposition is an important alternative method for enhancing the surface of microtubes/tubes. pHEMA could be coated with iCVD method, which is a simple to use, efficient, cheap, and uniform coating method, and is independent of surface shape. Furthermore, iCVD is the most suitable deposition technique for closed geometries such as microtubes, where physical deposition methods could not be implementable. In this study, the effect of thickness of swellable polymer crosslinked pHEMA coatings on CHF and boiling heat transfer enhancement was studied. The experiments were performed at two different mass fluxes, (5,000 kg/m<sup>2</sup>s to 20,000 kg/m<sup>2</sup>s). Crosslinked pHEMA was deposited on microtubes, whose inner diameters were 249 μm, 507 μm and 908 μm. The pHEMA coating thicknesses were ~50 nm, 100 nm and 150 nm, respectively.

#### **1.4 Literature Survey of Miniature Magnetic Actuator for Targeted Gene Delivery of Nucleic Acid Based Molecules (Third Part)**

Magnetofection is a basic and very efficient transfection technique, which occupies magnetic fields to concentrate particles containing nucleic acid into the target genes and cells. A wide spectrum of targeted gene delivery via magnetofection encourages researchers to study magnetic actuation effect. As a result, many studies related to gene delivery of nucleic acid-based are now available in the literature [66-97].

Scherer et al. [66] coupled gene vectors with super-paramagnetic nanoparticles and targeted gene delivery by application of magnetic field to overcome low efficiencies of non-viral gene



vectors. The duration of gene delivery was significantly decreased to minutes host tropism of adenoviral vectors to non-permissive cells were extended, and low retroviral titer was compensated. Moreover, they observed high transduction efficiencies in in-vitro test, which are reproduced with magnetic field-guided local transfection in the gastrointestinal tract and in blood vessels since magnetofection offers utilized tool for high throughput gene monitoring in vitro and may help to challenge obstructions in gene therapy in vivo. Lin et al. [67] studied in vitro gene delivery improvement by electrostatic forces and electroporation (EP) microchips. The authors revealed that the plasmid DNA could be magnetized to cell surfaces at unique regions using an electrostatic force since the cell could be manipulated in situ without detachment if adherent cell were used for electroporation. Bystrzejewski et al. [68] studied the synthesis of arc plasma of carbon-encapsulated FeNdB nanocrystallites in their experimental study. The authors found that simple magnetic nanoparticles such as Fe and Co may not be suitable for applications of biosensors fabrication because they may reduce sensor working efficiency due to the high potential of aggregation. In contrast to simple magnetic NPs, synthesized FeNdB NPs have no tendency to aggregate, high magnetization and signal noise ratio especially for biomedical investigations. Dobson [69] attached therapeutic and reporter genes to biocompatible magnetic nanoparticles to investigate non-viral transfection agents for gene delivery for in vitro and in vivo transfection via magnetofection. The experiments showed that magnetofection method provides rapid transfection and perfect transfection levels. Kopke et al. [70] investigated superparamagnetic iron oxide nanoparticles (SNPs) (consisted with magnetite ( $\text{Fe}_3\text{O}_4$ )) for the transportation of therapeutic molecules to the inner ear. The authors aimed to make middle ear implant capable to produce biomechanically relevant forces and provide auditory function by using SNPs. Oleic acid and dextran coated magnetite SNPs were covered with silica and polymer materials (such as D, L,-Lactide-co-glycolide) and resulted in generation of adequate forces to pull them across tissue in windows membrane models (in vitro culture, in vivo rat, guinea pig and human temporal bone). Huang et al. [71] developed an innovative electroporation (EP) system, which was designed according to magnetofection principle (use of magnetic nanoparticles-gene vectors) and has an EP microchip, which was combined with electrophoresis (ES), to make site-specific improvements of gene concentration. The authors used Lab on a chip to manipulate adherent cells in situ without detachment of the ES-EP microchip. The gene transfection efficiency was obtained as ~35.89 % by applying attracting electromagnetic field, while the efficiency was ~16.16 % in the absence of electromagnetic field. Hu et al. [72] investigated iron oxide/silica core-shell nanoparticles, which were

synthesized via self-assembled polyvinyl alcohol and those particles were actuated by a magnetic stimulus to release therapeutic agents. The results indicated that under high frequency of magnetic fields, the iron oxide/silica nanoparticles can be released by the magnet-induced heating and mechanical motion in the burst-like release of drug molecules. Gazeau et al. [73] indicated that therapeutic tools in nanoscale could be utilized for treatment of therapeutic hyperthermia and could meet requirements of future medicine as spatial targeting drug delivery and temporal control of therapy. Fung et al. [74] used electrodeposited ferromagnetic nickel nanowires to investigate efficiency of cellular internalization into 3T3 fibroblasts. The authors concluded that magnetic nanowires have great potential as therapeutic and interrogative platforms for medicine since agitation of the nanowires under low external magnetic field resulted in cell death, and the interleukin-6 (IL-6) gene expression of the fibroblast into nanowire encapsulated cellular manipulation was successfully examined by quantitative real-time polymerase chain reaction (qRT-PCR). Lee et al. [75] used magnetic nanoparticles covalently linked to siRNAs, which target cyclic Arg-Gly-Asp (RGD) peptides together with fluorescent dyes to make simultaneous delivery and multimodal imaging. The authors combined those siRNA molecules to the surface of nanoparticles with disulphide bonds and demonstrated that the nanoparticles were selectively internalized to target cells by integrin receptor-mediated endocytosis. Moreover, target-cell-specific gene silencing could be possible by releasing intact siRNA molecules through cleavage of disulphide bonds. Namiki et al. [76] investigated conjugation of magnetically guided in vitro and in vivo gene delivery using an assembly (termed LipoMag), which contained a magnetic core with a cationic lipid shell. The authors prepared LipoMag as phospholipids absorbed onto the inner hydrophobic acid layer via hydrophobic interactions and optimized gene silencing efficiency in different cells along with magnetic crystal-lipid formulation at several molar ratios of various lipids. Stride et al. [77] investigated enhancement of microbubble mediated gene delivery by simultaneous exposure to ultrasonic and magnetic fields to demonstrate whether it was possible to benefit the advantages of those techniques. The results indicated that the transfection of Chinese hamster ovary cells with naked plasmid DNA was significantly enhanced due to simultaneous exposure of the cell by ultrasound (10 s at 1 kHz pulse repetition frequency with 40 cycle 1 MHz sinusoidal pulses and 1 MPa peak to peak pressure) and magnetic field (cross-section of five square with N52 grade NdFeB magnets having 25 x 10 x 10 mm dimensions and transversal magnetization of 1.50 T arranged in Halbach array). Sajja et al. [78] studied enhancement of nanoparticles to enable and improve targeted delivery of therapeutic agents and the development of novel and

effective diagnostic and monitoring techniques to expand obstructions of molecular diagnostic providing point-of-care diagnosis. The authors demonstrated that an increase in efficiency of lower doses of drug and cancer cell destruction could be achieved by selective targeting of unique surface signatures of tumour cells, and nanotyping for clinical oncology is essential to predict cancer behaviour. Dave et al. [79] investigated biocompatible magnetic NPs180 (nanoparticles 180) to find an alternative non-viral delivery vehicle. The authors proved that the genetic material could be physically adsorbed or chemically conjugated to a magnetic nanoparticle, which was covered with transfection improved polymers. Magnetofection was the magnetic field gradient across the cell, and generated a kind of physical force on magnetically responsive nanoparticles. The results indicated that elimination of normally diffusion-limited localization of gene delivery agents to the targeted cell could provide reduction in sedimentation time and increase net transfection efficiency by various orders of magnitude. Kim et al. [80] inspected biofunctionalized magnetic-vortex microdiscs for targeted cancer-cell destruction. Microdiscs were made with lithography and have a spin-vortex ground state. It was found that spin-vortex mediated stimuli have advantages on compromised integrity of the cellular membrane and triggering programmed cell death. Moreover, the authors achieved 90 % cancer-cell destruction in vitro by applying low-frequency magnetic field of few tens of hertz when it was applied 10 minutes. Barakat [81] studied magnetically modulated nanosystems for a special drug-delivery platform by using magnetic nanoparticles having sizes ranging from 1 $\mu$ m to 10 $\mu$ m. The author stated that magnetic nanoparticles could be a perfect candidate for biomedical applications, and could be magnetically controlled by applying an external magnetic field. They have potential in cell separation, automated DNA extraction, gene targeting, drug delivery, MRI and hyperthermia. Besides, magnetic nanoparticles could be used in highly sensitive immunoassays and small substance recoveries if they are coated with appropriate materials. Veisheh [82] and Singh et al. [83] stated that the covalent bond of siRNA through magnetic nanoparticles via thioester links (not labile to protein) prevents siRNA degradation for the period of circulation in the bloodstream. Therefore, combining siRNA and nanoparticles using non-labile cross-linkers could make nanoparticles more stable. Amstad et al. [84] claimed that the ideal nanoscale drug delivery vehicle could allow control over the released dose in space and time by using stealth liposomes containing self-assembled super paramagnetic iron oxide nanoparticles (NPs), which were stabilized with palmityl-nitroDOPA along with the lipid membrane. The authors demonstrated that alternating magnetic fields could be manipulated for control in timing and dose of released delivery from vesicles. Gao et al. [85] described directed delivery

of drug-loaded magnetic polymeric particles using magnetically driven flexible nanoswimmers for the first time. According to their experimental results, flexible magnetic nickel-silver nanoswimmers having 5-6  $\mu\text{m}$  length and 200 nm diameters could actuate microsize particles at very high speeds ( $\sim 10 \mu\text{m s}^{-1}$ ). Mok and Zhang [86] investigated superparamagnetic iron oxide nanoparticle-based delivery systems for biotherapeutics and found that those systems have significant advantages on high target specificity, low adverse effects, high stability and increased efficiency compared to regular chemical drugs. Moreover, the authors reported that SPION-based materials could be used for developing such systems because they offer high biocompatibility and superparamagnetism, which provide long-term accumulation at target gene. Kim et al. [87] examined magnetic nanocomplexes and physiological challenges for cancer imaging and therapy. The results indicated that magnetic nanoparticles can provide a variety of drug delivery and imaging strategies together with modalities like magnetic hyperthermia when they are conjugated with bioactive molecules. The authors stated that more effective cancer therapies could be achieved via imaging with magnetic nanoparticles. Cohen and Shoushan [88] conducted research on magnetic nanoparticle based diagnostics and theranostics and summarized some of the recent progress in the synthesis and functionalization of MNPs (magnetic nanoparticles). The authors claimed that MNPs could be perfect scaffolds for loading targeting moieties, imaging drugs and inducing therapeutic effects, which makes them useful tools. Bao et al. [89] studied multifunctional magnetic nanoparticles for drug delivery and molecular imaging. The authors indicated that these nanoparticles through nanocrystalline synthesis have significant potential for providing contrast for different imaging modalities and targeted delivery of drug/gene and thermal therapies. In addition, multifunctional nanoparticles are excellent candidates in emerging medical fields such as multimodal imaging, theranostics and image-guided therapies. Hu et al. [90] investigated the use of functionalized magnetic nanoparticles to develop hBMSC differentiation as a target to a smooth muscle cell lineage via direct mechanical stimulation of platelet-derived growth factor receptor  $\alpha$  and  $\beta$  (PDGFR $\alpha$  and  $\beta$ ) by exposing to time-varying magnetic fields. According to conducted experiments on magneto-mechanical stimulation of PDGFR $\alpha$  in 3 hour period, up-regulation of smooth muscle resulted in  $\alpha$ -actin generation in both protein and mRNA levels. The authors verified that remote control concept could be utilized for locally-delivered mechanically induced differentiation of hBks. Subramanian et al. [91] inspected enhanced nanomagnetic gene transfection of human prenatal cardiac progenitor cells and adult cardiomyocytes and demonstrated that oscillating magnet array-based

nanomagnetic transfection could dramatically increase transfection efficiency in investigated cells when compared to static magnetofection. Moreover, the authors observed improved efficiency (up to 49 %) of adult cardiomyocytes transfection by seeding the cells onto Collagen I-coated plates with 24 % lipid reagents and 19 % electroporation. Lim et al. [92] investigated delivery of cancer therapeutics by nanotechnology and indicated advantageous features of nanoparticles as various formulations for organic/inorganic materials, simple modification of targeting molecules, efficient delivery to target sites and easy control of drug release via external and internal stimuli. For these reasons, the authors claimed that theranostics nanoparticles could be improved by incorporating imaging agents in drug carrier applications. Puri [93] inspected iron oxide magnetic nanoparticles in various mediums. The author found that those nanoparticles could offer magnetic manoeuvrability, easy control ability of transfection, biochemical surface functionalization and magnetic relaxation in ferrofluids and magnetic microspheres if some important properties such as particles, forces and scalar transport at different length scales are optimized. Du et al. [94] worked on biocompatible magnetic and molecular dual-targeting polyelectrolyte hybrid hollow microspheres for controlled drug release. The authors fabricated hybrid shell by electrostatic interaction between polyelectrolyte chitosan (CS) and citrate to modify ferroferric oxide nanoparticles ( $\text{Fe}_3\text{O}_4\text{-CA}$ ) toward the uniform polystyrene sulfonate microsphere templates. The dual targeting hybrid hollow microspheres showed exciting pH response and stability in high salt-concentration medium. The results demonstrated that the cell viability of the HepG2 cells decreased more quickly when they were treated by the FA in in vitro studies. Yim et al. [95] described a new device, which proposes a wireless biopsy method, where a magnetically actuated untethered soft capsule endoscope (MASCE) transports and releases a significant number of thermo-sensitive, untethered micro-grippers toward a desired target inside stomach and tissues. The device has excellent potential for multi-functional strategy for gastrointestinal capsule biopsy parallel autonomous and sub-millimeter scale tissue sampling.

Encouraged by the above mentioned results with targeted gene delivery methods and magnetic actuation effects on various cells, this work examines a new targeted gene delivery technique for nucleic acid-based molecules. A platform for gene delivery via magnetic actuation of nanoparticles was improved. The use of PEI-SPION (Super paramagnetic iron oxide nanoparticles) as transfection agents in in vitro studies was investigated with the effect of varying magnetic fields provided by a special magnetic system design, which was used as magnetic actuator offering different magnet's turn speeds and directions in the system.

Experimental results obtained from experimental magnetic actuator systems were compared to the experiments without magnetic actuation in MCF-7 and PC-3 cells. It is well known that gene therapy is a promising therapeutic method, and many studies have shown its therapeutic potential in treating various diseases, especially in cancer [96], but lack of ideal delivery system is the main obstacle for this method. The development of safe and efficient gene delivery system is still a major challenge for gene therapy, including its main application in cancer gene therapy. The non-viral gene carrier Polyethyleneimine (PEI) contains primary, secondary and tertiary amine, which can bind to both DNA and siRNA. PEI is one of the most widely studied cationic polymers for gene therapy. In addition, PEI can be modified by attaching small molecules, enabling a specific targeting ability [97]. In this study, our aim is to show effects of magnetic field on iron oxide nanoparticles and penetration properties of GFP-plasmid DNA attached PEI-SPION into breast cancer cells to reveal a method for further RNA interference studies.

## **CHAPTER 2**

### **EXPERIMENTAL SETUP AND PROCEDURE**

#### **2.1 Experimental Test Setup of Miniature Energy Harvesting Device Using External Fluid-Flows (First Part)**

##### **2.1.1 Device Overview**

The miniature device was designed in order to accomplish targeted optimal power reclamation and it included cardinal features such as durability, waterproof body, longevity and compatibility for the use under various conditions. Regarding the durability, its body and base were made of Aluminum because of its low density, its capability to resist corrosion, and its strength. Moreover, longevity was crucial for a long operating half-life. Locations, where the device would be placed, might not be easily accessible for all times. Therefore, in order to provide longevity, some components were used to improve the design. Concerning the waterproof characteristics, the Aluminum case was designed to protect the device from humidity, and the tails were made of a waterproof fabric, namely activated carbon fiber cotton. This miniature energy harvesting device is notably small and light and consists of few components. The device's dimensions are 0.13m x 0.04m x 0.6m, while its weight is just 540 gr. Thanks to its compactness; the device could be used in places, which are not easily accessible. As shown in the isometric 3-D view (Fig. 2.1), the device consists of generators, batteries, LCD screen and push button as electronic components. Four laterally positioned fish shaped tails were connected to four mini generators. The power generating mechanism consists of a 3.76 V battery, and mini generators located inside the device box (Fig. 2.2). The batteries were connected in parallel in order to increase the power value at a constant voltage value. The casing and inner structure were made of water-proof elements for protecting the vulnerable electronic components from the ambient fluid.

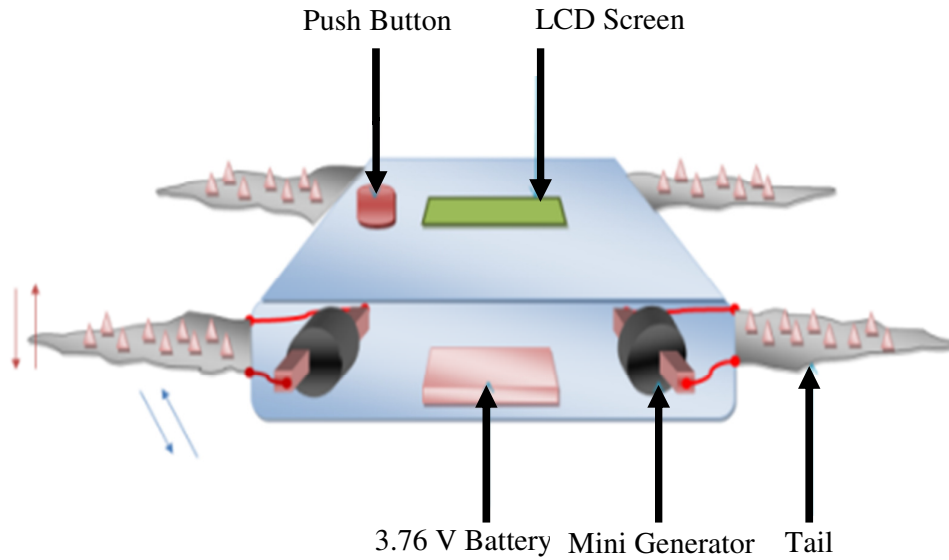


**Figure 2.1:** Isometric view of the power reclamation device

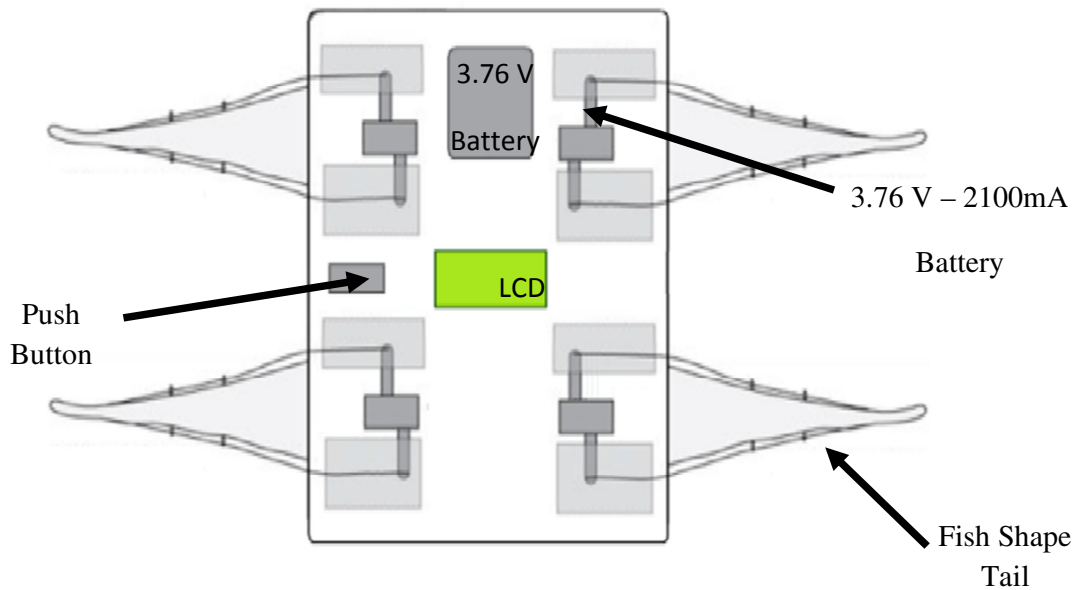


**Figure 2.2:** Schematic of the miniature energy harvesting device including its components

External fluid flow ( $Q$ ) is the main input, whereas power ( $P$ ) is the main output. The tails vibrate as results of external flows and translate energy to the mini generators, which harvest energy due to magnetic polarizations. The generator's output power could be utilized as an electric source to provide power for daily used devices.



### **2.1.2 Tail Design**

The tails of the miniature energy-harvesting device are responsible for capturing vibrations caused by external fluid flows. Because of their significant role, the tails had to be designed carefully. First of all, the tails had to be durable, which was accomplished by the carbon fiber-polyurethane composite tail skeleton (Fig. 2.3). The fiber leaves were integrated into the tail surface. Carbon fiber-polyurethane was chosen because of its capability to offer both strength and reduced weight. Polyurethane is a unique material, which provides high elasticity combined with toughness and durability. The tails are flexible and adjustable as well so that they would adapt to various flow rates.

The design enables the tails to vibrate even at very low displacements due to their surface structure, which generates low friction and enables multi trajectory movements. The tail design offers the conversion of vibration motion into circular motion (edge of the tails are connected to rotors), and the resulting axial movement of magnetic parts generates power. Increased vibration, due to higher flow velocities, causes enhanced power generation. One of the limitations for obtaining power generation is flow speed, which does not always have linear relationship with power. Another limitation is the adaptation of the device to the velocity change, since it is not always possible to obtain power when fluid velocity decreases. Even low frequencies in external flows could lead to power generation. The skeleton structure consists of multi joints and hinges. Each moving component is also flexible by itself.

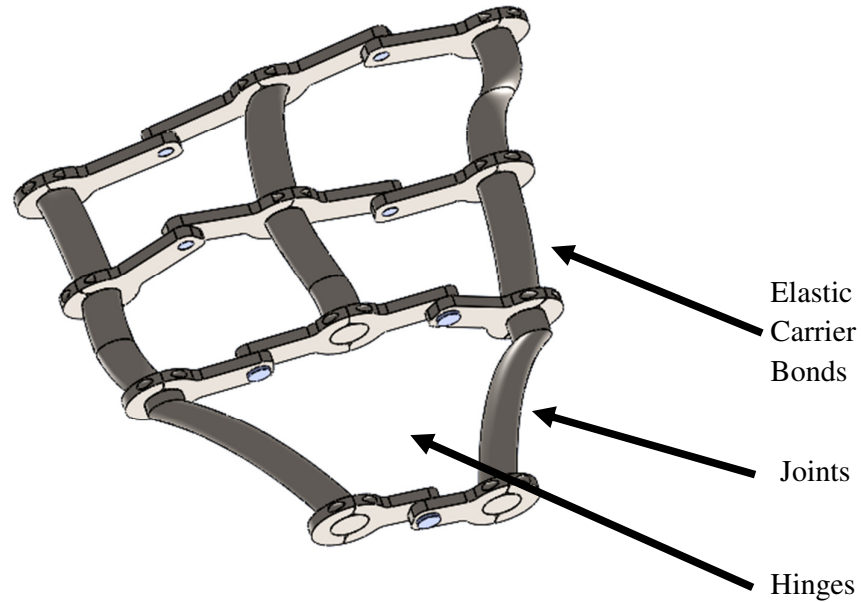


**Figure 2.3:** The design based on skeleton of Black Ghost Night Fish tail

Carbon fibers are combined with materials to form a composite. The surface was made of a composite of carbon fiber leaves and waterproof fabric, which offers low weight, reduced surface friction, high chemical resistance, low thermal expansion and high tensile strength (Fig. 2.4). Regarding the surface, it was also designed by taking inspiration from the Black Ghost Night Fish (*Apteronotus Albifrons*) body surface. The wavy shape offers more agility. Bulges and dents could cause mixing effects along tails while vibrating. Therefore, it enhances power reclamation capability. The tails are shown in detail in Fig. 2.5.

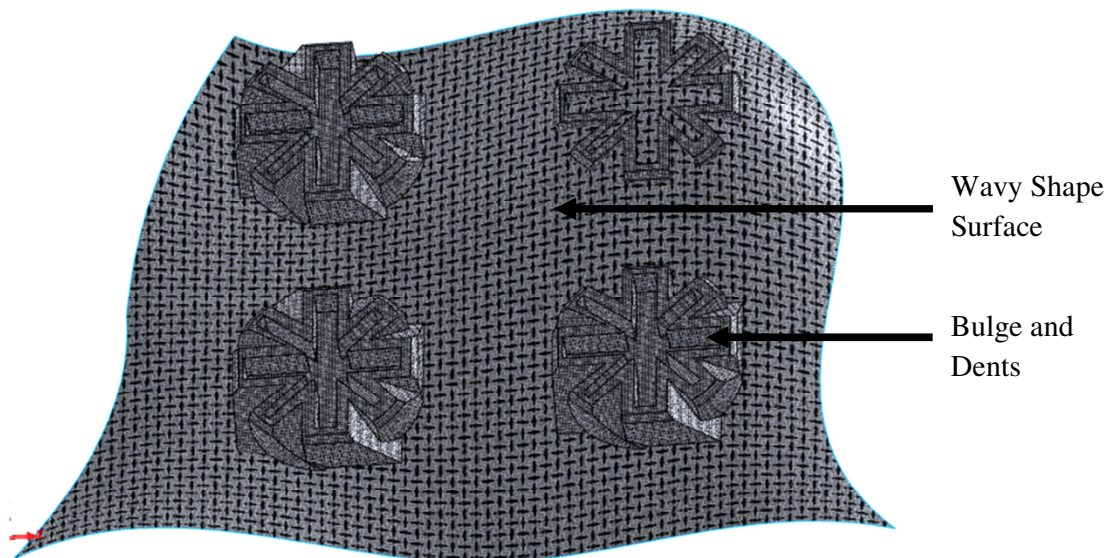


**Figure 2.4:** Surface of the Black Ghost Night Fish Tail Design

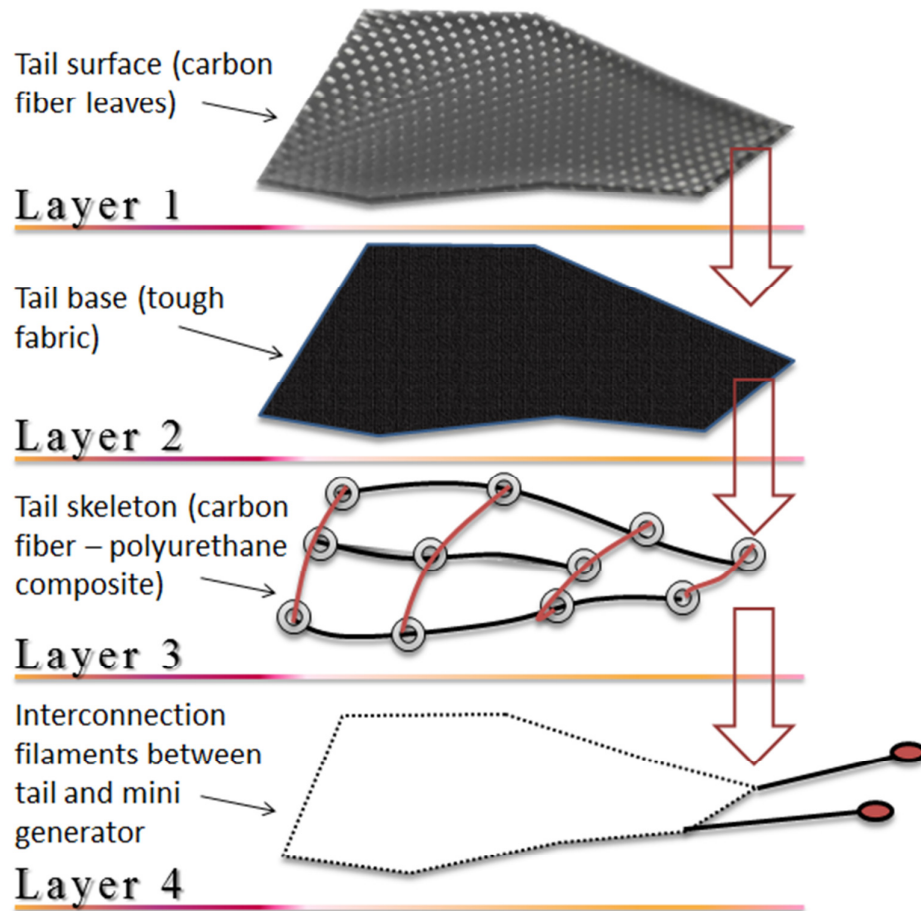


**Figure 2.5:** Illustration of the tail layers of the miniature energy harvesting device

The structure of the generator consists of an electroplate core and copper coils around magnet. The radii of armature, copper coils and mounting pins are  $\sim 2.7\text{cm}$ ,  $2.4\text{cm}$  and  $1.2\text{cm}$  respectively. Each generator has a resistance value due to field coil around spiral magnet. The internal resistance of generator directly affects the measured current and voltage values. Each coil resistance of generator is measured as  $0.81\ \Omega$ . This relatively small resistance value results in obtaining high current values.

## 2.2 Experimental Test Setup of Miniature System for Flow Boiling Enhancement in Microtubes with Crosslinked pHEMA Coatings (Second Part)

The schematic of the miniature device setup is illustrated in Fig. 2.6. The device setup consists of the test section, a storage cylinder, an Omega® flow meter, multiple pressure sensors, thermocouples, and proper tubing and fittings. Figure 2.7 displays the schematic of the test section.

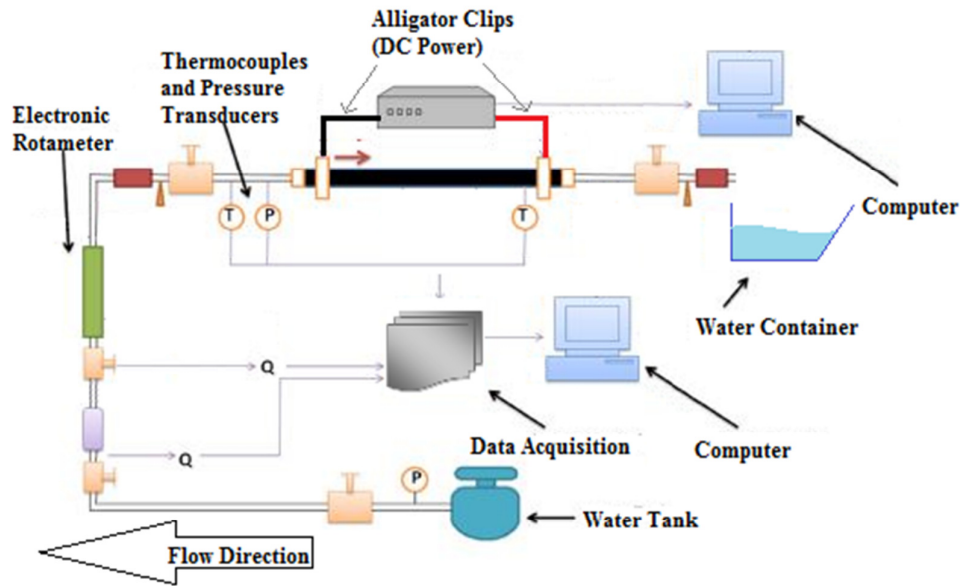


**Figure 2.6:** Schematic of the heat transfer experiment setup

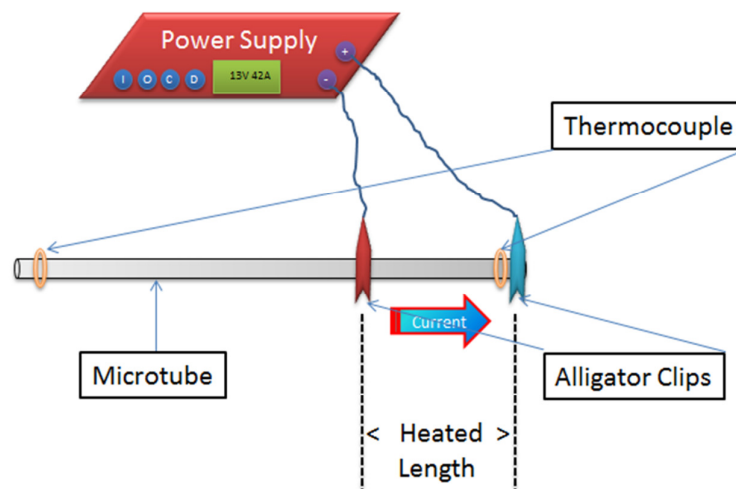


**Figure 2.7:** Schematic of the test section

### **2.3 Experimental Test Setup of Miniature Magnetic Actuator for Targeted Gene Delivery of Nucleic Acid Based Molecules (Third Part)**

In the third part of this work, a miniature magnetic actuator was designed in order to accomplish targeted gene delivery of nucleic acid-based molecules, and it includes fundamental features. Moving a magnetic field without distorting its shape is trivial if the source of magnetic field can be moved in the same direction. It was decided that such a mechanism would be cumbersome. Instead, the linear movement of the magnet was mimicked with magnets rotating around a common axis. The idea behind this design is using the synchronous rotation of symmetric and opposing magnets to generate a magnetic field, which peaks when the magnets are at the closest position and which diminishes while the magnets are at the farthest position. Rare earth magnets with 300 mT magnetic field strength are placed on to the each face of the square profile rotors with the  $(i-1)a$  mm distance from the reference edge, where  $i$  is the magnet number and  $a$  is the magnet diameter. The rotors are placed in such a way that the tube, which has 3 mm outer diameter, stays in between the rotors, which are actuated by a simple DC motor. Angular velocities are calculated from the position data, which are obtained from the encoder of the motor. The first design has been improved by reducing the angular separation of rare earth magnet pairs to obtain fewer discontinuities on the magnetic field, and better position tracking. This was achieved by changing rectangular rotors into hexagonal rotors. The magnetic actuator is illustrated in Fig. 2.8. The system consists of two magnetic rotors, DC motor (12V), power switch, speed control switch, power cables, miniature gears and proper stand and units for placing cell dish.

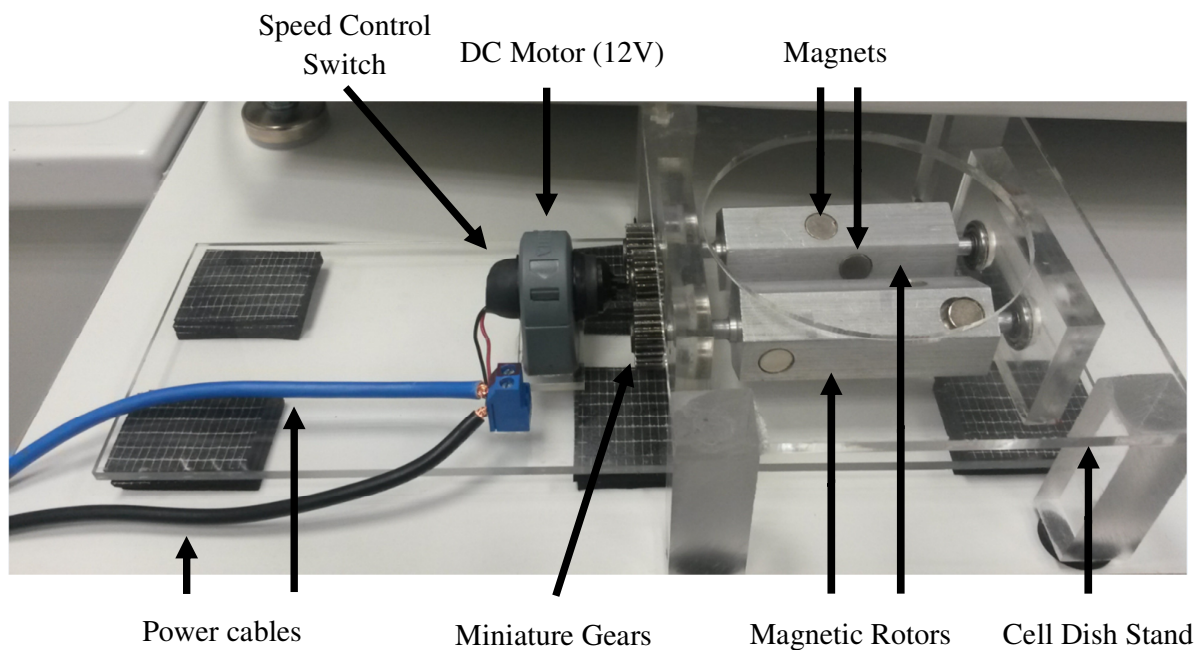


**Figure 2.8:** Schematics of magnetic actuator

The most important features of magnetic manipulation require control, and enhanced accuracy to achieve optimal magnetic conditions for gene delivery. Therefore, the magnetic actuator was designed in order to provide improved control ability, durability and less system complexity. Thanks to miniature gears and speed control switch, turn speed of magnetic rotors can be adjustable to the desired values. Hence, it provides control of magnetic field force. On the other hand, the direction of magnetic field plays an essential role. In order to supply continuous magnetic field, each magnets on the magnetic rotors are transversely placed. Hence the system provides magnetic fields in both vertical and horizontal directions due to magnetic vortices as shown in Fig. 2.9.

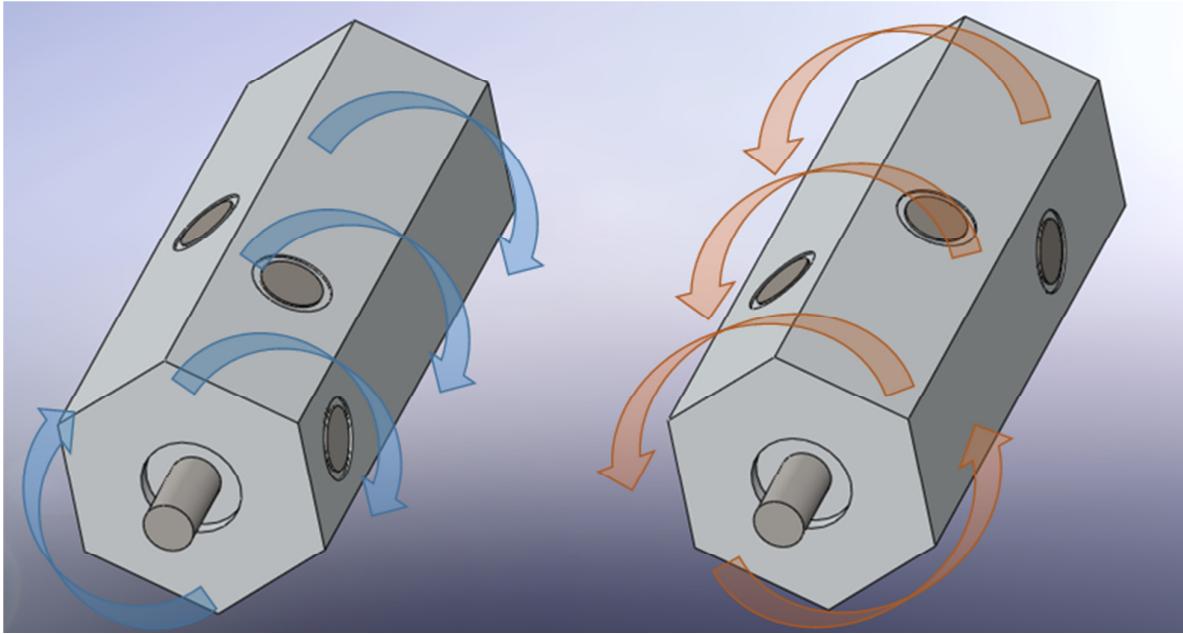


**Figure 2.9:** Magnetic field direction on magnetic rotors

#### **2.4 Experimental Procedure of Miniature Energy Harvesting Device Using External Fluid-Flows (First Part)**

In order to assess the efficiency of the device, power reclamation experiments are conducted using the device prototype under various test conditions. Accordingly, the experimental tests are performed with different flow velocities varying from 1 to 5 m/s. Plain water and two water-salt solutions with different salt concentrations (low-salinity water with a salt concentration of 150 gr per 1000 ml water and high-salinity water with a salt concentration of 350 gr per 1000 ml water) are examined to investigate the salt concentration effect. The schematic of the experimental setup is shown in Fig. 2.10. The experimental setup is prepared to perform the desired experiments for the above-mentioned velocities by using a fan.



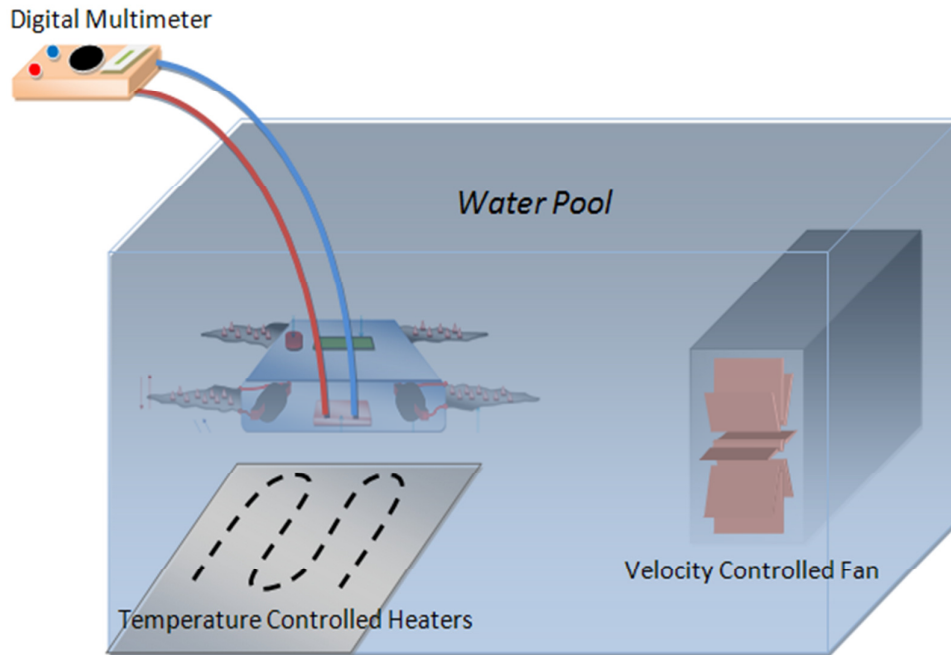


**Figure 2.10:** Experimental Setup of Miniature Energy Harvesting Device

## 2.5 Experimental Procedure of Miniature System for Flow Boiling Enhancement in Microtubes with Crosslinked pHEMA Coatings (Second Part)

In the second part of this work, two alligator clips, which were specially shaped with machining tools to minimize the heated length and to reach a width of 1mm, were attached to the microtube surface (with a 1cm heated length). Alligator clips were assembled with a prescribed distance from each other and connected to the high current power supply, which supplies an adjustable DC current and high power input to provide Joule heating to the desired sections of ~4 cm long microtubes of 249  $\mu\text{m}$ , 507  $\mu\text{m}$  and 908  $\mu\text{m}$  inner diameters. Conax<sup>®</sup> packing glands offer sealing between the microtube and the experimental loop. The test section was connected to the setup from the inlet side, whereas the outlet side was exposed to the atmosphere in order to guarantee atmospheric conditions at the outlet (exit) side. Moreover, one of Omega<sup>®</sup> thermocouples were assembled upstream the inlet of microtube in order to investigate bulk temperatures at the inlet. Pressure measurements were performed via Omega<sup>®</sup> pressure transducers with various ranges (between 0 - 3000 psi gauge pressure). Inlet pressures varied from 122 to 1552 kPa. An Omega<sup>®</sup> turbine meter was used



to collect flow rate data, which was obtained together with the voltage and current data. Collected data were transferred to the computer for data reduction. Local surface temperature at the outlet of the tube was measured via a thin Omega® thermocouple wire (~ 76µm thick). This thermocouple was connected to the microtube surface at the end of the heated length of the microtube, where the maximum temperature was expected along the test section via Omega® Bond and atmospheric conditions are present. Exit mass qualities vary from -0.079 to -0.147 in this study. During the experiments, the flow rate was fixed at the desired value by tuning the pressure difference between microtube inlet and exit. The temperature and pressure data were obtained from the Labview® interface. During the experiments, the experiments were performed under steady state conditions. By adjusting the current from power supply, the power was increased by up to ~0.5 Amps increments until the test setup lost its uniformity because of extreme overheating conditions (CHF condition). This procedure was repeated for different mass fluxes. Deionized water was utilized as working fluid, and inlet fluid temperature was the ambient temperature.

In the relevant literature the experimental setup was validated with single-phase heat transfer tests [98-99]. In order to calculate approximate heat losses, power was applied to the test section following evacuating de-ionized water from the test section. The temperature difference between the test section and atmosphere was recorded with the corresponding current value after the surface temperature of the test section reached to steady conditions. Since power values and temperature differences were recorded simultaneously, power versus temperature difference profile could be obtained in order to calculate the heat loss corresponding to each experimental data point, and a heat loss calibration curve was obtained. Accordingly, the average heat loss was found to be 5.6 %, and heat losses were taken into account in the data reduction.

## **2.6 Miniature Magnetic Actuator for Targeted Gene Delivery of Nucleic Acid Based Molecules (Third Part)**

In order to investigate effect of varying magnetic fields on targeted gene delivery of nucleic acid-based molecules, experiments are conducted using the miniature magnetic actuation setup under various test conditions. Targeted cells were cultivated in incubator

environment. Cultivated cells were placed to cell dish to be fit for miniature device setup. Processes of cell and nanoparticle preparation are explained in below.

### **2.6.1 Preparation of Polyethyleneimine-Superparamagnetic Nanoparticles**

Polyethyleneimine-superparamagnetic nanoparticles (PEI-SPION) were kindly provided from Koç University, Department of Chemistry, Turkey. In brief, oleic acid coated  $\text{Fe}_3\text{O}_4$  nanoparticles were obtained from the Ocean Nanotech LLC. The hydrophobic  $\text{Fe}_3\text{O}_4$  nanoparticles were silica coated by a modified reverse micro emulsion procedure by using tetraethyl orthosilicate. Polyethyleneimine (PEI) was added to the surface of the  $\text{Fe}_3\text{O}_4\text{-SiO}_2$  nanoparticles by stirring with trimethoxysilylpropyl modified polyethyleneimine (50 % in isopropanol).

### **2.6.2 Plasmid DNA isolation**

Plasmid DNA isolation was performed with plasmid DNA purification kit (Nucleobond Xtra Midi/Maxi, Macherey-Nagel, Germany). In this study pMAX-GFP plasmid was used (Addgene, Cambridge, USA). 100  $\mu\text{l}$  kanamycin was added into flask contains 200 ml LB Broth. E-coli contains pMAX-GFP plasmid put into LB Broth and was shaken overnight at  $37^\circ\text{C}$  at 240 rpm (Innova 4330 Incubator Shaker, New Brunswick Scientific, Germany). Then bacteria suspension is centrifuged in a Sorvall at 5000 rpm at  $+4^\circ\text{C}$  for 20 minutes. Supernatant was discarded and pellet was suspended with 8 ml suspension buffer. 8 ml Lysis buffer was added and incubated at room temperature for 5 minutes. After neutralization step with 8 ml neutralization buffer, lysate was loaded on column filter. After washing and elution steps, sample was precipitated with 3.5 ml isopropanol and centrifuged at 15000 g at  $+4^\circ\text{C}$  for 30 minutes. Supernatant was removed and 2 ml 70 % ethanol was added. Sample was centrifuged at 15000 g at room temperature for 5 minutes and supernatant was removed. Pellet was dried at room temperature for 5-10 minutes. DNA pellet was dissolved in TE buffer.

### **2.6.3 Cell Culture and Transfection**

MCF-7 (ATCC-HTB22) human breast cancer cell line and PC-3, human prostate cancer cells were cultured with DMEM (Sigma, Germany) supplemented with 10 % FBS (Biochrom KG, Germany), 1 % Penicillin-Streptomycin (Biological Industries, Israel), 1 % L-glutamin (Biological Industries, Israel).  $1, 5 \times 10^6$  cells were seeded on 10-cm culture plate in 8 ml cell culture medium. Cells were incubated for 48 hours at 37°C in a 5 % CO<sub>2</sub> atmosphere.

67 µl PEI-SPION was taken from stock suspension (Concentration of stock suspension of PEI-SPION was 3 mg/ml) and was added into Eppendorf tube contains 200 µl DMEM. After that, 16 µl of pMAX-GFP plasmid DNA was taken from stock solution (Concentration of stock solution of pMAX-GFP plasmid DNA was 2 µg/µl) and was added into another Eppendorf tube contains 200 µl DMEM. The mixture of Eppendorf tube with PEI-SPION was transferred into Eppendorf tube which contains pMAX-GFP plasmid DNA. Eppendorf tube was vortexed for 15 seconds. Eppendorf tube was incubated at room temperature for 10 minutes. Mixture was added on the cell line dropwise. So that, pMAX-GFP plasmid DNA concentration was 4 µg/ml and PEI-SPION concentration was 25 µg/ml in cell culture medium. Cells were washed with PBS after 6-8 hours. Cells were incubated with DMEM supplemented with 10 % FBS, 1 % Penicillin-Streptomycin and 1 % L-glutamine for 48 hours and then analysed with microscopy.

### **2.7 Model and Simulations (First Part)**

In the first part of this work, energy harvesting simulations are performed to assess the energy harvesting capability of the device. For this, a miniature device tail is modelled to estimate the maximum possible reclaimable power. The tail of the device is modelled with the Solid Works 2008 SP 2.1 software with the same dimensions as the real tail. Moreover, the tail skeleton and surface materials are chosen as carbon fiber leaves and carbon fiber poly-urethane composite in similar lines to the real tail. The model is then transferred to the COMSOL Multiphysics version 4.2 software for the simulations.

### 2.7.1 Governing Equations

Laminar flow assumption is made for solving the governing equations (weakly compressible stationary Navier–Stokes equations). Accordingly, Navier-Stokes equations are expressed as:

$$\nabla \cdot (\rho \mathbf{u}) = 0 \quad (2.1)$$

$$\rho \mathbf{u} \cdot \nabla \mathbf{u} = -\nabla p + \nabla \cdot \left( \mu (\nabla \mathbf{u} + (\nabla \mathbf{u})^T) - \frac{2}{3} \mu (\nabla \mathbf{u}) \mathbf{I} \right) \quad (2.2)$$

where  $\rho$  is fluid density,  $u$  is fluid velocity,  $\mu$  is fluid viscosity,  $T$  is transpose of the matrix and  $\mathbf{I}$  is the unit vector

The boundary conditions for velocity at the tail surface, inlet fluid velocity ( $u_0$ ) and exit pressure ( $p$ ) are as follows:

$$\mathbf{u} \Big|_{\text{surface}=x,y,z} = \mathbf{0} \quad (2.3)$$

$$\mathbf{u} \Big|_{x=0,y,z} = \mathbf{u}_0 \quad (2.4)$$

$$p \Big|_{x=L,y,z} = p_{atm} \quad (2.5)$$

The shear stress is proportional to tail displacements due to vibrations. Vibrations are caused by harmonic fluid waves because of variable flow rates. The variable flow velocity due to harmonic progressive waves is shown in Eqn. (2.6), where  $A$  is amplitude and  $\omega$  is angular velocity of the wave:

$$\mathbf{u} \Big|_{x=0,y,z} = \mathbf{u}_0 = A [\cos(\omega t)] \quad (2.6)$$

In the simulations, this formula is used for defining the fluid velocity profile. Regarding the amplitude, the velocity values from real experiments are used. Accordingly, fluid velocity amplitudes vary between 1 to 5 m/s.

### 2.7.2 Mesh and Solver Settings

The COMSOL Multiphysics 3.5a solver is used for solving Navier-Stokes equations. The simulations are performed with a workstation having an Intel Xeon 2.67 GHz processor with 24 GB RAM. The operating system is Windows Vista Server Edition. Due to the complex tail shape, the time required for one simulation to be completed is approximately 22-24 hours. In order to simulate displacements on the tail, two different meshes are used. A cube (20 cm each side) is used as the domain to isolate the simulated tail (Fig. 2.11). The experimental parameters such as fluid velocity and density are defined inside the cube. A user-controlled fixed mesh is used. The total number of the degrees of freedom varies from 548373 to 801569, while 2666 elements are present in the mesh.

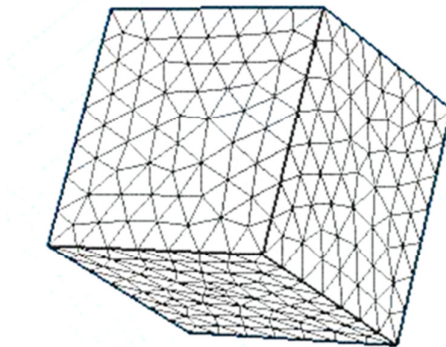


**Figure 2.11:** Fixed Mesh for Virtual Environment Cube

For the tail (located inside the cube), a moving mesh is used for tail movements. Regarding the material selection, carbon fiber (included in the material library of the COMSOL

Multiphysics software 4.2) is chosen for simulations. The configuration used in simulations was first modelled in Solid Works 2008 SP 2.1, and then transferred to COMSOL Multiphysics software 4.2. This configuration was generated in similar lines to the experimental configuration. Moving mesh is a method of adaptive meshing, which solves the continuous domain of interest into a grid of many individual points on the solid object. Total number of degrees of freedom varies from 1428354 to 2193809 in this study. Triangle type element is used, while there are 6000 elements present in the mesh. In this moving mesh, the grid is dynamic and tracking the features of the result is performed as computation progresses. Several parameters are defined to generate the moving mesh. First, fixed mesh is defined according to the initial position of the tail before the fluid flow occurs. Prescribed mesh displacement is defined according to displacement range obtained from the analysis and experimental observations. The prescribed deformation is defined according to experimental parameters as a function of fluid velocities in x, y, z directions. The tail with moving mesh inside the cube and mesh configurations is displayed in Figs. 2.12 and 2.13.

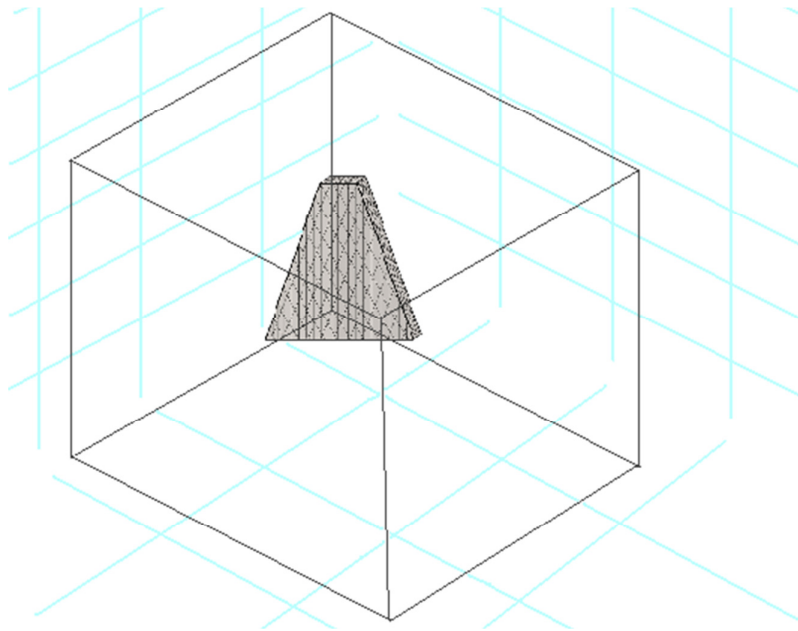


**Figure 2.12:** Moving Mesh for the Tail in the Cube

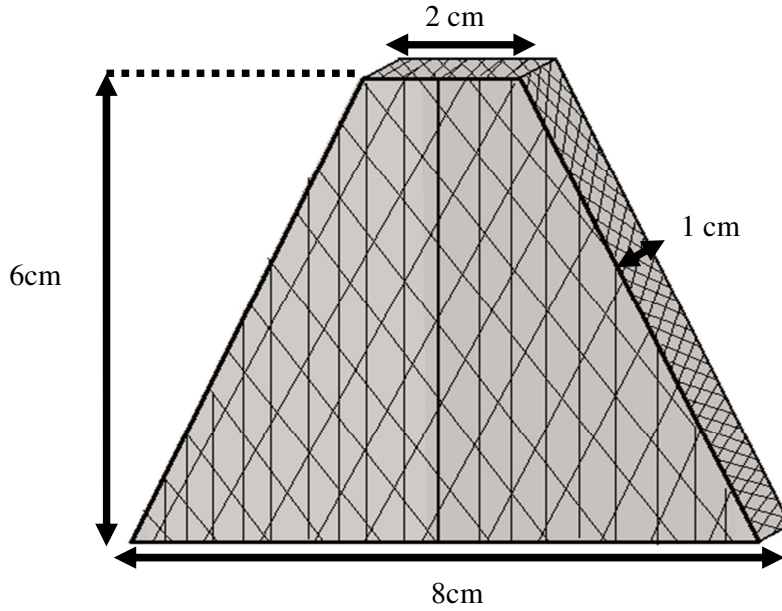


**Figure 2.13:** Zoom in View of Moving Mesh for the tail\*

### 2.7.3 Post Processing of the Results

After solving Navier-Stokes equations, forces acting on the tail surface can be obtained in post processing. The maximum reclaimable power is obtained from the following integration along the tail surface as:

$$P_m = \int_S (\hat{\mathbf{n}} \cdot \underline{\underline{\delta}}) \circ \vec{\mathbf{u}} dS \quad (2.7)$$

where  $\hat{\mathbf{n}}$  is unit normal vector,  $\underline{\underline{\delta}}$  is stress tensor and  $\vec{\mathbf{u}}$  is flow velocity vector.

In the simulations, the tail is fixed from the long bottom side, where it is connected to the generator. Therefore, fixed type mesh is used for this side. For the remaining sides, a controlled moving mesh is employed in order to account for vibrations and oscillations on the tail surface. Accordingly, the tail vibrates within defined displacements ranges inside the box. Same moving mesh properties are defined for each side of the tail. The displacement range in

simulation is defined as  $\pm 2$  cm. This range is chosen in parallel lines with the observations from experiments on the tail of the device. In the simulations, the fluid velocity amplitudes vary from 1 to 5 m/s. Initial position and one representative position due to vibrations are shown in Figs. 2.14 and 2.15. In order to analyse flow characteristics, streamlines for the flow (with velocity amplitude of 5 m/s) across a tail are obtained. As can be seen from Fig. 2.16, the flow become separated downstream the tail. In the wake region behind the tail, vortices can be clearly seen. It can be also observed that the flow can follow the geometry of the above surface of the tail, while it cannot do so behind the tail resulting in flow separation and consequent vortices. All these results agree well with cross flow characteristics across solid bodies reported in the literature [100].

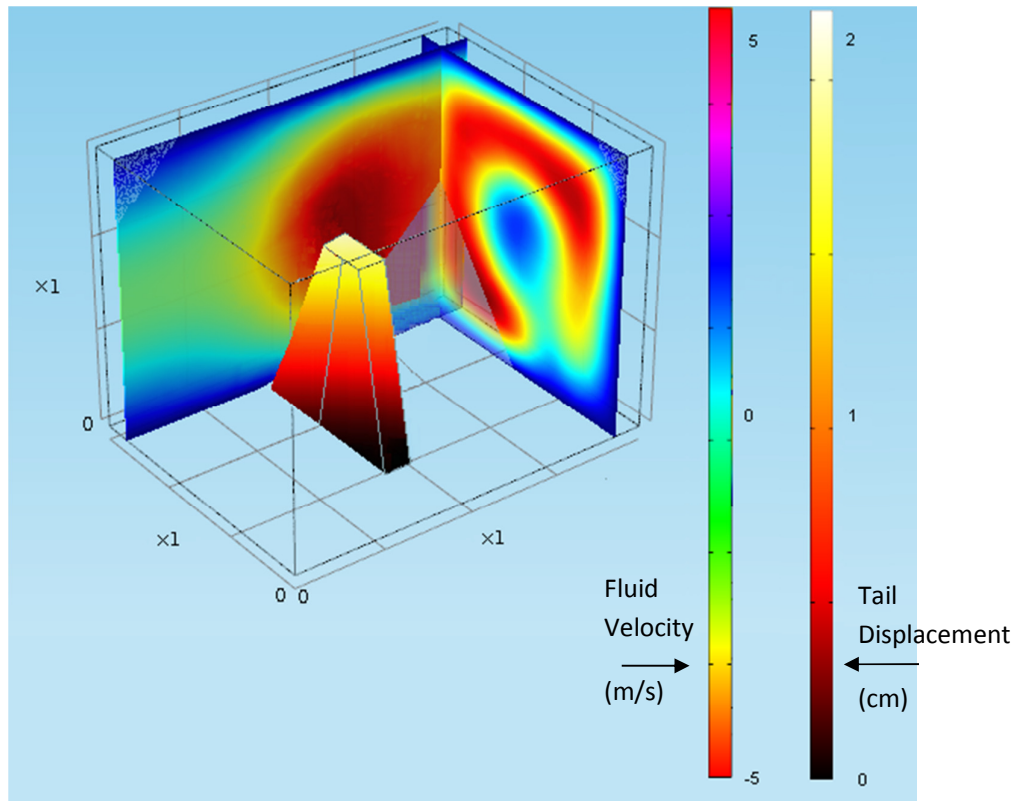


**Figure 2.14:** Initial Position of the Tail.



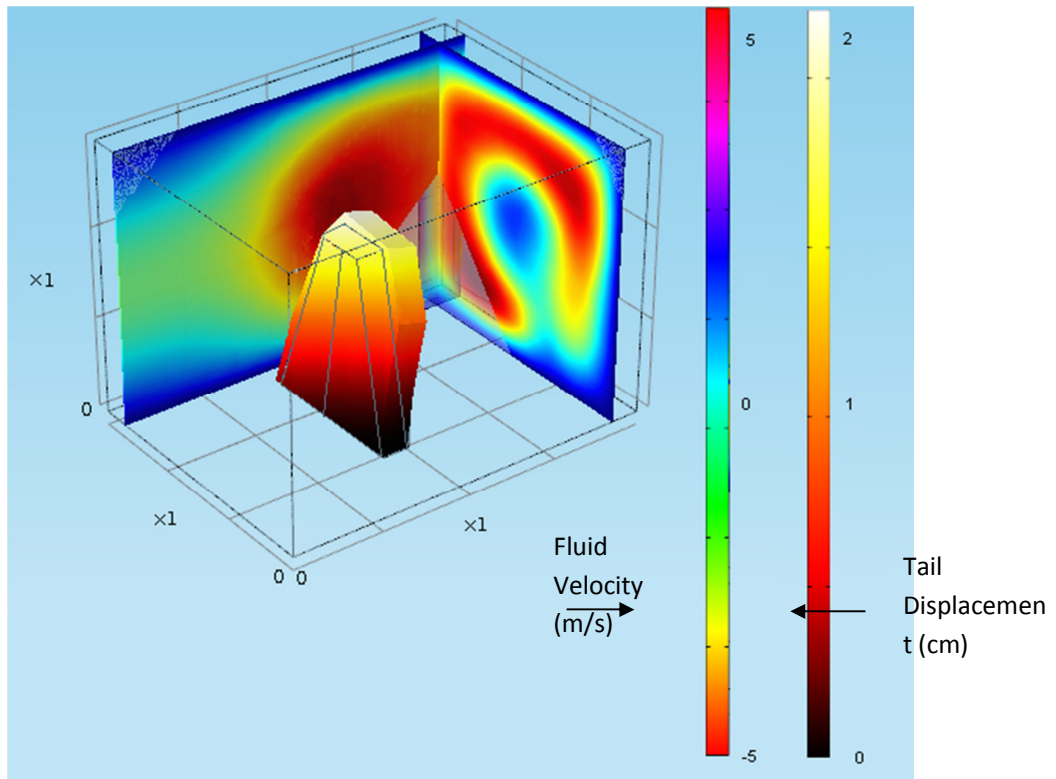


**Figure 2.15:** Tail at a Displacement Value of 2 cm due to Vibrations Caused by Flow Oscillations

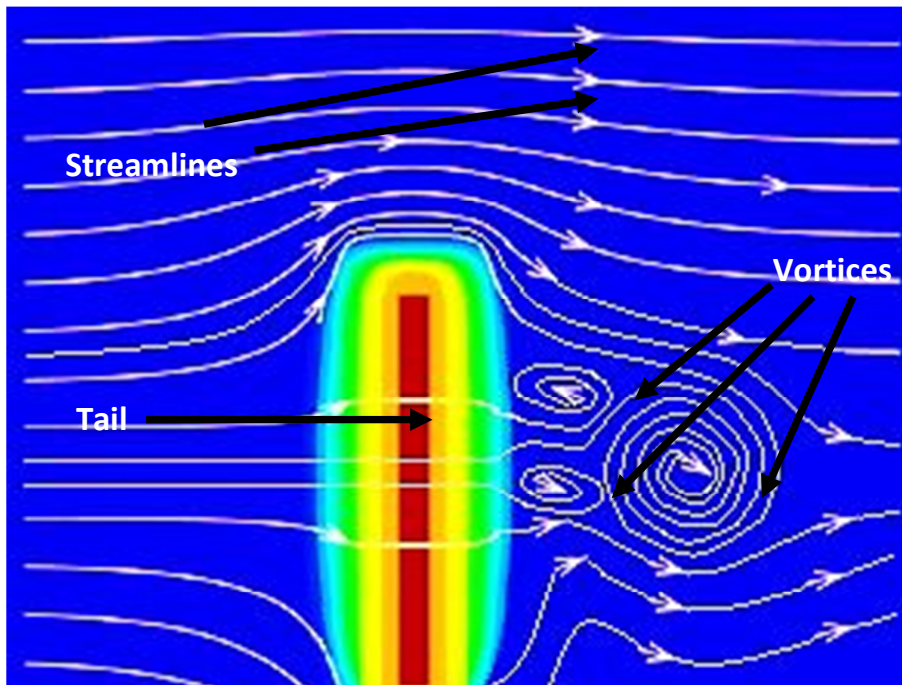


**Figure 2.16:** Flow Streamlines for the Initial Position of the Tail.

## 2.8 Data Reduction (Second Part)

For the second part, the voltage, current, flow rate, and temperature data is reduced to attain heat transfer coefficients and CHF (critical heat flux).

The mass flux can be found using the following formula:

$$G = \dot{m}/Ac \quad (2.8)$$

where  $Ac$  is the cross section of the microtube.

CHF is expressed as:

$$q''_{CHF} = \frac{\left( P_{elec} - \dot{Q}_{loss} \right)}{\pi d_i L_h} \quad (2.9)$$

where  $\left( P_{elec} - \dot{Q}_{loss} \right)$  is the applied net power,  $d_i$  is the inner hydraulic diameter, and  $L_h$  is the heated length.

Two-phase heat transfer coefficient at the exit of the tube is expressed as:

$$h_{tp} = \frac{\left( P_{elec} - \dot{Q}_{loss} \right)}{\pi d_i L_h (T_{w,i} - T_{w,o})} \quad (2.10)$$

Assuming 1-D steady state heat conduction with uniform heat generation, the local inner surface temperature of the microtube,  $T_{w,i}$ , is expressed in terms of the measured local outer surface temperature,  $T_{w,o}$ , as:

$$T_{w,i} = T_{w,o} + \frac{\dot{q}}{4k_w} (r_o^2 - r_i^2) - \frac{\dot{q}}{2k_w} r_o^2 \log\left(\frac{r_o}{r_i}\right) \quad (2.11)$$

where  $k_w$  is heat thermal conductivity of the wall,  $r_o$  is outer radius of the microtube,  $r_i$  is inner radius of the microtube, and  $\dot{q}$  is the volumetric heat generation.  $\dot{q}$  is expressed as a function of net power, inner microtube radius, outer microtube radius, and heated length as:

$$\dot{q} = \frac{\left( P_{elec} - \dot{Q}_{loss} \right)}{\pi(r_o^2 - r_i^2)L_h} \quad (2.12)$$

Local exit mass quality was deduced based on energy balance:

$$x_e = \frac{\dot{q} \pi d_i L_h - \dot{m} c_{p,e} (T_{sat,e} - T_i)}{\dot{m} h_{FG,e}} \quad (2.13)$$

where  $\dot{m}$  is mass flow rate,  $c_p$  is specific heat,  $T_i$  is inlet temperature, and  $h_{FG}$  is latent heat of vaporization.

The uncertainty of the measured values for the second part is given in Table 1. They were provided by the manufacturer's specification sheet, whereas the uncertainties were obtained using the propagation of uncertainty method developed by Kline and McClintock [101]. According to this method, if for an experimental result,  $r$ , computed from  $J$  measured variables  $X_{1...J}$ , the data reduction equation is:

$$r = r(X_1, X_2, \dots, X_J) \quad (2.14)$$

Then, the corresponding uncertainty in the experimental result is given by:

$$U_r^2 = \left( \frac{\partial r}{\partial X_1} \right)^2 U_{X_1}^2 + \left( \frac{\partial r}{\partial X_2} \right)^2 U_{X_2}^2 + \dots + \left( \frac{\partial r}{\partial X_J} \right)^2 U_{X_J}^2 \quad (2.15)$$

where  $U_r$  is the uncertainty in the result,  $U_{X_i}$  is the uncertainty in the variable  $X_i$ , etc. Moreover, the outer diameters were directly measured using a high precision calibre with an uncertainty of  $\pm 1 \mu\text{m}$ . The inner diameter was carefully obtained by relating it to the outer diameter via visualization through computer vision techniques.

| <b>Uncertainty</b>                            | <b>Error</b>                     |
|---|----------------------------------|
| Inner diameter, $d_i$                         | $\pm 2 \mu\text{m}$              |
| Temperature, $T$                              | $\pm 0.1 \text{ }^\circ\text{C}$ |
| Electrical power, $P$                         | $\pm 0.2 \%$                     |
| Heat flux, $q''$                              | $\pm 3.2 \%$                     |
| Mass flux, $G$                                | $\pm 2.6 \%$                     |
| Two-phase heat transfer coefficient, $h_{tp}$ | $\pm 12.2 \%$                    |
| Coating thickness                             | $\pm 5 \text{ nm}$               |

**Table 2.1:** Uncertainties of measured values

## CHAPTER 3

### RESULTS AND DISCUSSION

#### Motivation for performed research

Miniature devices described in this thesis are applicable to multiple areas. However, the work was motivated by a significant goal: to design and develop energy efficient miniature devices for energy harvesting, thermal management and biomedical applications. The performed research is divided into three main components according to device types: energy harvesting device, flow boiling investigation system and magnetic actuation device. The major aims serving for the motivation of this research are as follows:

- The miniature power reclamation device is designed for underwater usage such as wild life observation, military and security applications, requiring electricity and places which are not easily accessible due to depth, flow and unreachable coordinates.
- The proposed device aims to provide significant features such as durability, sustainability and light weight.
- Tail and body design of the miniature power reclamation device aims at the operation under different working fluid and various inner flow circulations.
- The miniature power reclamation device aims to provide less complexity and cheap materials which are commonly available in the market.
- The device also targets to sense global warming effects by observing the displacement of deep currents and icebergs.
- The miniature system having microchannel for boiling applications aims to investigate flow boiling on crosslinked pHEMA coated microtubes having different coating thickness
- The miniature flow boiling system aims to see effects of crosslinked pHEMA coating on critical heat flux and boiling heat transfer
- The miniature flow boiling system targets to show that iCVD is a useful tool for coating microchannel having various hydraulic diameters because of its 3D coating capability.

- A miniature device is designed for investigating effect of varying magnetic fields on targeted gene delivery of nucleic acid-based molecules as providing a miniature magnetic system, which will be used as magnetic actuator offering different magnet's turn speeds and directions in the system.
- The miniature magnetic actuator aims to deliver necessary drugs and genes for patients and their transport under safe conditions.
- The device aims to have a compact system that could operate with low energy consumption, low waste disposal, and parallel and fast processing capability and high mixing capacity.

### **3.1 First Part - Power Reclamation Efficiency of Miniature Energy Harvesting Device Using External Fluid Flows**

#### **3.1 Simulation Results**

Power reclamation experiments are conducted using the device prototype under various test conditions and simulated with COMSOL 4.2 software. Accordingly, the experimental tests are performed with different flow velocities varying from 1 to 5 m/s. Plain water and two water-salt solutions with different salt concentrations (low-salinity water with a salt concentration of 150 gr per 1000 ml water and high-salinity water with a salt concentration of 350 gr per 1000 ml water) are examined to investigate the salt concentration effect. The simulations are performed for various flow velocity profiles. The average power values are computed corresponding to various time dependent flow velocity profiles (Eqn. 2.6) by averaging instantaneous power values over the time. Each flow velocity profile is given manually as the input velocity. Obtained results showed the maximum possible reclaimable average power as a function of the given velocity amplitudes. The simulation results of reclaimable power from a single mini generator by simulating the tail at different fluid velocities (for plain water) are shown in Fig. 3.1. The maximum reclaimable power is found as 6.45 W from one single tail corresponding to flow velocity amplitude of 5 m/s (for plain water), while the minimum reclaimable power is attained as 2.12 Watts corresponding to flow velocity amplitude of 1 m/s. A linear relationship between the maximum reclaimable power and flow velocity amplitude is apparent.

#### **3.2 Experimental Results**

The power output is found from the Ohm's law. The current in the device is measured by a digital multimeter. Since the resistance value of the generator is known, power output could be easily obtained ( $P(W) = I^2 \cdot R$ ). The maximum reclaimed power is found as 4.3 W when the fluid velocity is set to 5 m/s and the fluid is plain water, while the minimum reclaimed power is 1.54 W when the fluid velocity is set to 1 m/s, and the fluid is high salinity water. The reclaimed power is directly proportional to fluid velocity as shown in Fig. 3.1. On the other hand, fluid concentration has a negative effect on the reclaimed power due to enhanced viscous effects introduced by high-salt concentrations.

The comparison between the maximum reclaimable power estimated by computer simulations of the tail and the experimental results is displayed in Fig. 10. According to this comparison, 33.8 % of the reclaimable power is lost during operation of the device in average. The difference might be attributed to frictional losses and losses in the generator, which is 5 % according to the datasheet provided by manufacturers. The maximum reclaimable powers according to simulations are higher than those obtained from the experiments, when the working fluid is plain water for both cases. Since the temperature is within a few degrees under the experimental conditions, irreversible losses due to heat transfer are not significant. Frictional losses at connecting points and losses in the generator are the sources for efficiency losses. Vibration capturing capabilities of tails due to their flexibility, light weight and special surface (made of Carbon fiber leaves) design have a positive effect on generated electricity. In comparison to other energy harvesting systems manipulating thermal energy, magnetic energy, and fuel cells, the proposed energy reclamation device offers several advantages. The simple structure of the device benefits from reduced cost and easy implementation. Although the tail design seems complicated, materials used here could easily be provided from local providers. The components basically consist of mini generators, tails, batteries, voltage output port, on-off switch and water proof metal case. Moreover, the proposed device does not require any specific input from ambient conditions. Fundamentally, this device requires external fluid flows, which are already present in natural resources such as rivers, oceans and seas. The power generation principle is based on vibrations of the tails, which could originate from water flow or waves. Taking the outlet power and voltage performance of the present miniature device into consideration, required working hours under different working fluids to run a given daily used device for 1 hour are listed in Table 3.1. Therefore, this device has the potential for providing necessary power to run many daily used electronic devices.



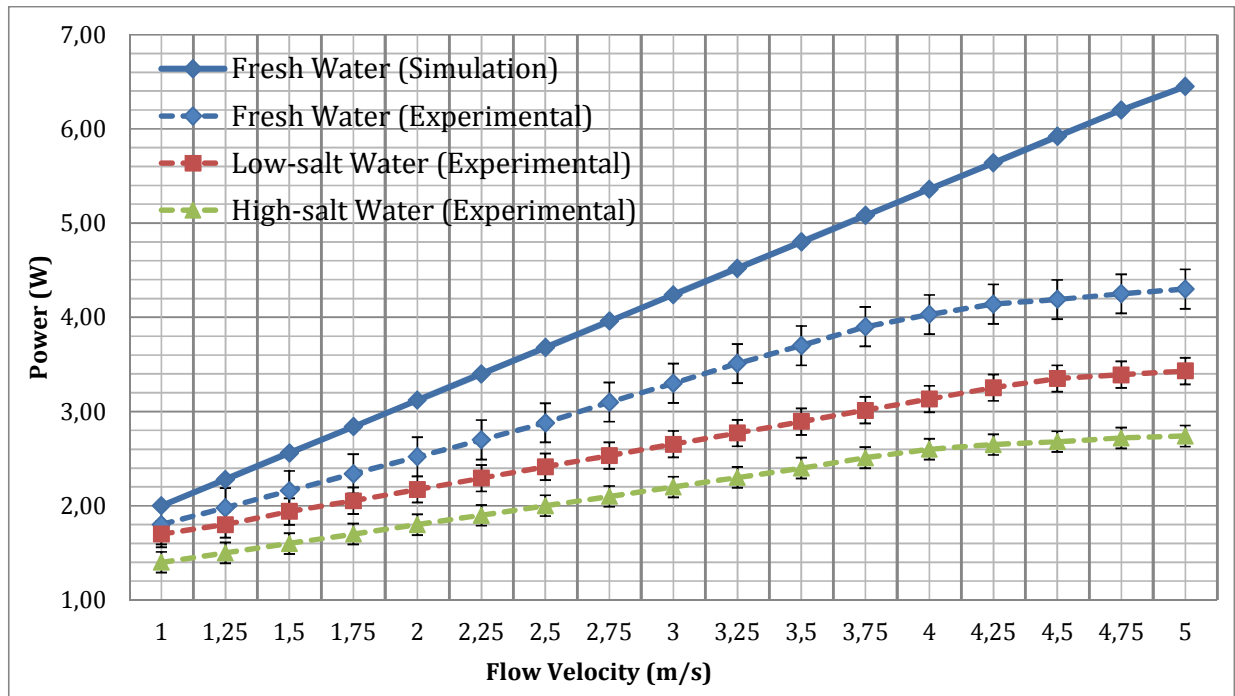


**Figure 3.1:** Outlet Power Result of COMSOL Simulation (Plain Water) and Experimental Results under Different Working Fluids (Plain Water, Low-salinity and High salinity Water).

| Device Name           | Estimated Power Consumption of Some Example Devices to Run ~1 | Plain Water | Low-Salinity Water | High-Salinity |
|-----------------------|---|-------------|--------------------|---------------|
| Led Light (~60 Piece) | ~800 mA – 3 Volts   | ~1 hour     | ~1h 25min          | ~1h 45min     |
| Voltage Regulator     | ~1500 mA – 4.2 Volts  | ~1h 50min   | ~2h 15min          | ~2h 50min     |
| Mini Aquarium Filter  | ~500 mA – 6 Volts   | ~1 h 10min  | ~1h 35min          | ~1h 55min     |
| Mini Aquarium Pump    | ~2000 mA – 5 Volts  | ~2h 30 min  | ~3h 20min          | ~4 hours      |
| Mini GPS Receiver     | ~200 mA – 1.4 Volts   | ~30 min     | ~44 min            | ~1h 10min     |
| Underwater Mini       | ~750mA – 6 Volts  | ~1h 30 min  | ~2hours            | ~2h 15 min    |
| Mini Thermometer      | ~300 mA – 1.5 Volts   | ~40 min     | ~55 min            | ~1h 20min     |
| Mini Seismometer      | ~500 mA – 4.5 Volts   | ~1 h 15min  | ~1h 50min          | ~2 hours      |

**Table 3.1:** Estimated Working Duration of the Energy Harvesting Device to Run Given Daily Used Devices for ~1 Hour

### 3.2 Second Part - Flow Boiling Enhancement in Microtubes with Crosslinked pHEMA Coating Having Different Coating Thickness

Before boiling heat transfer tests, single-phase pressure drop tests under the same mass fluxes ( $G = 5,000$  and  $20,000 \text{ kg/m}^2\text{s}$ ) for all used microtubes were conducted and the results were validated with single-phase correlations with friction factor results. There is a good agreement between experimental results and available correlations (Colebrook correlation [102] for turbulent flow conditions ( $Re > 2300$ ),  $f = 64/Re$  for laminar flow conditions ( $Re < 2300$ )) (Fig. 3.2). All of the experimental data fall within  $\pm 15\%$  of the predicted values. In relevant literature [98], single-phase heat transfer results on similar microtube configurations were found to be close to the theoretical predictions from available correlations under similar experimental conditions for the single-phase flow, which serves for another validation of the current experimental setup.

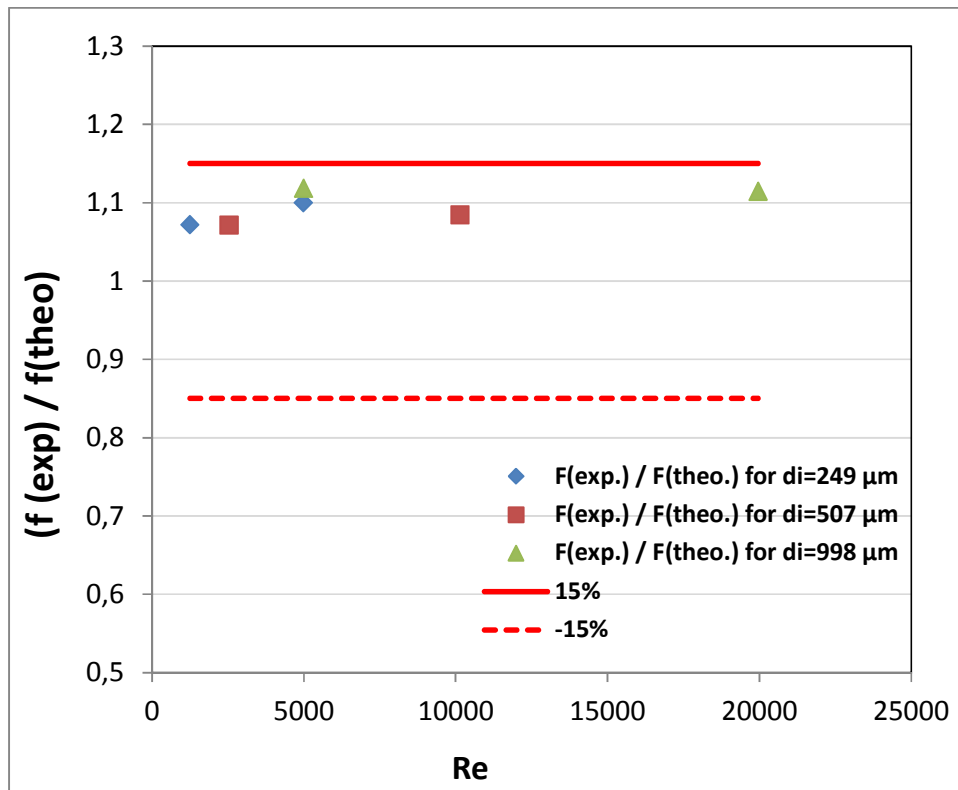
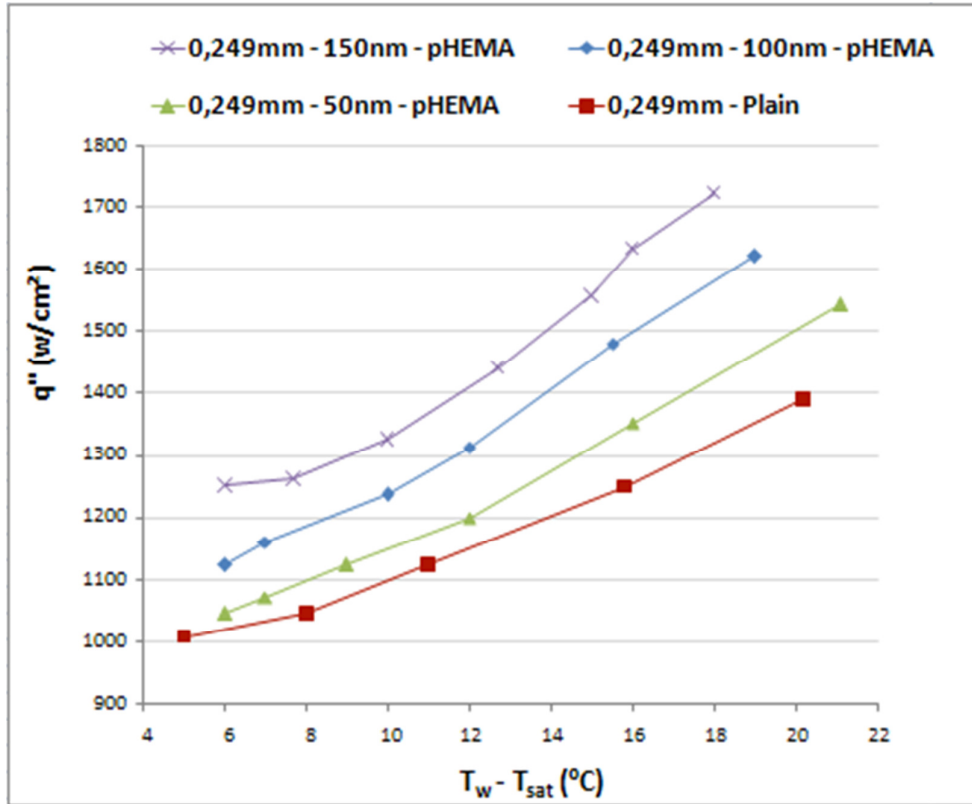


Figure 3.2:  $f_{\text{experimental}} / f_{\text{theoretical}}$  – Reynolds number profiles

### 3.2.1 Boiling Curves

In Fig. 3.3, boiling curves for non-coated and crosslinked pHEMA coated microtubes having an inner diameter of 249  $\mu\text{m}$  with coating thicknesses of  $\sim 50$  nm, 100 nm and 150 were shown at the mass flux of 5,000  $\text{kg}/\text{m}^2\text{s}$ .



**Figure 3.3:** Boiling Curves for Plain Surface Microtubes and pHEMA Coated Microtubes (50 nm, 100 nm and 150 nm thick coatings) with an Inner Diameter of 249  $\mu\text{m}$  at the Mass Flux of 5,000  $\text{kg}/\text{m}^2\text{s}$ .

The largest CHF enhancement is observed at the pHEMA coated microtube having the thickest coating ( $\sim 150$ nm). Compared to the non-coated microtube, maximum enhancement is around 20.4 %, while enhancements are 17.3 % and 13.2 % for coating thicknesses of 50 nm and 100 nm, respectively. In the relevant literature, it was found that contact angle decreases with the increase of nanostructure coating thickness [103]. Accordingly, lower contact angle promotes wetting [104]. Moreover, surface characteristics are also considerably changed with pHEMA coating since thicker coatings result in more porous structure.

In Fig. 3.4, identical crosslinker configurations are used for investigating CHF enhancements on microtubes of a diameter of 507  $\mu\text{m}$  at the mass flux of 5,000  $\text{kg}/\text{m}^2\text{s}$ . Similar trends in boiling curves can be observed. CHF enhancement ratios are less than those corresponding to the microtube of diameter of 249  $\mu\text{m}$ . CHF enhancements in this case are 10.1 %, 14 % and 15.3 % for coating thicknesses of 50 nm, 100 nm and 150 nm, respectively.

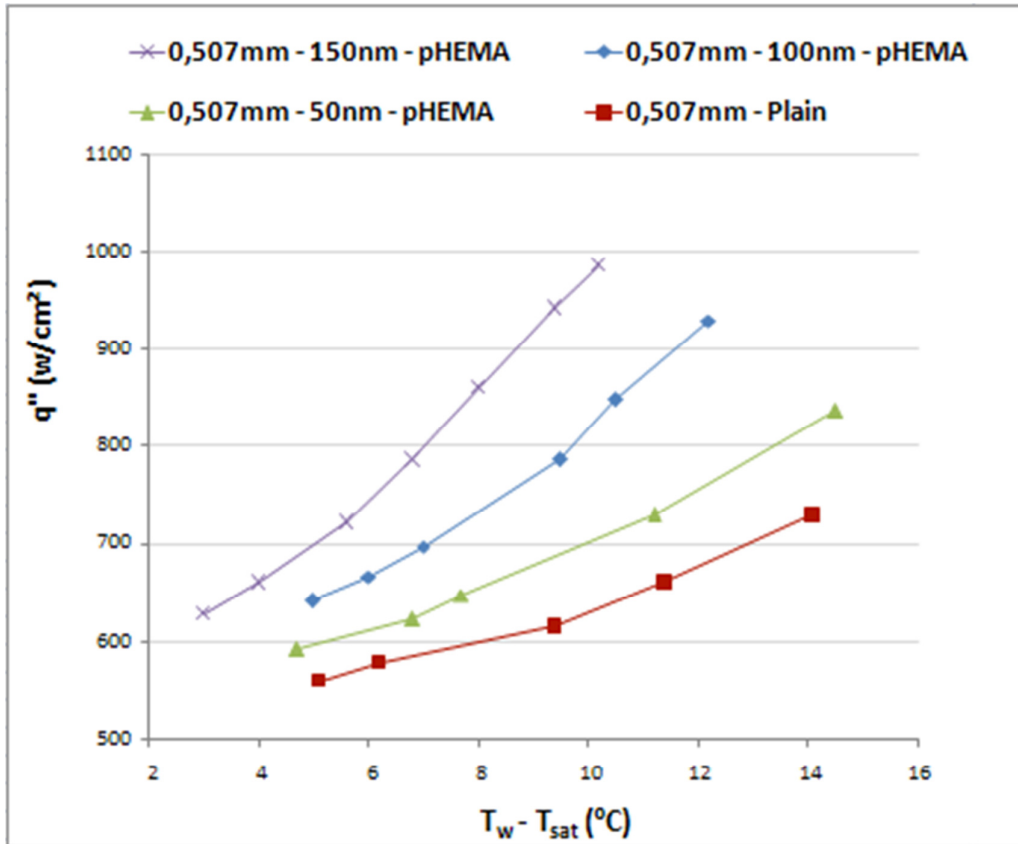


**Figure 3.4:** Boiling Curves for Plain Surface Microtubes and pHEMA Coated Microtubes (50 nm, 100 nm and 150 nm thick coatings) with an Inner Diameter of 507  $\mu\text{m}$  at the Mass Flux of 5,000  $\text{kg}/\text{m}^2\text{s}$ .

The boiling curves for the microtube having an inner diameter of 908  $\mu\text{m}$  are displayed in Fig. 3.5. Accordingly, the same trends related to coating thickness as in other cases can be noted in boiling curves. pHEMA coatings result in enhancement ratios of 8.9 %, 11 % and 12.5 % for coating thicknesses of 50 nm, 100 nm and 150 nm, respectively.

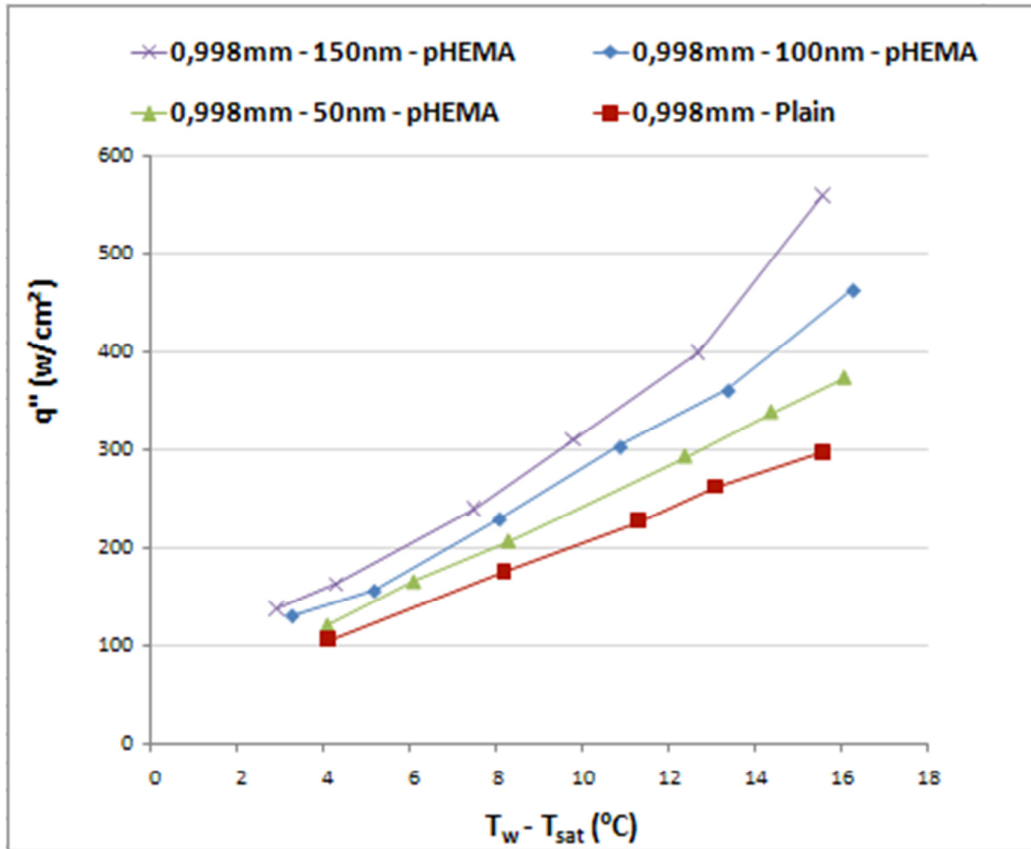


**Figure 3.5:** Boiling Curves for Plain Surface Microtubes and pHEMA Coated Microtubes (50 nm, 100 nm and 150 nm thick coatings) with an Inner Diameter of 998  $\mu\text{m}$  at the Mass Flux of 5,000  $\text{kg/m}^2\text{s}$ .

Figure 3.6, 3.7 and 3.8 show boiling curves at the mass flux of 20,000  $\text{kg/m}^2\text{s}$ . As can be seen from these figures, the highest enhancement in CHF occurs in the microtube having the smallest diameter. Moreover, the highest CHF enhancement is observed in the microtube with the thickest pHEMA coating in this case. The CHF enhancement ratios are 29.7 %, 26 % and 23.1 % for coating thicknesses of 50 nm, 100 nm and 150 nm, respectively. As shown in Figs. 3.7 and 3.8, similar trends are present for the microtubes having 507  $\mu\text{m}$  and 908  $\mu\text{m}$  inner diameters. The maximum CHF enhancement ratio is found as 24.8 % in the microtube having an inner diameter of 507  $\mu\text{m}$  and corresponds to the thickest pHEMA coating, while the maximum enhancement ratio is 20.1 % in the microtube having an inner diameter of 908  $\mu\text{m}$  for the thickest coating.

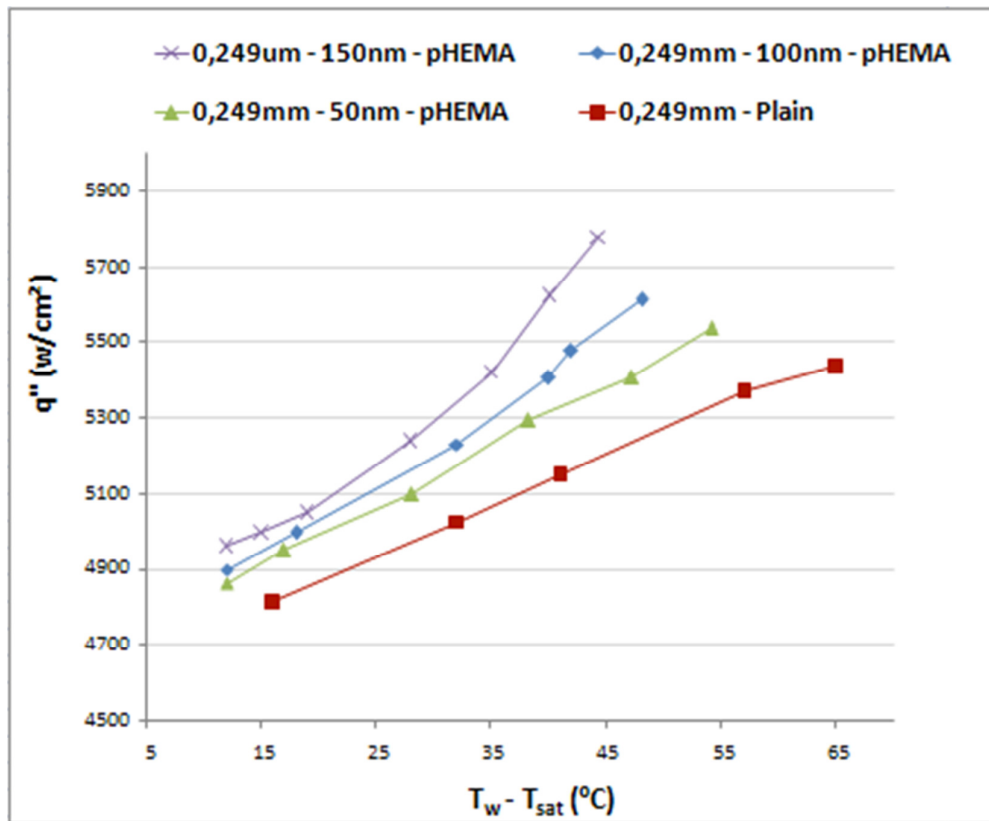


**Figure 3.6:** Boiling Curves for Plain Surface Microtubes and pHEMA Coated Microtubes (50 nm, 100 nm and 150 nm thick coatings) with an Inner Diameter of 249  $\mu\text{m}$  at the Mass Flux of 20,000  $\text{kg}/\text{m}^2\text{s}$ .

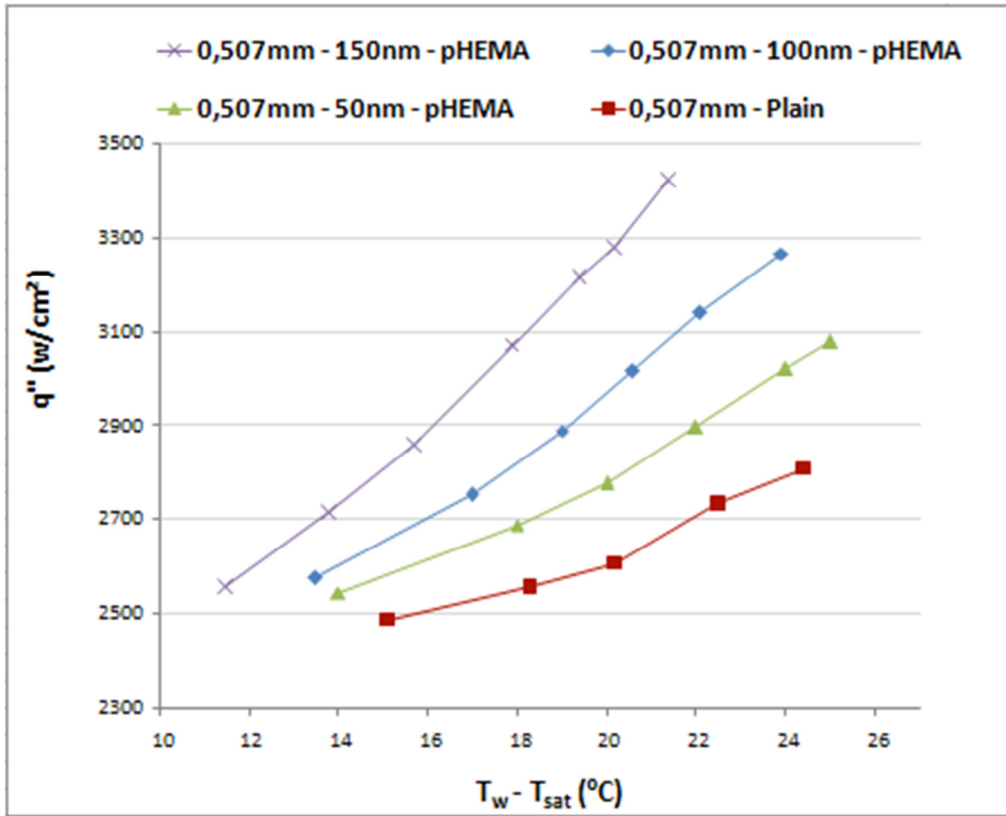


**Figure 3.7:** Boiling Curves for Plain Surface Microtubes and pHEMA Coated Microtubes (50 nm, 100 nm and 150 nm thick coatings) with an Inner Diameter of 507  $\mu$ m at the Mass Flux of 20,000 kg/m<sup>2</sup>s.

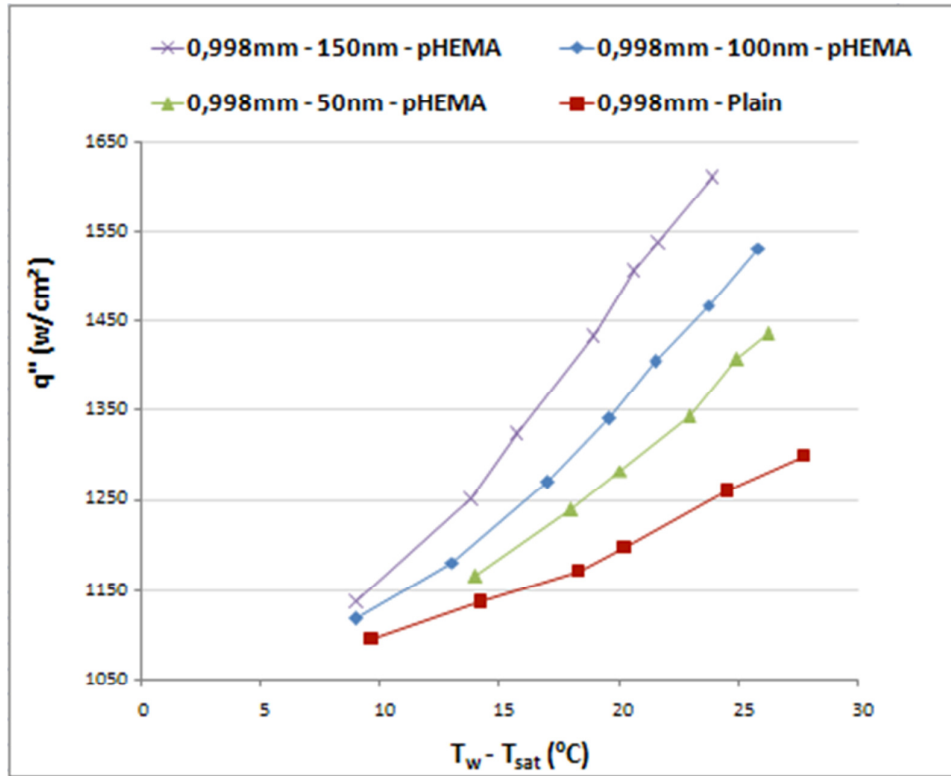


**Figure 3.8:** Boiling Curves for Plain Surface Microtubes and pHEMA Coated Microtubes (50 nm, 100 nm and 150 nm thick coatings) with an Inner Diameter of 998  $\mu\text{m}$  at the Mass Flux of 20,000  $\text{kg}/\text{m}^2\text{s}$ .

Swelling property and smaller contact angle result in CHF improvement in coated tubes. This effect is more dominant for the thickest coating configuration. The contact angle is approximately  $75^\circ$  between flowing water and non-coated microtube wall, while the contact angle is about  $45^\circ$  between water and crosslinked pHEMA coated inner surface. Crosslinked pHEMA coating also results in extra wetting layer on inner microtube walls [105], which can be extended with thicker coatings. For enhanced surfaces, where passive enhancement is performed, suction-evaporation mode exists at higher heat fluxes [106]. In this mode, it was reported that the liquid is sucked through the porous layer on the enhanced surface through inactive pores. Then, this sucked liquid spreads and evaporates from active pores [107]. This mechanism for enhancement is amplified by the capillary-porous structure and structural parameters such as the coating thickness, and porosity. Since crosslinked pHEMA coating offers a highly capillary-porous structure, which is improved with an increase with the coating thickness, CHF condition is delayed with an increase with pHEMA coating thickness [108].



According to the results, it is found that CHF considerably decreases when the microtube diameter increases. Previous studies have similar findings regarding the effects of diameter [99, 109, 110]. Increased bubble velocity relative to the bulk fluid and condensation effects in smaller diameter channels result in an increase in CHF [110]. Moreover, the length of heated tube is significantly large compared to the tube diameter. It is proven that the emerging bubbles occupy a bigger portion of the microtube cross-section especially for small diameters [112]. This interaction between the fluid flow and emerging bubbles may have an effect on flow boiling leading to significant diameter effects on CHF compared to bigger size channels. It can be clearly seen that mass flux has significant effects on CHF according to the experimental results. CHF has an increasing trend with mass flux. In the literature, mass flux effects on CHF were investigated, and it was found that there was an increasing trend in CHF with the mass flux [38, 111, 113, 114]. The underlying mechanisms for DNB (Departure from nucleate boiling) are explained with physical observations such as growing bubbles, vapor clots and bubbles crowding microtubes wall surface. Due to better liquid replenishment to the tube's inner wall at higher mass flux values, the CHF condition is delayed at higher flow rates. Growing bubbles, bubbles crowding channel surfaces, and slugs or vapor clots are possible scenarios for triggering DNB type CHF conditions [115]. Since they can be more easily removed at higher flow rates and more effective liquid replenishment to the tube wall occurs, CHF condition is delayed to higher heat flux values. CHF has a linear relationship with mass flux in contrast to conventional channel results [116], which might be explained by possible bubble-to-channel interactions reported in the literature [117].

### **3.2.2 Heat Transfer Results**

Figures 3.9, 3.10 and 3.11 display experimental two phase heat transfer coefficient profiles at different microtube sizes (249  $\mu\text{m}$ , 507  $\mu\text{m}$  and 908  $\mu\text{m}$ ) and mass flux of 5,000  $\text{kg}/\text{m}^2\text{s}$ .

In Figs. 22a-c, two phase heat transfer coefficients are displayed at the mass flux of 5,000  $\text{kg}/\text{m}^2\text{s}$  for the microtubes having diameters of 249  $\mu\text{m}$ , 507  $\mu\text{m}$  and 908  $\mu\text{m}$ , respectively. According to the results, local two phase heat transfer coefficient (htp-local) considerably increases with pHEMA coating, and it has an increasing trend with the pHEMA coating thickness.

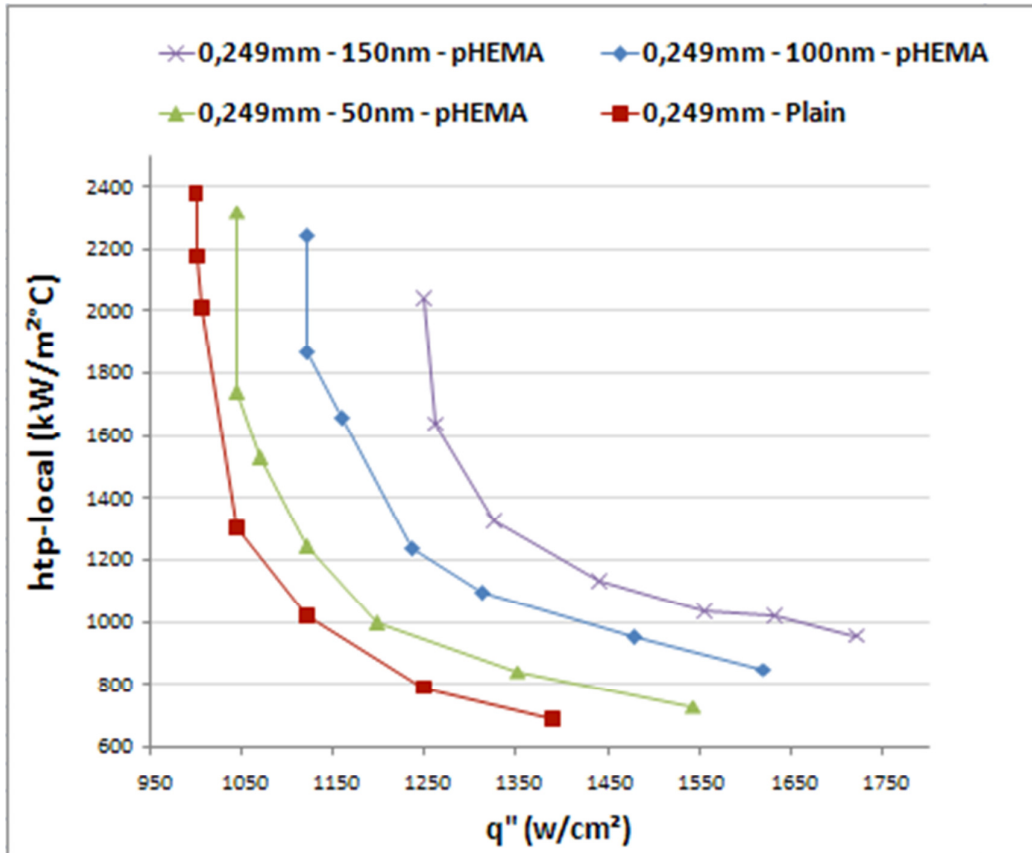


**Figure 3.9:** Two Phase Heat Transfer Coefficient for Plain Surface Microtubes and pHEMA Coated Microtubes (50 nm, 100 nm and 150 nm Thick Coatings) with an Inner Diameter of 249  $\mu\text{m}$  at the Mass Flux of 5,000  $\text{kg}/\text{m}^2\text{s}$

Two phase heat transfer coefficient enhancements up to 97.4 % are obtained in the microtube having the smallest diameter with the thickest configuration, which is because high crosslinker coating thickness increases nucleation site density due to more porous structure and also leads to an increase in bubble generation frequency. Boiling heat transfer (at a fixed heat flux) enhancements up to 85 % and 77,1 % are obtained at the mass flux of 5,000  $\text{kg}/\text{m}^2\text{s}$  for the microtubes of inner diameters of 507  $\mu\text{m}$  and 908  $\mu\text{m}$ , respectively. The largest enhancements are again obtained from the thickest crosslinked pHEMA coated tube configurations.

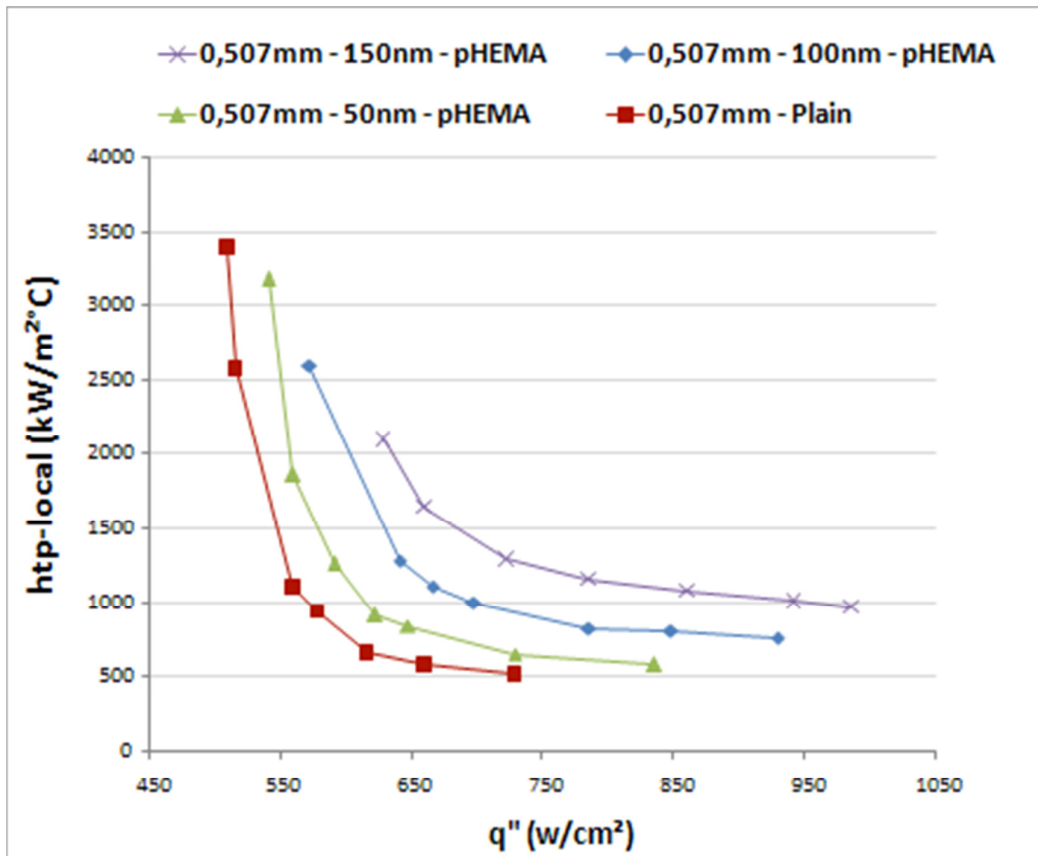


**Figure 3.10:** Two Phase Heat Transfer Coefficient for Plain Surface Microtubes and pHEMA Coated Microtubes (50 nm, 100 nm and 150 nm Thick Coatings) with an Inner Diameter of 507  $\mu\text{m}$  at the Mass Flux of 5,000  $\text{kg/m}^2\text{s}$

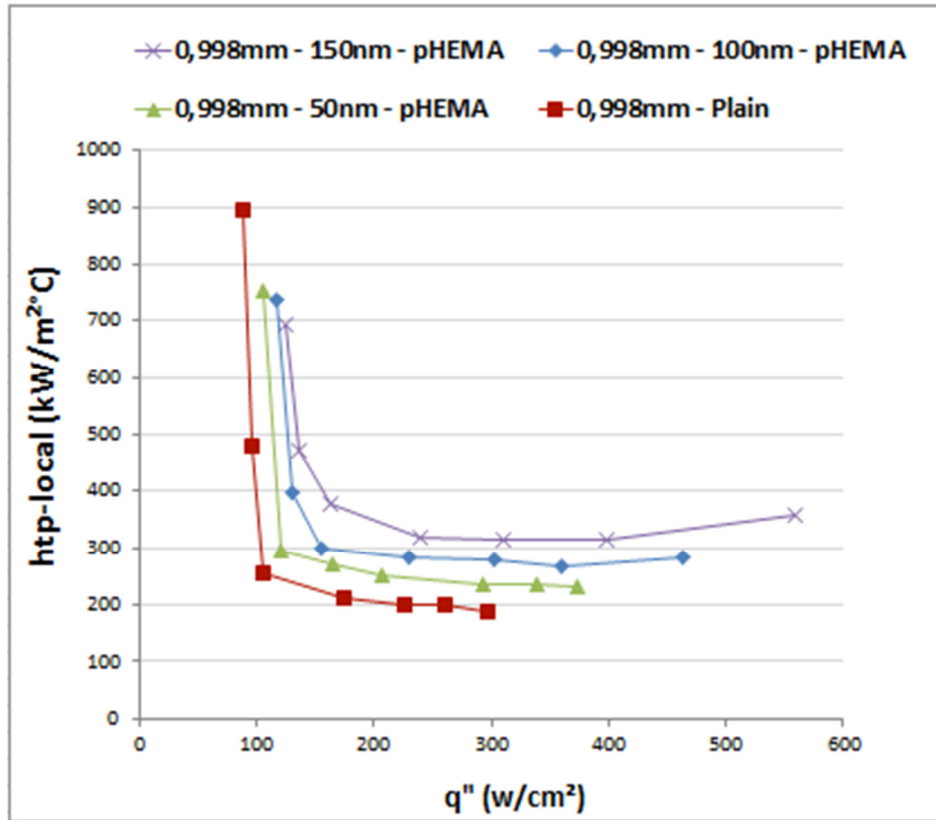


**Figure 3.11:** Two Phase Heat Transfer Coefficient for Plain Surface Microtubes and pHEMA Coated Microtubes (50 nm, 100 nm and 150 nm Thick Coatings) with an Inner Diameter of 507  $\mu\text{m}$  at the Mass Flux of 5,000  $\text{kg}/\text{m}^2\text{s}$

In Figs. 3.12, 3.13 and 3.14 two phase heat transfer coefficients are shown as a function of heat flux performed for microtubes of different inner diameters (249  $\mu\text{m}$ , 507  $\mu\text{m}$  and 908  $\mu\text{m}$ ) and coating thicknesses (50 nm, 100 nm and 150 nm) at the mass flux of  $G=20,000 \text{ kg}/\text{m}^2\text{s}$ . Similar trends in  $h_{tp\text{-local}}$  compared to Figs. 3.9, 3.10 and 3.11 are observed at this mass flux value. As expected, the highest enhancements are attained from the smaller size microtube and the thickest coating. Enhancement ratios in boiling heat transfer coefficients up to 126.2 % are obtained in the smallest size microtube (of diameter of 249  $\mu\text{m}$ ), while maximum enhancements in boiling heat transfer coefficients are 90.1 % and 86.4 % for the microtubes of 507  $\mu\text{m}$  and 908  $\mu\text{m}$  inner diameters, respectively.

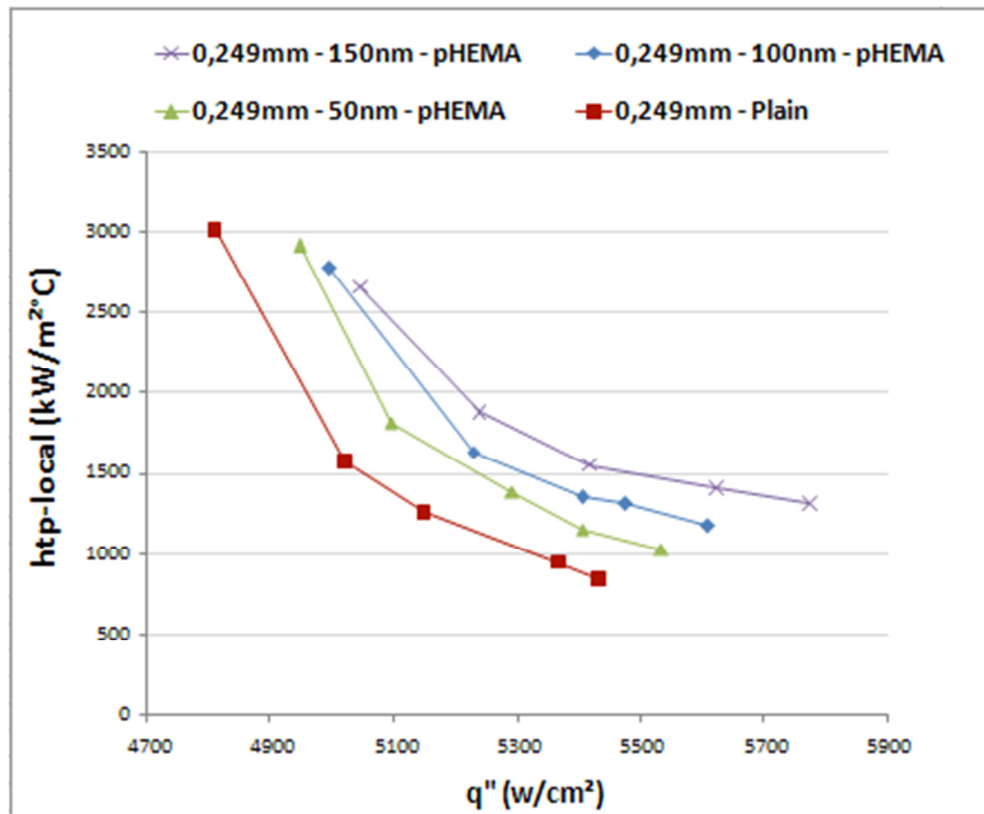


**Figure 3.12:** Two Phase Heat Transfer Coefficient for Plain Surface Microtubes and pHEMA Coated Microtubes (50 nm, 100 nm and 150 nm Thick Coatings) with an Inner Diameter of 249  $\mu\text{m}$  at the Mass Flux of 20,000  $\text{kg}/\text{m}^2\text{s}$

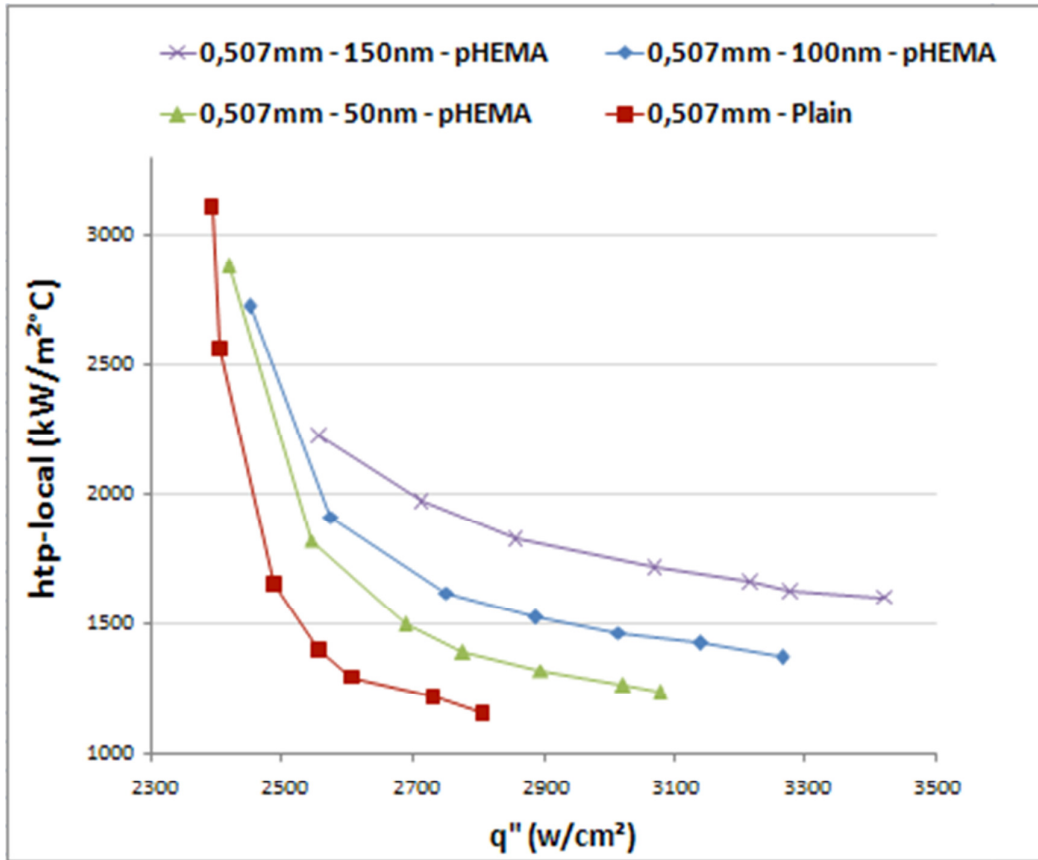


**Figure 3.13:** Two Phase Heat Transfer Coefficient for Plain Surface Microtubes and pHEMA Coated Microtubes (50 nm, 100 nm and 150 nm Thick Coatings) with an Inner Diameter of 507  $\mu\text{m}$  at the Mass Flux of 20,000  $\text{kg/m}^2\text{s}$

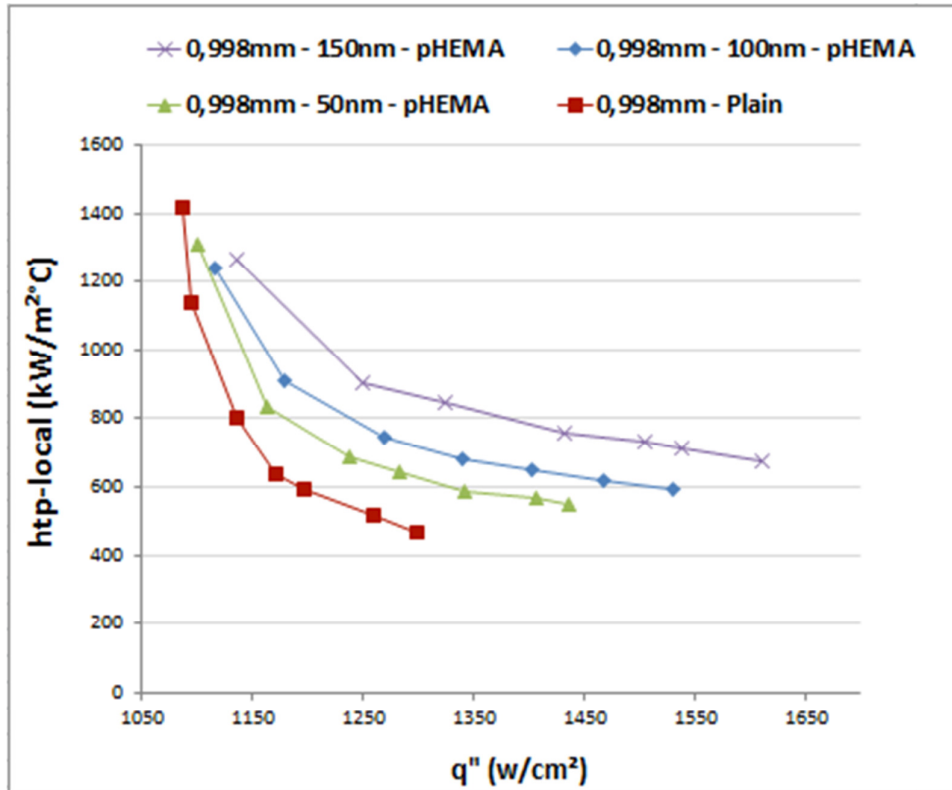


**Figure 3.14:** Two Phase Heat Transfer Coefficient for Plain Surface Microtubes and pHEMA Coated Microtubes (50 nm, 100 nm and 150 nm Thick Coatings) with an Inner Diameter of 998  $\mu\text{m}$  at the Mass Flux of 20,000  $\text{kg}/\text{m}^2\text{s}$

### 3.2.3 Raman Spectroscopy Results

To validate pHEMA is reliable and sustainable method as a stable and durable coating alternative, crosslinked pHEMA coating was tested with Raman Spectroscopy. Raman spectroscopy is a kind of technique based on vibrational spectroscopy and is the most common spectroscopic technique used to assess molecular motion and fingerprinting species. Based on inelastic scattering of a monochromatic excitation source, routine energy range can be up to 200 – 4000  $\text{cm}^{-1}$  [118]. Raman Spectrometry was used for the analysis of pHEMA coatings. Raman spectral analysis was conducted at the Renishaw inVia Raman Microscope attached with a 532 nm green laser and 2400 lines/mm grating. pHEMA coatings were tested apart from the experiments to investigate the strength and reliability. In Figs.3.15 and 3.16, treated and non-treated plates were compared based on Raman spectrum. The pHEMA coated plates were exposed to very high temperature (255°C) by heating the plate using a film heater

for a time period of 87 minutes. Moreover, to observe the impact of pressured water flows on pHEMA coatings, the pHEMA coated plate was manually subjected to water flow ( $G=5,000-20,000 \text{ kg/m}^2\text{s}$  flowing inside  $249 \mu\text{m}$ ,  $507 \mu\text{m}$  and  $998 \mu\text{m}$  microtubes) with the same mass fluxes as under the experimental conditions.

As seen in Fig. 3.16, pHEMA coating was present after the treatment due to a similar Raman spectrum compared to the untreated plate. It was proof of the pHEMA is reliable and sustainable method as a stable and durable coating alternative. According to Fig. 3.16, the biggest band appearing at  $2952 \text{ cm}^{-1}$  is due to the  $\nu$  as  $\text{CH}_2$  stretching mode [119]. It is known that between  $2800 - 3100 \text{ cm}^{-1}$  valence vibrations of  $\text{CH}_2$  and  $\text{CH}_3$  were becoming dominant [120]. The Raman peak located at  $1454 \text{ cm}^{-1}$  result from the deformation of C-H group. It is critical to analyze if the spectrum contains any C=C related Raman peak. Because the polymer inside the tubes was deposited with free radical polymerization the C=C bonds were expected to be broken during the synthesis. HEMA produces 2 significant C=C related Raman peaks:  $1280 \text{ cm}^{-1}$  ( $\text{C}=\text{CH}_2$  stretching vibration) and  $1454 \text{ cm}^{-1}$  (C=C aliphatic stretching vibration). The absence of these peaks proves that C=C bonds in the methacrylate group were opened forming pHEMA chains. Other peaks and corresponding modes were as follows:  $1730 \text{ cm}^{-1}$  ( $\nu\text{C}=\text{O}$ ),  $636 \text{ cm}^{-1}$  ( $\nu\text{sCCO}$ ) and  $964 \text{ cm}^{-1}$  ( $\rho\text{CH}_3$ ) ( $\nu$ : stretching,  $\rho$ : rocking, s: symmetric, as: asymmetric) [121].

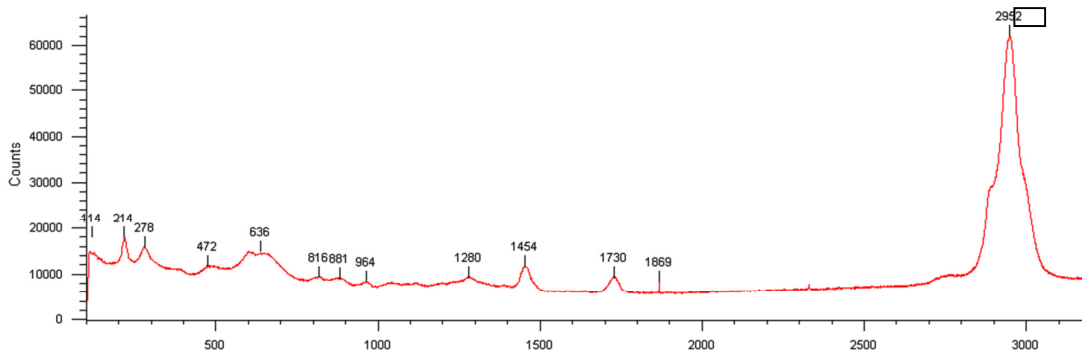


**Figure 3.15:** Raman Spectrum Taken from the Inner Surface of the Untreated Sample Microtube Having  $249 \mu\text{m}$  Inner Diameters



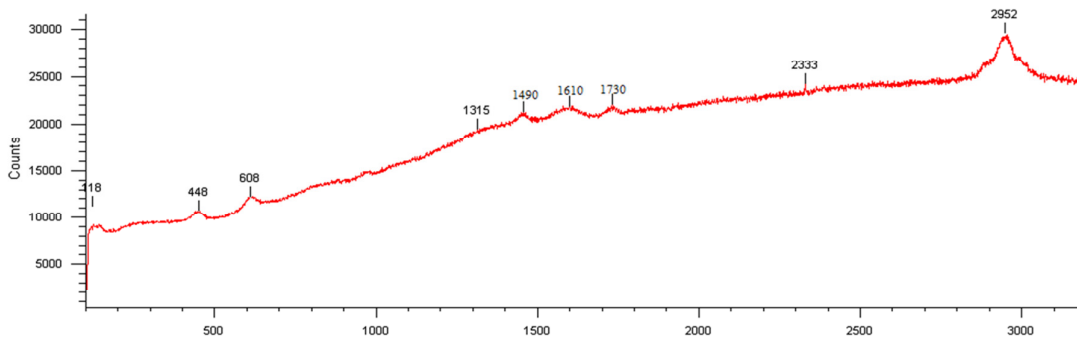


**Figure 3.16:** Raman Spectrum Taken from the Inner Surface of the Treated Sample Microtube Having 249  $\mu\text{m}$  Inner Diameters

### 3.2.4 Visualization Tests

In order to verify a crosslinked pHEMA coating is durable and improve boiling heat transfer, visualization tests were performed. In the literature, the advantages of nanostructure coating and deposition on boiling heat transfer were extensively discussed [122-123]. The underlying mechanism for enhanced boiling heat transfer performance with crosslinked pHEMA coating may be attributed to its ability of increasing the nucleation site density by providing more active nucleation sites because of its very porous structure and by enhancing incidence of bubble occurring from surface which is more dominant for thicker coatings.

In the visualization tests, the applied heat flux was fixed to  $40 \text{ W/cm}^2$  for both non-coated and pHEMA coated plate surfaces, which were heated by cartridge heaters in a pool with transparent sides (Fig. 3.17). A Phantom V310 high speed camera was used for this task, while the image resolution, sample rate, and exposure time were  $1200 \times 800$  pixels, 2800 fps, and 100  $\mu\text{s}$ , respectively. Images were recorded for approximately 60 seconds for an applied heat flux, which was selected to monitor the performance of the plates at the isolated bubble regimes.

In order to observe plates from the lateral side, the experimental setup made of glass was prepared. An aluminium base (19 mm x 19 mm) was constructed for a cartridge heater of length of 19.25 mm and of a diameter of 4.5 mm. The base was also surrounded with glass walls with height of 20 cm to have a similar shape as pool. To prevent any leakage, the setup was sealed with liquid gasket. Moreover, pHEMA and non-coated plates were placed at on the surface of the bottom of aluminium base with Omega® Bond thermal grease. For determining the average bubble departure frequency from the plates, total number of emerged bubbles from plates were counted and averaged over monitoring time. Average bubble departure diameter from both pHEMA and non-coated plates were calculated by measuring the diameter of each bubble individually and averaging the sum of all diameters over the total number of emerged bubbles. The reliability of data was proven with long recording time since a cycle of bubble growth and release has an order of magnitude of milliseconds.

Figures 3.18 and 3.19 displaying bubbles emerging from non-coated and pHEMA coated (with a coating thickness of 150 nm) surfaces. As can be seen from the figures, at 40 W/cm<sup>2</sup> heat flux (at ~9.5 K wall superheat) more individual bubbles emerged for the pHEMA coated plate (~3 and ~7 bubbles were emerging on average from 1cm<sup>2</sup> hot plate for non-coated and pHEMA coated plates, respectively). The duration of a bubble growth cycle is also shorter for the pHEMA coated surface (~10 ms) compared to the non-coated surface (~50 ms). The bubble departure diameters are ~2 mm and ~4 mm for non-coated and pHEMA coated plates, respectively. From the figures, it is clear that pHEMA coated plate increases the number of the nucleation site significantly compared to non-coated plate, and these figures serve as a proof of boiling heat transfer enhancement on coated surfaces.

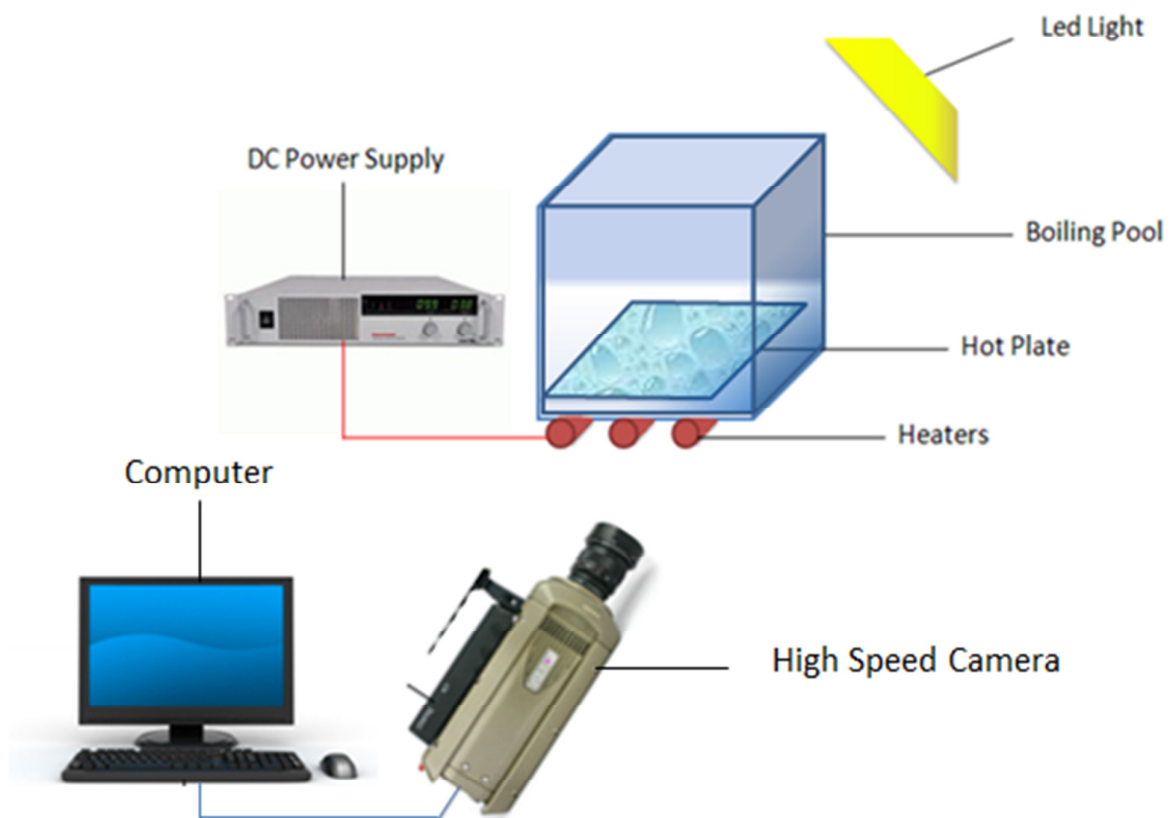


**Figure 3.17:** The Schematic of the Experimental Setup for Visualization

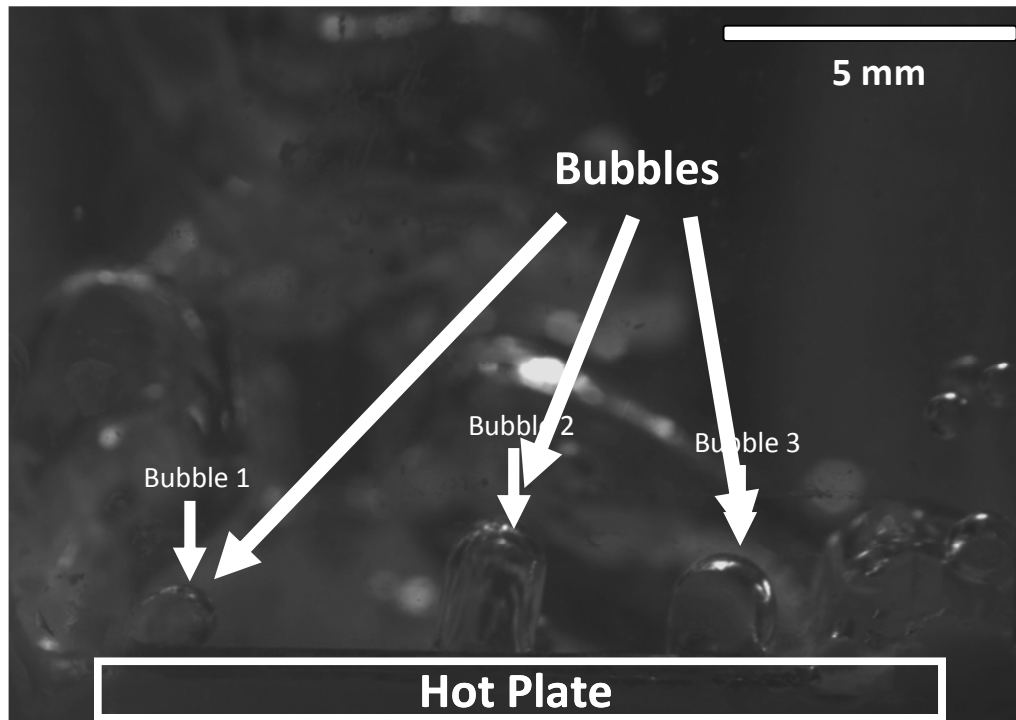


**Figure 3.18:** Bubbles emerging from the non-coated Plate

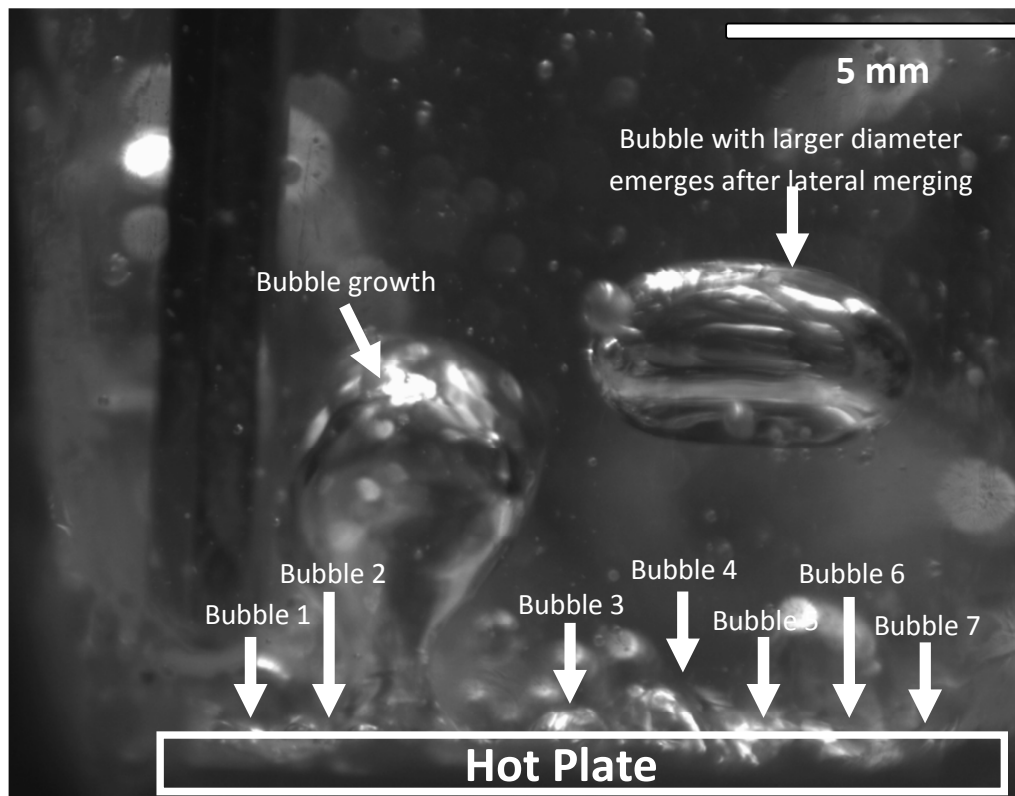


**Figure 3.19:** Bubbles emerging from the Crosslinked pHEMA Coated Plate

The results prove that crosslinked pHEMA coatings improve boiling heat transfer for micro scale cooling applications, where enhancement may be not possible with common surface enhancement and micro fabrication methods. This method may provide a feasible solution, when geometrical modifications are not possible with physical deposition methods in cases such as closed geometries.

### **3.3 Third Part - Varying Magnetic Field on Targeted Gene Delivery of Nucleic Acid-Based Molecules**

#### **3.3.1 PEI Transfection Results**

Before PEI-SPION transfection via miniature magnetic actuation device test, non-viral transfection agents of Polyethyleneimine (PEI) were transfected to the targeted PC-3 cells to validate single PEI complexes could be transfected without any complication and toxicity. The results were validated with different experimental combination, which contain different ratio of DNA and PEI molecules. During the experiments, different amounts of DNA (0.5 g/ml, 1 g/ml, 2 g/ml and 2.5 g/ml) molecules and GFP (Green Fluorescent Proteins) (5, 10, 20, and 25 microgram) complexes were tested. The largest PEI transfection efficiency is obtained ~50 % at 2.5 g/ml DNA with 25 microgram PEI (Fig. 3.20) while the minimum transfection is found ~10 % at 0.5 g/ml DNA with 5 microgram PEI (Fig. 3.21). In both figures, green bright spots are representing transfected PEI complexes on PC-3 cells. Experimental results revealed that the transfection efficiency was dramatically increased in the experiment having combination of 2.5 g/ml DNA with 25 microgram PEI. On the other hand, there are only few particles transfected for the experiment has minimum transfection efficiency. The combination that gives maximum transfection efficiency is used in PEI-SPION transfection experiments.

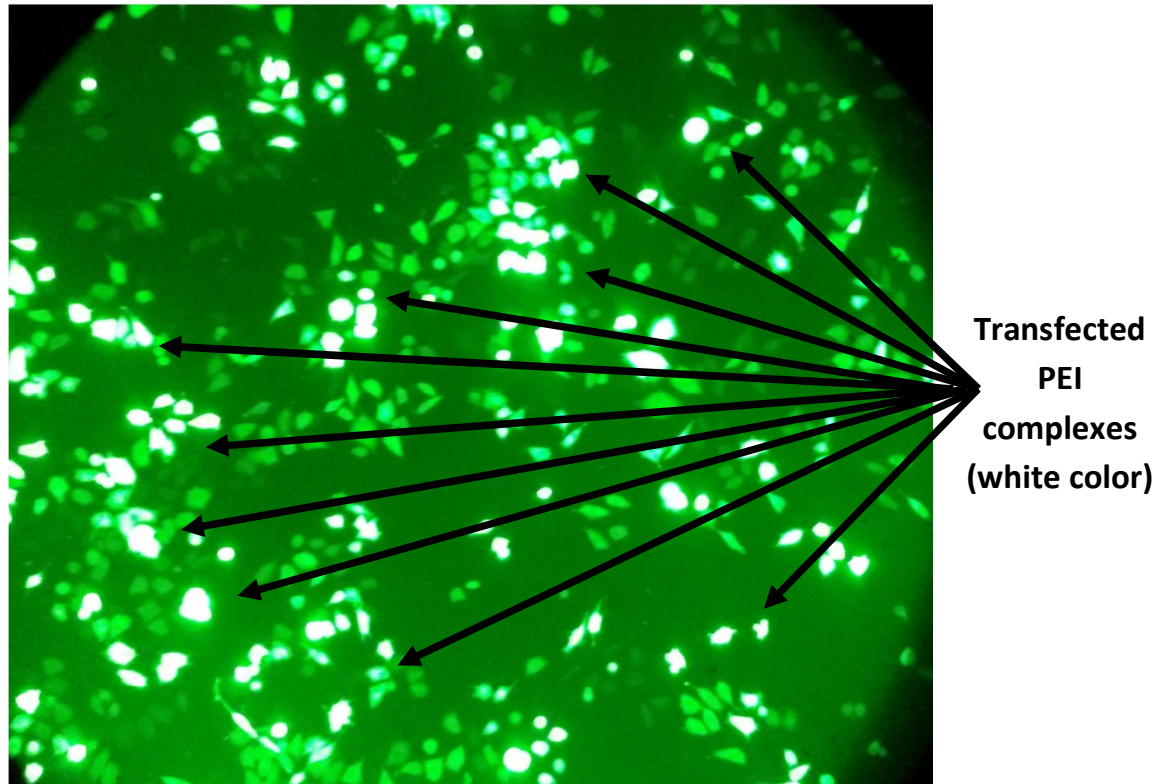


**Figure 3.20:** Transfection results of 2.5 g/ml DNA with 25 microgram PEI

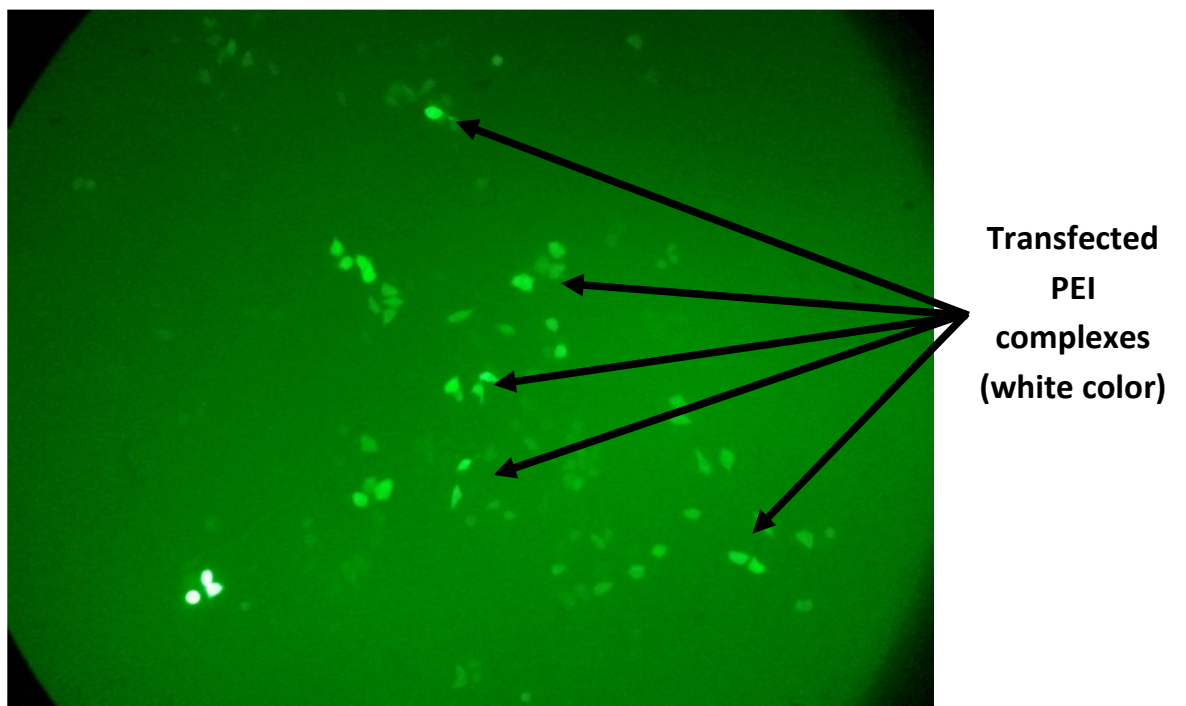


**Figure 3.21:** Transfection results of 0.5 g/ml DNA with 5 microgram PEI

### 3.3.2 PEI – SPION Transfection Results

In order to investigate effect of varying magnetic fields on targeted gene delivery of nucleic acid-based molecules, experiments are conducted using the miniature magnetic actuation device under various test conditions. Accordingly, the experimental tests are performed with different magnetic rotor turn velocities varying from 0.108 to 0.216 m/s when the supplied voltage was 12 V and currents were 2.1 Amp and 4.2 Amp, respectively. The miniature magnetic actuation device during the experiment is shown in Fig. 3.22. In order to assess the relationship between magnetic rotor velocity and supplied power, calculated voltage/current curve is given in Fig. 3.23.

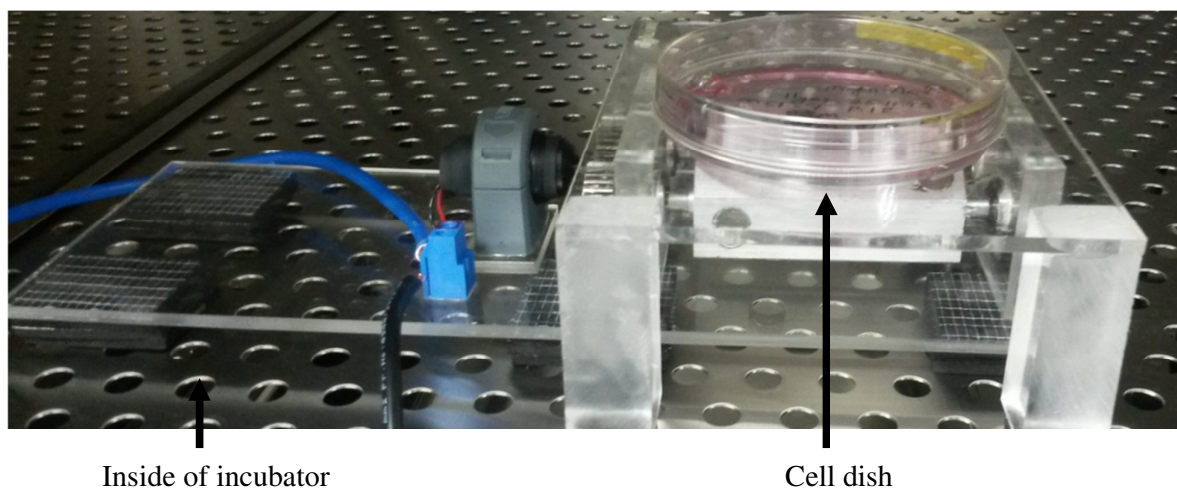


**Figure 3.22:** Magnetic actuator setup inside incubator at 37 C°



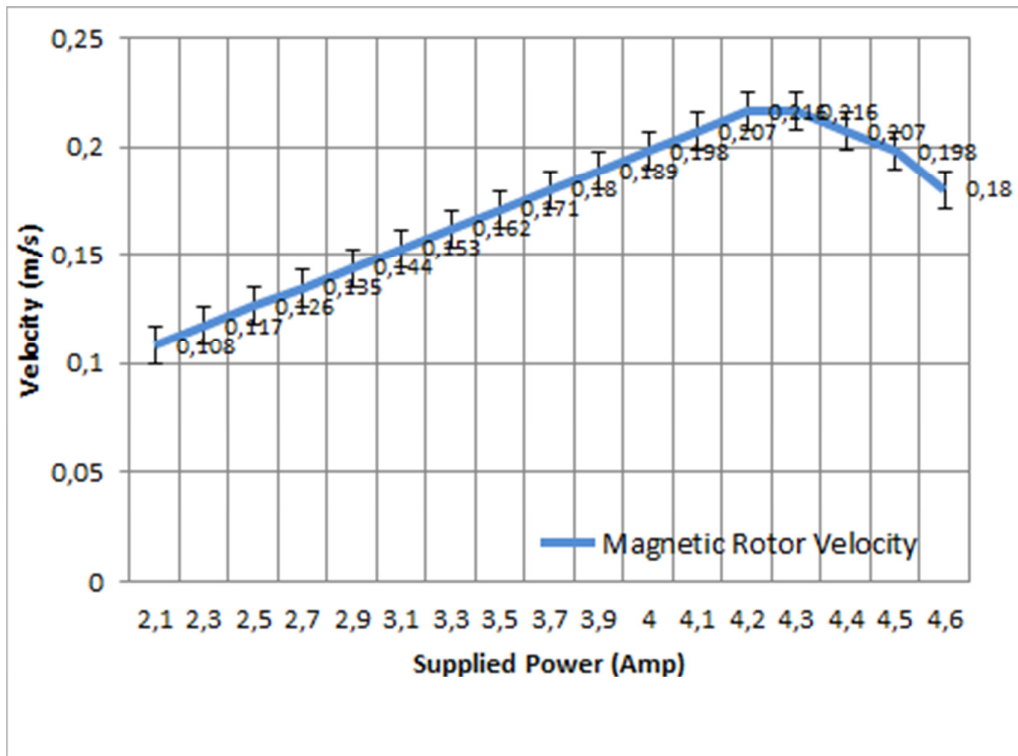


**Figure 3.23:** Power vs velocity curve for magnetic rotors

The use of PEI-SPION (Super paramagnetic iron oxide nanoparticles) as transfection agents in in vitro studies was investigated with the effect of varying magnetic fields provided by a special magnetic system design, which was used as magnetic actuator offering different magnet's turn speeds in the system. PEI complexes bind to DNA via the electrostatic binding interaction between secondary amine groups of PEI and phosphate backbone of DNA. On the other hand, PEI complexes bind to DNA via the electrostatic binding interaction between secondary amine groups of PEI and phosphate backbone of DNA [124]. In the relevant literature [125], it was showed that silica layer over iron oxide core can easily bind to amine groups of PEI with amine-to-silica interaction.

In order to assess magnetic field effect on targeted gene delivery, MCF-7 breast cancer cells and PC-3 prostate cancer cells were chosen as targeted cell to perform gene delivery. pMAX-GFP plasmid DNA was utilized to transfect cells by using PEI-SPION complex. MCF-7 cells were illustrated in Fig. 3.24. Both cancer cells in cell culture medium inside cell dish were viewed via Carl-Zeiss Primo Star microscope before and after experiments. The images were taken with 10X zoom under high brightness of UV (ultraviolet) light.



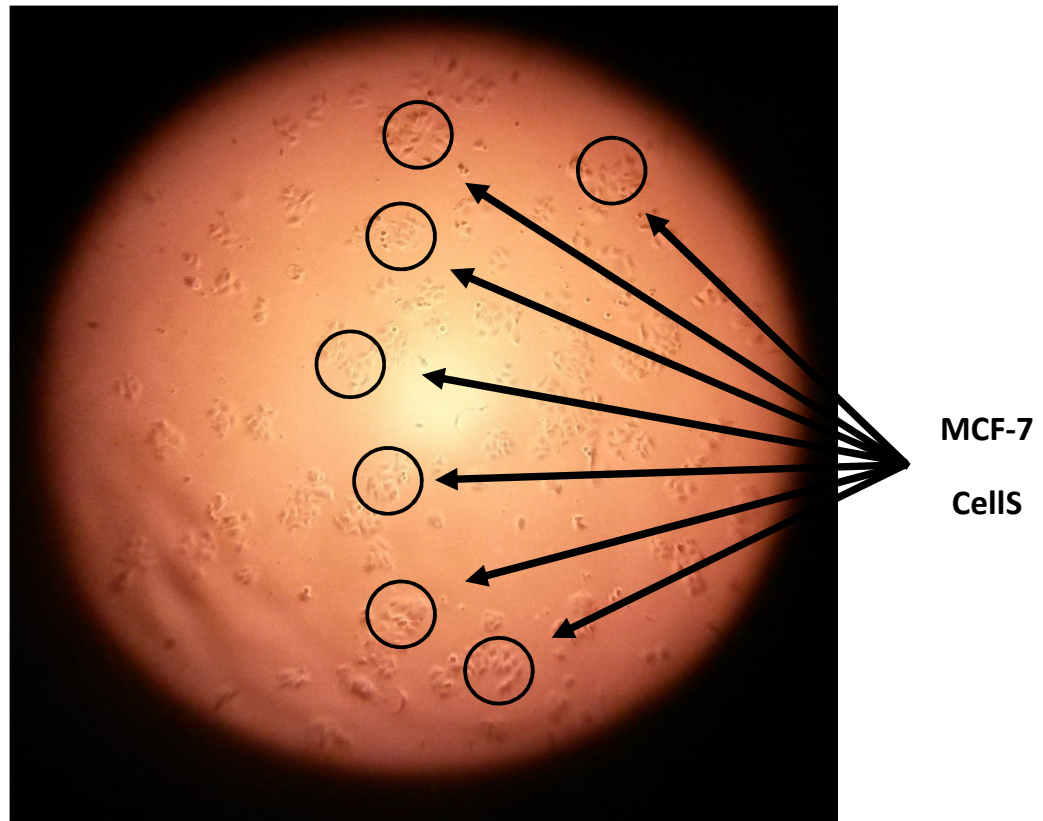


**Figure 3.24:** MCF-7 Breast Cancer Cells

The experiments were conducted under temperature of 37 C° inside incubator. To understand magnetic field effects on transfection, cells were exposed magnetic field 6 hours. Cells were checked under the microscope after 24 hours post-transfection.

Experimental results, were obtained via miniature magnetic actuation device, were compared to their counterpart experiment under non-magnetic field conditions. Significant enhancements for targeted gene delivery were attained for both cells. In figures 3.25 & 3.26, experimental results of magnetic and non-magnetic conditions of MCF-7 cells under fluorescent light and light microscopy image were shown, respectively. The maximum transfection efficiency is obtained ~30% for MCF-7 cells under magnetic field when it is ~25% for non-magnetic field.

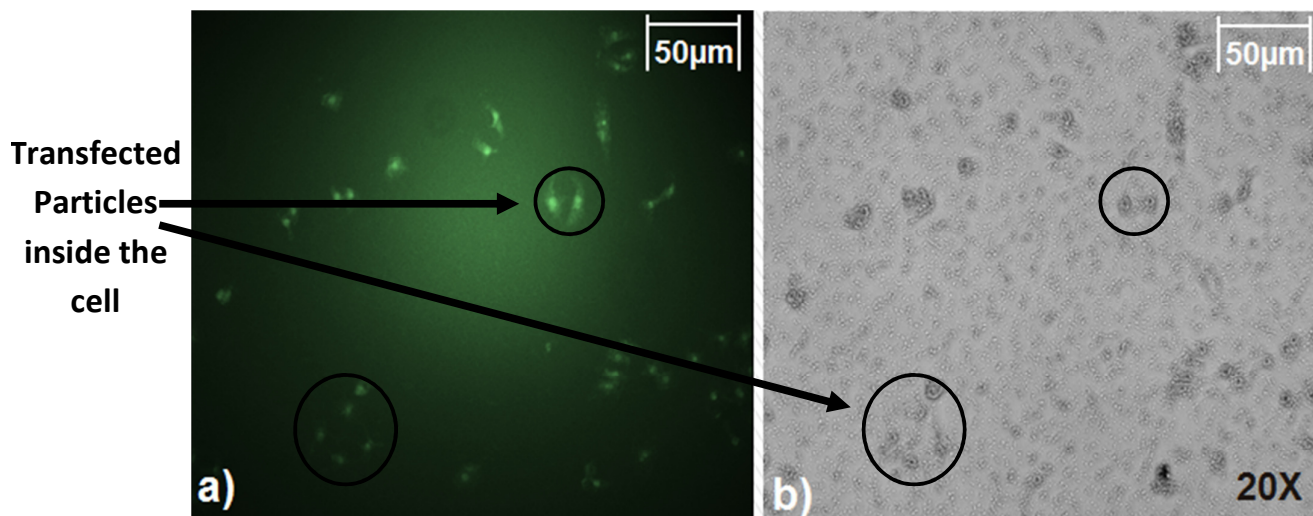


**Figure 3.25:** Experimental results without device MCF-7 cell under Fluorescent light (a) and light microscopy (b) image

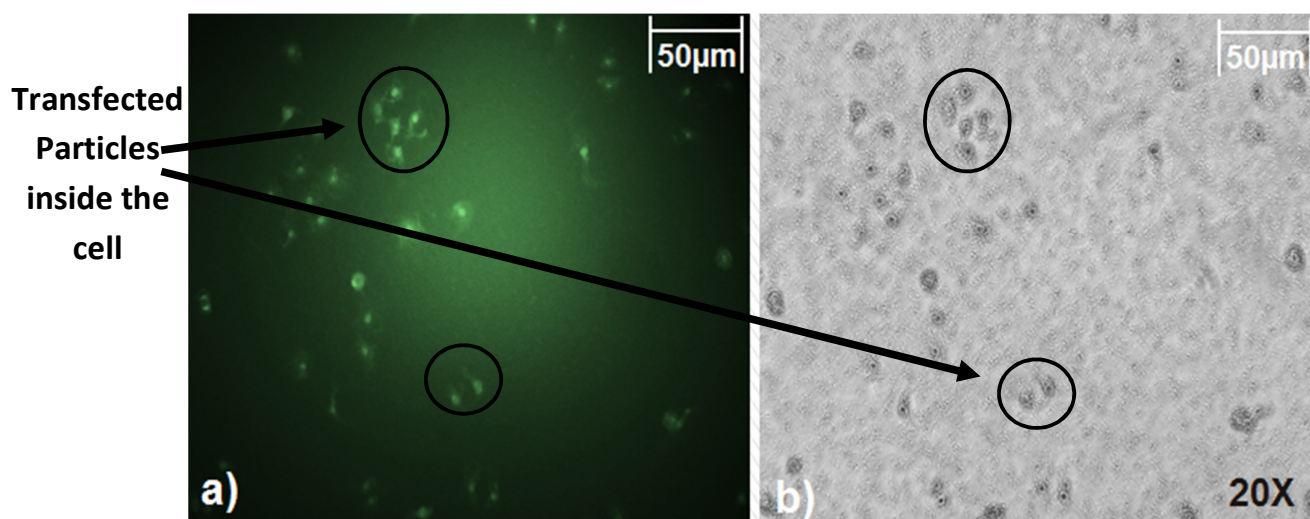


**Figure 3.26:** Experimental results with device MCF-7 cell under Fluorescent light (a) and light microscopy

Transfection results for PC-3 cells were shown in Fig. 3.26. The maximum transfection efficiency is reached ~25% and ~20% for magnetic and non-magnetic field respectively.

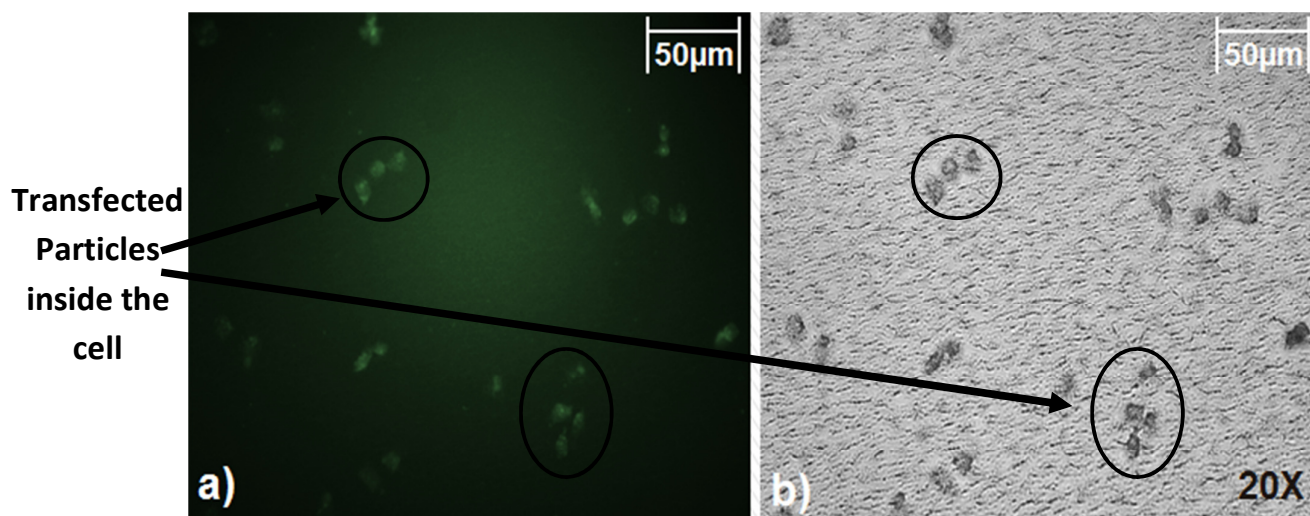


**Figure 3.27:** Experimental results without device PC-3 cell under Fluorescent light (a) and light microscopy (b) image

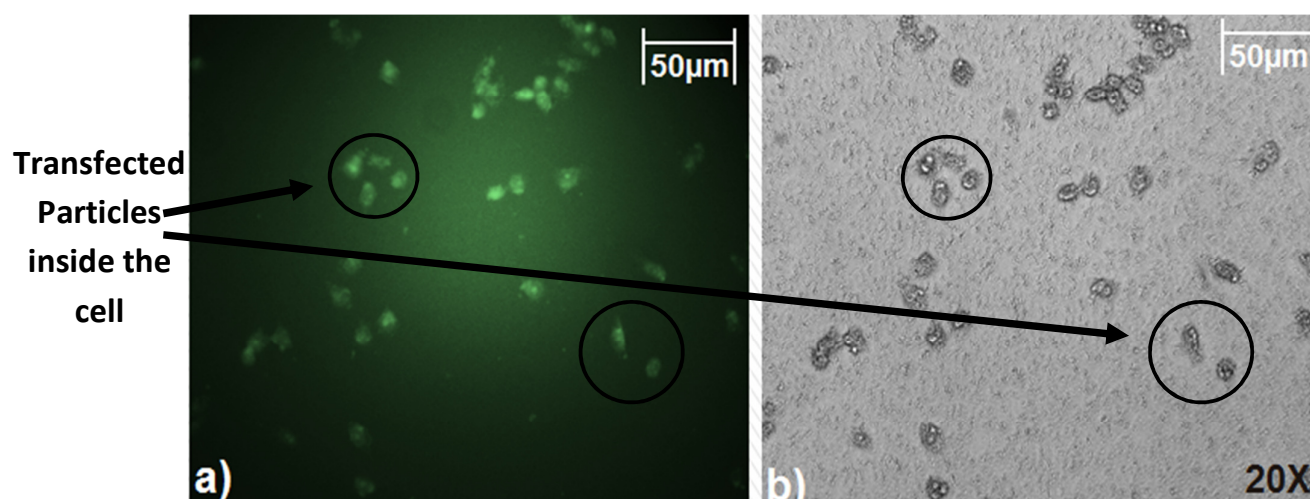


**Figure 3.28:** Experimental results with PC-3 cell under Fluorescent light (a) and light microscopy (b) image

In previous studies, PEG (Polyethyleneglycol)-PEI-SPION was used for transfection agent in SGC-7901 (Human Gastric Carcinoma) cell line [126]. This work showed that PEI-SPION (Polyethyleneimine – Super Paramagnetic Iron Oxide Nanoparticles) can be perfect candidate for gene delivery of nucleic acid based molecules as being transfection agents in in vitro studies. Positive effect of magnetic field could be turned to account by magnetic manipulation with miniature magnetic actuation device. It is proven that several RNAs with interference properties on gene regulation (e.g. miRNAs, siRNAs) can be used for further studies for gene regulation of human breast and prostate cancer cells for treatment purposes.

## MAJOR FINDINGS

- Energy efficient miniature devices could be utilised for energy harvesting, thermal management and biomedical applications involving academic research, industrial processes, medical surgeries and daily operations.
- An energy efficient miniature power reclamation device is uniquely designed by taking inspiration from Black Ghost Knife Fish for underwater usages, which require electricity.
- The miniature power reclamation device could be used for military and security purposes and serve for a power source for GPS and lighting especially at locations, which are not easily accessible due to depth, flow and unreachable coordinates.
- Global warming effects could be observed with miniature power reclamation device as monitoring changes under the water.
- A miniature system is developed for flow boiling enhancement in microtubes with crosslinked pHEMA coatings having different coating thicknesses. Significant enhancements in CHF (Critical Heat Flux) (up to 29.7%) and boiling heat transfer (up to 126.2%) were attained.
- The miniature flow boiling investigation system revealed significant enhanced features offered by crosslinked pHEMA coatings such increasing swelling property, nucleation site density and bubble generation frequency.
- Thanks to the miniature flow boiling investigation system, iCVD was proven to be a very practical method for pHEMA coatings in micro scale channels/tubes, in which the application of existing conventional methods is limited.
- The enhancements in boiling heat transfer and critical heat flux, which are obtained via miniature flow boiling investigation system, could be utilized for offering more efficient cooling and heating systems.
- The miniature flow boiling system could be supported by the visualization tests to validate durability and sustainability.
- A miniature magnetic actuation device is developed for investigation of effect of varying magnetic fields on targeted gene delivery of nucleic acid-based molecules. Significant enhancements of targeted gene delivery were attained for MCF-7 (Human breast cancer cells) and PC-3 (Human prostate cancer cells). The maximum transfection efficiency is obtained as ~30% for MCF-7 cells under magnetic field

while it is ~25% for the absence of magnetic field. On the other hand, transfection efficiency is ~25% and ~20% for PC-3 cells, respectively.

- The miniature magnetic actuation device provides continuous magnetic field in both vertical and horizontal directions due to magnetic vortices and enhanced magnetic rotor speed control. Thanks to improved control ability, durability and less system complexity, it could be utilized in biomedical engineering.
- The miniature magnetic actuation device demonstrated that PEI-SPION (Polyethyleneimine – Super Paramagnetic Iron Oxide Nanoparticles) can be a perfect candidate for gene delivery of nucleic acid based molecules as being transfection agents in in - vitro studies. Positive effects on the results with varying magnetic fields could be realized with the miniature magnetic actuation device.

## CHAPTER 4

### CONTRIBUTION TO THE SCIENTIFIC KNOWLEDGE

The need for more efficient and practical solutions for emerging areas such energy harvesting, thermal management and biomedical applications is continuously increasing. Miniature devices and related compact systems offer efficient tools for overcoming this need. The experimental investigations performed in this thesis study are aimed to contribute to the literature in the design and develop of futuristic energy efficient miniature devices.

The first part, a miniature energy harvesting device, contributes to scientific knowledge by:

- Proposing a miniature energy harvesting device could be used for underwater usage such as wild life observation, military and security applications, requiring electricity and places which are not easily accessible due to depth, flow and unreachable coordinates.
- Providing important simulation model and experimental data for understanding behaviour of a miniature device tail in aqueous medium.
- Helping observation for global warming effects by observing the displacement of deep currents and icebergs.

The second part, a miniature flow boiling system, contributes to scientific knowledge by:

- Proving that pHEMA coating on microchannel can increase the boiling heat transfer performance, offer more active nucleation sites and enhance the CHF value, by forming an extra wetting layer and porous structure on tube walls due to its swelling property in aqueous medium.
- Showing that iCVD is a useful tool for coating microchannel having various hydraulic diameters because of its 3D coating capability.

The third part, a miniature magnetic actuator, contributes to scientific knowledge by:

- Proposing a miniature magnetic actuator device could be used for delivery of necessary drugs and genes for patients and their transport under safe conditions.

- Proposing a compact system that could operate with low energy consumption, low waste disposal, and parallel and fast processing capability and high mixing capacity.
- Providing significant data for cancer treatment methodology.



## CHAPTER 5

### CONCLUSIONS

In the first part, energy harvesting capability of a miniature power reclamation device based on external liquid flows was investigated. The tails of the device vibrate as a result of external flows and translate energy to the mini generators, which harvest energy due to magnetic polarizations. Experimental tests were performed within a range of flow velocities (1.0 m/s ~ 5.0 m/s) for various fluid densities (plain water, low-salt and high-salt water). A device tail was simulated to estimate the maximum possible reclaimable power using COMSOL Multiphysics 4.2 software. It was observed that the reclaimed power was directly proportional to fluid velocity, and fluid concentration had a negative effect on the reclaimed power. Promising results related to energy harvesting results were obtained. Accordingly, the device could generate power of 17.2W, while the maximum reclaimable power was obtained as 25.7W. This device could be uniquely designed for the underwater usages such as wild life observation, military and security applications, requiring electricity. In such applications, the aim is to produce energy on those locations, which are not easily accessible due to depth, flow and unreachable coordinates. Moreover, the effects of global warming could be also sensed with the help of the proposed device by observing the displacement of deep currents and icebergs. Besides, the output energy from the device could be utilized as a power source for both lighting and GPS location devices installed on buoys in open sea.

In the second part, flow boiling heat transfer performance was investigated in microtubes with different crosslinked pHEMA coating thicknesses (50nm, 100nm and 150nm) and in plain microtubes having inner diameters of 249  $\mu\text{m}$ , 507  $\mu\text{m}$  and 908  $\mu\text{m}$  at mass fluxes of 5,000  $\text{kg/m}^2\text{s}$  and 20,000  $\text{kg/m}^2\text{s}$ . Significant increase in CHF (critical heat flux) and heat transfer coefficient with crosslink pHEMA coatings were obtained. The major findings of this study are as follows:

- The swelling property of the pHEMA coatings has a positive effect on CHF due to the resulting increase in surface wettability.
- Larger coating thicknesses result in larger increase in CHF.



- Crosslinked pHEMA coating improves boiling heat transfer performance since it increases the nucleation site density by offering more active nucleation sites due to its porous structure, raises bubble generation frequency from the surface, and improves liquid replenishment to the surface after bubble departures. This effect is more pronounced for thicker coatings.
- iCVD was proven to be a very practical method for pHEMA coatings in micro scale channels/tubes, in which the application of existing conventional methods is limited.
- The results were supported by the visualization tests performed on both plain and pHEMA coated rectangular plates.

In the third part, a platform for gene delivery via magnetic actuation of nanoparticles was developed. PEI-SPION (Super paramagnetic iron oxide nanoparticles) was investigated as transfection agents in in vitro studies with the effect of varying magnetic fields offered by a miniature magnetic actuator design. The proposed device could be used as an energy efficient magnetic actuator, which offers different magnet's turn speeds. The major findings of this study are as follows:

- Magnetic field has a positive effect on targeted gene delivery of nucleic acid-based PEI-SPION molecules.
- Higher magnet's turn speed result in higher transfection rate.
- Transfection rate is independent of magnet's turn direction.
- It is proven that the miniature magnetic actuator setup could be used for investigation of transfection agents in both in-vitro and in-vivo studies.
- It is proven that the miniature magnetic actuator could deliver drug and genes to the targeted cell with low energy consumption, low waste disposal, and parallel and fast processing capacity, high mixing capability, and enhanced safety.

## REFERENCES

- [1] Justin R.F., 2007, “A comparison of power harvesting techniques and related energy storage issues”, Master of Science Thesis; Department of Mechanical Engineering, Virginia Polytechnic Institute and State University, Blacksburg, VA
- [2] Blatt F.J., Schroeder F.A., Foiles C.L., Greig D., 1976, “Thermoelectric power of materials”, New York: Plenum Press, pp. 136 - 155
- [3] Myers R.L., 2006, “The basics of physics”, 18<sup>th</sup> IEEE International Micro Electro Mechanical Systems Conference and Exhibition: Westport, CT, USA
- [4] Elliot R.S., 1993, “Electromagnetics: history, theory, and applications”, IEEE Press Piscataway; pp. 73-92
- [5] Wang D.A., Ko H.H., 2010, “Piezoelectric energy harvesting from flow-induced vibration”. *Journal of Micromechanics and Microengineering*, **20**, pp. 254 – 263.
- [6] Aureli M., Prince C., Porfiri M., Peterson S.D., 2010, “Energy harvesting from base excitation of ionic polymer metal composites in fluid environments”, *Smart Materials & Structures*, **19**, 32 – 45.
- [7] Hobbs W.B., Hu D.L., 2011, “Tree-inspired piezoelectric energy harvesting”, *Journal of Fluids and Structures*, **20**, pp. 1-12
- [8] Song J., Zhou J., Wang Z.L., 2006, “Piezoelectric and semiconducting coupled power generating process of a single ZnO belt/wire: A technology for harvesting electricity from the environment”, *Nano letters*, **6**, pp. 1656–1662
- [9] Howels C.A., 2009, “Piezoelectric harvesting”, *Energy Conversion and Management*; **50**, pp. 1847-1850
- [10] Tang L., Paidoussis M.P., Jiang J., 2009, “Cantilevered flexible plates in axial flow: Energy transfer and the concept of flutter-mill”, *Journal of Sound and Vibration*, **326**, pp. 263-276
- [11] Akaydin H.D., Elvin N., Andreopoulos Y., 2009, “Energy harvesting from highly unsteady fluid flows using piezoelectric materials”. *Journal of Intelligent Material Systems and Structures*, **21**, pp. 1263–1278
- [12] Giacomello A., Porfiri M., 2011, “Underwater energy harvesting from a heavy flag hosting ionic polymer metal composites”, *Journal of Applied Physics*, **109**, pp. 633 – 642.

- [13] Vanderpool D., Yoon J.H., Pilon L., 2008, “Simulations of a prototypical device using pyroelectric materials for harvesting waste heat”, *International Journal of Heat and Mass Transfer*, **51**, pp. 5052–5062.
- [14] Boland J., Yuan-Heng C., Suzuki Y., Tai Y.C., 2003, “Micro electret power generator”, 16<sup>th</sup> IEEE International Micro Electro Mechanical Systems Conference and Exhibition: Kyoto, JAPAN
- [15] Muselli M., Notton G., Louche A., 1999, “Design of hybrid – photovoltaic power generator, with optimization of energy management”, Centre de Recherche Energie et Systèmes
- [16] Taylor G.W., Burns J.R., Kammann S.A., Powers W.B., Welsh T.R., 2001, “The energy harvesting eel: a small subsurface ocean/river power generator”, *IEEE Journal of Applied Physics*; **11**, pp. 101–143
- [17] Kulah H., Najafi K., 2004, “An electromagnetic micro power generator for low-frequency environmental vibrations”, 17<sup>th</sup> IEEE International Micro Electro Mechanical Systems Conference and Exhibition: Maastricht, NETHERLANDS
- [18] Wiegele T.G., 1996, “Micro-turbo-generator design and fabrication: a preliminary study”, 31<sup>st</sup> Energy Conversion Engineering Conference IECEC 96 - Proceedings of the 31st Intersociety: Washington DC, USA
- [19] Tsutsumino T., Suzuki Y., Kasagi N., Sakane Y., 2006, “Seismic power generator using high-performance polymer electret”, 19<sup>th</sup> IEEE International Micro Electro Mechanical Systems Conference and Exhibition: Istanbul, TURKEY
- [20] Jeon Y.B., Sood R., Jeong J.H., Kim S.G., 2005, “MEMS power generator with transverse mode thin film PZT”, *Sensors and Actuators A: Physical*, **122**, pp.16–22
- [21] Soderlund L., Eriksson J.T., Salonen J., Vihriala H., Perala R., 1996, “A permanent-magnet generator for wind power applications, *IEEE Transactions on Magnetics*, **32**, pp. 230-249
- [22] Sarı I., Balkan T., Kulah H., 2008, “An electromagnetic micro power generator for wideband environmental vibrations”, *Sensors and Actuators A: Physical*, **145-146**, pp. 405–413
- [23] Yang W.M., Chou S.K., Shu C., Li Z.W., Xue H., 2004, “A prototype microthermophotovoltaic power generator”, *Applied Physics Letters*, **84**, pp. 55–63
- [24] Büren T., Tröster G., 2006, “Design and optimization of a linear vibration-driven electromagnetic micro-power generator”, *Sensors and Actuators A: Physical*, **135**, pp. 765–775

- [25] Williams C.B., Shearwood C., Harradine M.A., Mellor P.H., Birch T.S., Yates R.B., 2001, "Development of an electromagnetic micro-generator", IEEE/RSJ International Conference on Intelligent Robots, Wailea, Hawaii, USA
- [26] White N.M., Glynn J.M., Beeby S.P., 2001, "A novel thick-film piezoelectric micro-generator", *Smart Materials and Structures*, **10**, pp. 132–149
- [27] Mahmoud M.A., El-Saadany E.F., Mansour R.R., 2006, "Planar electret based electrostatic micro-generator", 6<sup>th</sup> International Workshop on Micro and Nanotechnology for Power Generator and Energy Conversion Applications: Berkeley, USA
- [28] Beeby S.P., Tudor M.J., Koukharenko E., White N.M., O'Donnell T., Saha C., Kulkarni S., Roy S., 2005, "Micromachined silicon generator for harvesting power from vibrations", 5<sup>th</sup> International Workshop on Micro and Nanotechnology for Power Generator and Energy Conversion Applications: Tokyo, JAPAN
- [29] Arakawa Y., Suzuki Y., 2004, "Micro seismic power generator using electrets polymer film", 4<sup>th</sup> International Workshop on Micro and Nanotechnology for Power Generator and Energy Conversion Applications: Kyoto, JAPAN
- [30] Glatz W., Simon M., Christopher H., 2006, "Optimization and fabrication of thick flexible polymer based micro thermoelectric generator", *Sensors and Actuators*, **132**, pp. 337–345
- [31] Jacquot A., Liu W.L., Chen G., Fleurial J.P., Dauscher A., Lenoir B., 2002, "Fabrication and modeling of an in-plane thermoelectric micro-generator", 2<sup>nd</sup> Twenty-First International Conferences - Thermoelectrics proceedings: Long Beach, CA
- [32] Jones K.D., Lindsey K., Platzer M.F., 2002, "An investigation of the fluid-structure interaction in an oscillating-wing micro-hydropower generator", WIT eLibrary; Wessex Institute
- [33] Toriyama T., Yajima M., Sugiyama S., 2001, "Thermoelectric micro power generator utilizing self-standing polysilicon-metal thermopile", 14<sup>th</sup> IEEE International Micro Electro Mechanical Systems Conference and Exhibition: Orlando, FL, USA
- [34] Kwon K., Lee S.J., Longnan L., Han C., and Kim D., 2013, "Energy harvesting system using reverse electro dialysis with nanoporous polycarbonate track-etch membranes", *International Journal of Energy Research*; DOI: 10.1002/er.3111
- [35] Okamoto H., Suzuki T., Mori K., Cao Z., Onuki T., Kuwano H., 2009, "The advantages and potential of electric-based vibration-driven micro energy harvesters", *International Journal of Energy Research*, **33**, pp. 1180-1190

- [36] Danielson O., Eriksson M., Leijon M., 2006, "Study of a longitudinal flux permanent magnet linear generator for wave energy convertors", *International Journal of Energy Research*, **30**, pp. 1130-1145
- [37] Koşar A., 2009, "A model predict saturated critical heat flux in minichannels and microtubes", *International Journal of Thermal Science*, **48**, pp. 261-270
- [38] Koşar A., Schneider B., Peles Y., 2007, "Hydrodynamic cavitation and boiling in refrigerant (r-123) flow inside microtubes", *International Journal of Heat and Mass Transfer*, **50**, pp. 2828- 2854
- [39] Koşar A., Peles Y., 2007, "Critical heat flux of r-123 in silicon-based microtubes", *Journal of Heat Transfer*, 129, pp 844-851
- [40] Kandlikar S.G., 2002, "Fundamental issues related to flow boiling in minichannels and microtubes", *Experimental Thermal and Fluid Science*, **26**, pp. 389 – 407
- [41] Lin, L., 1998, "Microscale thermal bubble formation: thermophysical phenomena and applications", *Microscale Thermophysical Engineering*, **2 (2)**
- [42] Yu W., France D.M., Wambsganns M.W., Hull J.R., 2002, "Two-phase pressure drop boiling heat transfer and critical heat flux to water in a small-diameter horizontal tube", *International Journal of Multiphase Flow*, **28**, pp. 927-941
- [43] Tran N.T., Chyu M.C., Wambsganss W.M., France D.M., 2000, "Two phase pressure drop of refrigerants during flow boiling in small channels: an experimental investigation and correlation development", *International Journal of Multiphase Flow*, **26**, pp. 1739 – 1754
- [44] Ribatski G., Wojtan L., Thome J.R., 2006, "An analysis of experimental data and prediction methods for two-phase frictional pressure drop and flow boiling heat transfer in micro-scale channels", *Experimental Thermal and Fluid Science*, **31**, pp. 1-19
- [45] Thome R.J., 2004, "Boiling in microtubes: a review of experiment and theory", *International Journal of Heat and Fluid Flow*, **25**, pp 128-139
- [46] Bertsch S.S., Groll E.A., Suresh V.G., 2008, "Review and comparative analysis of studies on saturated flow boiling in small channels", *Nanoscale and Microscale Thermophysical Engineering*, **12**
- [47] Kaya A., Ozdemir M.R., Kosar A., 2013, "High mass flux flow boiling and critical heat flux in microscale", *International Journal of Thermal Sciences*, **65**, pp. 70-78
- [48] Koşar A., Peles Y., Bergles A.E., 2009, "Experimental investigation of critical heat flux in microtubes for flow-field probes", *ASME 7th ICNMM Conference*, June 22-24, Pohang, South Korea

- [49] Kandlikar S.G., Shoji M., Dhir V.K., 1999, "Handbook of phase change", Taylor & Francis, USA
- [50] Hwang G.S., Kaviany M., 2006, "Critical heat flux in thin, uniform particle coatings", *International Journal of Heat and Mass Transfer*, **49**, pp. 844-849
- [51] Sarwar M.S., Jeong Y.H., Soon H.C., 2007, "Subcooled flow boiling chf enhancements with porous surface coatings", *International Journal of Heat and Mass Transfer*, **50**, pp. 3649-3657
- [52] Khanikar V., Mudawar I., Fisher T., 2009, "Effects of carbon nanotube coating on flow boiling in a microtube", *International Journal of Heat and Mass Transfer*, **52**, pp. 3805-3817
- [53] Jeong H.Y., Sarwar S.M., Chang H.S., 2008, "Flow boiling CHF enhancement with surfactant solutions under atmospheric pressure", *International Journal of Heat and Mass Transfer*, **51**, pp. 1913-1919
- [54] Kim H., Kim M., 2009, "Experimental study of the characteristics and mechanism of pool boiling chf enhancement using nanofluids", *Heat and Mass Transfer*, **45**, pp. 991-998
- [55] Şeşen M., Khudhayer W., Karabacak T., Koşar A., 2010, "Compact nanostructure integrated pool boiler for microscale cooling applications", *Micro & Nano Letters*, **5**
- [56] Kim I.T., Jeong H.Y., Chang H.S., 2010, "An experimental study on chf enhancement in flow boiling using Al<sub>2</sub>O<sub>3</sub> nano-fluid", *International Journal of Heat and Mass Transfer*, **53**, pp. 1015-1022
- [57] Park D.S., Lee W.S., Kang S., Bang C.I., Kim H.J., Shin S.H., Lee W.D., Lee W.D., 2010, "Effects of nanofluids containing graphene / graphene-oxide nanosheets on critical heat flux", *Applied Physics Letters*, **97**
- [58] Forrest E., Williamson E., Buongiorno J., Hu W.L., Rubner, M., Cohen, R., 2010, "Augmentation of nucleate boiling heat transfer and critical heat flux using nanoparticle thin-film coatings", *International Journal of Heat and Mass Transfer*, **53**, pp. 58-67.
- [59] Morshed, A.M., Fanghao, Y., Yakut, M.A., Khan, J.A., Li C., 2012, "Enhanced flow boiling in a microtube with integration of nano wires", *Applied Thermal Engineering*, **32**, pp. 68-75.
- [60] Phan H.T., Caney N., Marty P., Colasson S., Gavillet J., 2012, "Flow boiling of water on nanocoated surfaces in a microtube", *Journal of Heat Transfer*, **134**
- [61] Ahn H.S., Kang S.H., Lee C., Kim J., Kim M.H., 2012, "The effect of liquid spreading due to micro-structures of flow boiling critical heat flux", *International Journal of Multiphase Flow*, **43**, pp. 1-12.

- [62] Betz R.A., Jenkins J., Kim C., Attinger D., 2013, "Boiling heat transfer on superhydrophilic, superhydrophobic, and superbiphilic surfaces", *International Journal of Heat and Mass Transfer*, **57**, pp. 733 - 741
- [63] Saeidi D., Alemrajabi A.A., 2013, "Experimental investigation of pool boiling heat transfer and critical heat flux of nanostructured surfaces", *International Journal of Heat and Mass Transfer*, **60**, pp. 430 - 449
- [64] Tang Y., Tang B., Li Q., Qing J., Lu L., Chen K., 2013, "Pool-boiling enhancement by novel metallic nanoporous surface", *Experimental Thermal and Fluid Science*, **44**, pp. 194 – 198
- [65] Yongwei C., Mingyan L., Longfei H., 2013, "CaCO<sub>3</sub> fouling on microscale-nanoscale hydrophobic titania-fluoroalkylsilane films in pool boiling", *AIChE Journal*, **59**, pp. 2662 – 2678
- [66] Scherer F., Anton M., Schillinger U., Henke J., Bergemann C., Krüger A., Gansbacher B., Plank C., 2002, "Magnetofection: enhancing and targeting gene delivery by magnetic force in vitro and in vivo", *Gene Therapy*, **9**, pp. 102–109.
- [67] Lin Y., Li M., Wu C., 2004, "Simulation and experimental demonstration of the electric field assisted electroporation microchip for in vitro gene delivery enhancement", *Lab on a Chip*, **4**, pp. 104 – 108
- [68] Bystrzejewski, M., Huczko, A., Lange, H., 2005, "Arc plasma route to carbon-encapsulated magnetic nanoparticles for biomedical applications", *Sensors and Actuators B: Chemical*, **109**, pp. 81-85
- [69] Dobson, J., 2006, "gene therapy progress and prospects: magnetic nanoparticle-based gene delivery", *Gene Therapy*, **13**, pp. 283-287
- [70] Kopke R.D., Wassel R.A., Mondalek F., Grady B., Chen K., Liu J., Gibson D., Dormer K.J., 2006, "Magnetic nanoparticles: inner ear targeted molecule delivery and middle ear implant", *Audiology and Neurotology*, **11**, pp. 123 - 133
- [71] Huang K.S., Lin Y.C., Su, C.C., Fang, C.S, 2006, "Enhancement of an electroporation system for gene delivery using electrophoresis with a planar electrode", *Lab on a Chip*, **7**, pp. 86 - 92
- [72] Hu S., Liu D., Tung W., Liao C., Chen S., 2008, "Surfactant-free, self-assembled pva-iron oxide/silica core-shell nano carriers for highly sensitive, magnetically controlled drug release and ultrahigh cancer cell uptake efficiency", *Advanced Functional Materials*, **18**, pp. 2946 – 2955

- [73] Gazeau F., Lévy M., Wilhelm C., 2008, “Optimizing magnetic nanoparticle design for nanothermotherapy”, *Nanomedicine*, **3**, pp. 831-844
- [74] Fung A.O., Kapadia V., Pierstorff E., Ho D., Chen Y., 2008, “Induction of cell death by magnetic actuation of nickel nanowires internalized by fibroblasts”, *The Journal of Physical Chemistry C*, **112**, pp. 15085 - 15088
- [75] Lee H., Lee K., Moon S.H., Lee Y., Park, T.G., Cheon J., 2009, “All-in-one target-cell-specific magnetic nanoparticles for simultaneous molecular imaging and siRNA delivery”, *Angewandte Chemie International Edition*, **48**, pp. 4174 – 4179
- [76] Namiki Y., Namiki T., Yoshida H., Ishii Y., Tsubota A., Koido S., Nariai K., Mitsunaga M., Yanagisawa S., Kashiwagi H., Mabashi Y., Yumoto Y., Hoshina S., Fujise K., Tada N., 2009, “A novel magnetic crystal–lipid nanostructure for magnetically guided in vivo gene delivery”, *Nature Nanotechnology*, **4**, pp. 598 – 606
- [77] Stride E., Porter C., Prieto A.G., Pankhurst Q., 2009, “Enhancement of microbubble mediated gene delivery by simultaneous exposure to ultrasonic and magnetic fields”, *Ultrasound in Medicine & Biology*, **35**, pp. 861 – 868
- [78] Sajja H.K., East M.P., Mao H., Wang A.Y., Nie S., Yang L., 2009, “Development of multifunctional nanoparticles for targeted drug delivery and non-invasive imaging of therapeutic effect”, *Current Drug Discovery Technologies*, **6**, pp. 43 – 51
- [79] Dave S.R., Xiaohu G., 2009, "Monodisperse magnetic nanoparticles for biodetection, imaging, and drug delivery: a versatile and evolving technology", *Wiley Interdisciplinary Reviews: Nanomedicine and Nanobiotechnology*, **1**, pp. 583 - 609
- [80] Kim D.H., Rozhkova E.A., Ulasov I.V., Bader S.D., Rajh T., Lesniak M.S., Novosad V., 2009, “Biofunctionalized magnetic-vortex microdiscs for targeted cancer-cell destruction”, *Nature Materials*, **9**, pp. 165-171
- [81] Barakat N.S., 2009, “Magnetically modulated nanosystems: a unique drug-delivery platform”, *Nanomedicine*, **4**, pp. 799-812
- [82] Singh N., Agrawal A., Leung A.K.L., Sharp P.A., Bhatia S.N., Am J., 2010, “Effect of nanoparticle conjugation on gene silencing by rna interference”, *American Chemical Society*, **132**, pp. 8241 – 8243
- [83] Veiseh O., Kievit F.M., Mok H., Ayesh J., Clark C., Fang C., Leung M., Arami H., Park J.O., Zhang M., 2011, “Cell transcytosing poly-arginine coated magnetic nanovector for safe and effective siRNA delivery”, *Biomaterials*, **32** (24), pp. 5717 – 5725.



- [84] Amstad E., Kohlbrecher J., Müller E., Schweizer T., Textor M., Reimhult E., 2011, “Triggered release from liposomes through magnetic actuation of iron oxide nanoparticle containing membranes”, *Nano Letters*, **11**, pp. 1664 – 1670
- [85] Gao W., Kagan D., Pak O.S., Clawson C., Campuzano S., Chuluun E. C., Shipton E., Fullerton E.E., Zhang L., Lauga E., Wang J., 2012, “Cargo-towing fuel-free magnetic nanoswimmers for targeted drug delivery”, *Small*, **8**, pp. 460-467
- [86] Mok H., Zhang M., 2013, “Superparamagnetic iron oxide nanoparticle-based delivery systems for biotherapeutics”, *Expert Opinion on Drug Delivery*, **10**, pp. 73 - 87
- [87] Kim E., Lee K., Huh Y.M., Haam S., 2013, “Magnetic nanocomplexes and the physiological challenges associated with their use for cancer imaging and therapy”, *Journal of Materials Chemistry B*, **1**, pp. 729 - 739
- [88] Cohen Y., Shoushan S.Y., 2013, “magnetic nanoparticles-based diagnostics and theranostics”, *Current Opinion in Biotechnology*, **24**, pp. 672 – 681
- [89] Bao G., Mitragotri S., Tong S., 2013, “Multifunctional nanoparticles for drug delivery and molecular imaging”, *Annual Review of Biomedical Engineering*, **15**, pp. 253 – 282
- [90] Hu B., Dobson J., El Haj A.J., 2013, “Control of smooth muscle  $\alpha$ -actin (sma) up-regulation in hbmscs using remote magnetic particle mechano-activation”, *Nanomedicine: Nanotechnology, Biology and Medicine*
- [91] Subramanian M., Lim J., Dobson J., 2013, “Enhanced nanomagnetic gene transfection of human prenatal cardiac progenitor cells and adult cardiomyocytes”, *Plos One*, **8**
- [92] Lim E.K., Jang E., Lee K., Haam S., Huh Y.M., 2013, “Delivery of cancer therapeutics using nanotechnology”, *Pharmaceutics*, **5**, pp. 294 - 317
- [93] Puri I.K., 2013, “Therapeutic magnetic fields”, *Annual Review of Fluid Mechanics*, **46**
- [94] Du P., Zeng J., Mu B., Liu P., 2013, “Biocompatible magnetic and molecular dual-targeting polyelectrolyte hybrid hollow microspheres for controlled drug release”, *Molecular Pharmaceutics*, **10**, pp. 1705 - 1715
- [95] Yim S., Gultepe E., Gracias D.H., Sitti M., 2013, “Biopsy using a magnetic capsule endoscope carrying releasing and retrieving untethered micro-grippers”, *Biomedical Engineering, IEEE Transactions on*, **13**, pp. 99 - 105
- [96] Kim S.H., Jeong J.H., Lee S.H., Kim S.W., Park T.G., 2006, “PEG conjugated VEGF siRNA for anti-angiogenic gene therapy”, *Control Release*: **116**, pp. 9 – 123
- [97] Chen Y., Lian G., Liao C., Wang W., Zeng L., Qian C., Huang K., Shuai X., 2013, “Characterization of polyethylene glycol-grafted polyethylenimine and superparamagnetic

iron oxide nanoparticles (PEG-G-PEI-SPION) as an mri-visible vector for sirna delivery in gastric cancer in vitro and in vivo”, *Gastroenterol* , **48**, pp. 809–821

[98] Özdemir M.R., Koşar A., 2013, “Thermally developing single-phase flows in microtubes”, *Journal of Heat Transfer*, **135** (7)

[99] Özdemir M.R., Kaya A., Koşar A., 2011, “Low mass quality flow boiling in microtubes at high mass fluxes”, *ASME Journal of Thermal Sciences and Engineering Applications*, **3**

[100] Munson B.R., Huebsch W.W., Rothmayer A.P., 2012, “Fundamentals of fluid mechanics”, Wiley 7th Edition, pp. 103-125

[101] Kline S., McClintock F.A., 1953, “Describing uncertainties in single-sample experiments”, *Mechanical Engineering (ASME)*, **75**, pp. 3-8

[102] Colebrook C.F., 1939, “Turbulent flow in pipes, with particular reference on the transition between the smooth and rough pipe laws”, *Journal of Institution of Civil Engineers London* **11** (4), pp. 133–156

[103] Zhai L., Cebeci F.Ç., Cohen R.E., Rubner M.F., 2004, “Stable superhydrophobic coatings from polyelectrolyte multilayers”, *Nano Letters*, **4**, pp. 1349 – 1353

[104] Lenz P., Lipowsky R., 1998, “Morphological transitions of wetting layers on structured surfaces”, *Physical Review Letters*, **80**, pp. 1920 – 1923

[105] Ji S., Liu C., Son J.G., Gotrik K., Craig G.W., Gopalan P., Himpfel F.J., Char K., Nealey P.F., 2008, “Generalization of the use of random copolymers to control the wetting behavior of block copolymer films”, *Macromolecules*, **41**, pp. 9098 – 9103

[106] Webb R. L., 1994, “Principles of enhanced heat transfer”, New York: John Wiley and Sons, Chapter 11.

[107] Yabe A., Mori Y., Hijikata K., 1995, “Active heat transfer enhancement by utilizing electric fields”, *Annual Review of Heat Transfer*, **7**, pp. 193 – 244.

[108] Yabe A., Taketani T., Maki H., Takahashi K., Nakadai Y., 1992, “Experimental study of electro-hydrodynamically (EHD) enhanced evaporator for nonazeotropic mixtures”, *ASHRAE Transactions*, **98**, pp. 455 – 460.

[109] Kandlikar S.G., 2010, “A scale analysis based theoretical force balance model for critical heat flux (CHF) during saturated flow boiling in microchannels and minichannels”, *Journal of Heat Transfer*, **132**, pp. 1-13

[110] Mudawar I., Bowers M.B., 1999, “Ultra-high critical heat flux (CHF) for subcooled water flow boiling: chf data and parametric effects for small diameter tubes”, *International Journal of Heat and Mass Transfer*, **42**, pp. 1405 – 1428

- [111] Bergles, A.E., 1963, “Subcooled burnout in tubes of small diameter”, ASME Paper No. 63-WA-182
- [112] Kuo J.C., Kosar A., Peles Y., Virost S., Mishra C., Jensen M.K., 2006, “Bubble dynamics during boiling in enhanced surface microtubes”, *Journal of Microelectromechanical Systems*, 15, pp. 1514-1527
- [113] Groeneveld D.C., 1996, “The 1995 look-up table for critical heat flux in tubes”, *Applied Thermal Engineering*, **163**, pp. 1-23
- [114] Celata G.P., 1993, “Recent achievements in the thermal hydraulics of high heat flux components in fusion reactors”, *Experimental Thermal and Fluid Science*, 7, pp. 263-278
- [115] Vandervort, C. L., Bergles, A. E., Jensen, M. K., 1994, “An experimental study of critical heat flux in very high heat flux subcooled boiling”, *International Journal of Heat and Mass Transfer*, 37 (1), pp. 161-173.
- [116] Hall D. D., Mudawar I., 2000, “Critical heat flux (CHF) for water flow in tubes – ii: subcooled CHF correlations”, *International Journal of Heat and Mass Transfer*, **43 (14)**, pp. 2605-2640.
- [117] Brutin D., Tadrist L., 2004, “Pressure drop and heat transfer analysis of flow boiling in a minichannel: influence of the inlet condition on two-phase flow stability”, *International Journal of Heat and Mass Transfer*, **47**, pp. 2365-2377.
- [118] Harvey S.D., Vucelick M.E., Lee N.R., Wright B.W., 2002, “Blind field test evaluation of raman spectroscopy as a forensic tool”, *Forensic Science International*, **125**, pp. 12-21
- [119] Constantini A., Luciani G., Annunziata G., Silvestri B., Branda F., 2006, “Swelling properties and bioactivity of silica gel/pHEMA nanocomposites”, *Journals of Material Science: Materials in Medicine*, **17**, pp. 319-325
- [120] Ozaydin-Ince G., Demirel G., Gleason K.K., Demirel M.C., 2010, “highly swellable free-standing hydrogel nanotube forests soft matter”, **6**, 1635-1639
- [121] Colthup N.B., Daly L.H., Wiberley S.E., 1990, “Introduction to infrared and Raman spectroscopy”, Academic Press, pp. 20-24
- [122] Ali Y. M., Yang F., Fang R., Chen L., Khan J., 2011, “Thermohydraulic characteristics of a single-phase microtube heat sink coated with copper nanowires”, *Frontiers in Heat and Mass Transfer*, 2, pp. 451 – 534
- [123] McHale J. P., Garimella S., 2010, “Bubble nucleation characteristics in pool boiling of a wetting liquid on smooth and rough surfaces”, *International Journal of Multiphase Flow*, 36, pp. 249-260.

[124] Mc Bain S.C., Yiu H.P., El Haj A., Dobson J., 2007, "Polyethylenimine functionalized iron oxide nanoparticles as agents for DNA delivery and transfection", *Material Chemistry*, 17, pp. 2561–2565.

[125] Jang E.S., Park K.S., 2012, "Lipofectamine-2000 assisted magnetofection to fibroblast cells using polyethyleneimine- $\text{Fe}_3\text{O}_4$ - $\text{SiO}_2$  nanoparticles", *Bull. Korean Chem. Society*, 8

[126] Chen Y., Lian G., Liao C., Wang W., Zeng L., Qian C., Huang K., Shuai, X., 2012, "Characterization of polyethylene glycol-grafted polyethylenimine and superparamagnetic iron oxide nanoparticles (PEG-g-PEI-SPION) as an MRI-visible vector for siRNA delivery in gastric cancer in vitro and in vivo", *Journal of Gastroenterology*, 48 (7), pp. 809 – 821.